ABSTRACT

Title of Dissertation: THE MECHANISMS AND ROLES OF POST-TRANSLATIONAL PROCESSING OF THE *DROSOPHILA* FIBROBLAST GROWTH FACTOR BRANCHLESS DURING DEVELOPMENT

Alexander Ronayne Sohr, Doctor of Philosophy, 2019

Dissertation directed by: Dr. Sougata Roy
Department of Cell Biology and Molecular Genetics
University of Maryland

During embryonic development, cells communicate with each other to cooperate to form organized tissues. Cells spatiotemporally coordinate with each other by communicating with signaling proteins such as Fibroblast Growth Factor (FGF) that travel from source to target cells to activate various functions. To better understand cell communication during tissue morphogenesis, this study aimed to address a fundamental question: how different cellular and molecular mechanisms in signal-producing cells prepare and release signals at the correct time and location and at an appropriate level. This research focuses on the intercellular communication of the *Drosophila* FGF Branchless (Bnl) to elucidate this question. Bnl is dynamically produced in restricted groups of cells to induce morphogenesis of tracheal airway

epithelial tubes. Tracheal cells receive the signal over distance by extending long receptor-containing filopodia, or cytonemes, to dynamically contact the Bnl-source. This work discovered two post-translational modifications of Bnl that regulate its polarized intracellular trafficking and cytoneme-mediated intercellular dispersal. During intracellular trafficking through the source cell Golgi network, Bnl is endo-proteolytically cleaved at a single site by the protease Furin-1. This cleavage activates polarized intracellular trafficking of the truncated signal exclusively to the surface of the source cells that faces the recipient tracheal cells. Thus, the intracellular cleavage acts as a switch to catalyze the efficient trafficking of the signal to the correct location from where cytonemes can subsequently receive it. Secondly, in the endoplasmic reticulum of source cells, Bnl is modified with a glycosylphosphatidylinositol (GPI) moiety at its C-terminus. This lipid moiety tethers Bnl molecules to the outer leaflet of the cell membrane, inhibiting its free release and ensuring signal exchange solely by direct physical contacts established by cytonemes. Therefore, this study discovered how Bnl is prepared by the source cells to ensure its subsequent target-specific intercellular dispersion through cytonemes. Conserved FGF family proteins are essential for regulating a broad spectrum of biological functions and defects in spatiotemporal levels of FGF signaling leads to severe diseases. Given the conservation of developmental signaling mechanisms in all organisms, the discovery of new regulatory mechanisms of FGF signaling has fundamental implications for understanding development and disease in humans.

THE MECHANISMS AND ROLES OF POST-TRANSLATIONAL PROCESSING OF THE *DROSOPHILA* FIBROBLAST GROWTH FACTOR BRANCHLESS DURING DEVELOPMENT

by

Alexander Ronayne Sohr

Dissertation submitted to the Faculty of the Graduate School of the
University of Maryland, College Park, in partial fulfillment
of the requirements for the degree of
Doctor of Philosophy
2019

Advisory Committee:
Professor Sougata Roy, Chair
Professor Norma Andrews
Professor Wenxia Song
Professor Eric Haag
Professor Leslie Pick, Dean's Representative

Dedication

To my incredible wife, Marly, for her unwavering love and support, and our daughter, who we will finally get to meet very soon!

Acknowledgements

The full list of people and how they have helped me achieve this goal would be another dissertation in itself, so I have done my best to be brief:

First and foremost, I would like to thank my wife, Marly, for being my rock. Through all the ups and downs of this experience you were the main constant and I am so incredibly lucky that you are in my life. I can't imagine having done this without you.

Next, I want to thank my entire family, especially my mom, my dad, my brother and sister, Drew, and P and Cathy. Every one of you has uniquely helped me and provided me with invaluable tools, time, and support to get here. It isn't possible to fit the gratitude I feel into a few simple sentences. Instead, I do my best to return the favor of love and support.

My committee consisting of Leslie, Eric, Norma, and Wenxia have been extremely supportive and have helped me find direction with my work and become a better scientist. I especially thank Leslie for her role as a mentor to me since I rotated in her lab. Time is extremely precious, and I sincerely appreciate each of you for spending a substantial amount of yours in helping me throughout this process.

Thank you to all of my lab members, past and present. It has been so fun getting to know each of you and grow together as coworkers and friends. I am always a text or call away if you ever need any help or advice, or just need me to reach something on a

high shelf in the lab. I want to especially acknowledge Lijuan, who was always incredibly generous with her time and so willing to help me no matter how many questions I pestered her with.

Finally, I would like to thank my mentor, advisor, and friend, Sougata. I feel very lucky and honored to have been your first graduate student and know that all of your future graduate students are lucky as well. I could always tell that you sincerely wanted the best for me as a scientist and as a person and I am extremely grateful for the support you have provided and continue to provide.

Table of Contents

Chapter 1: Introduction

1.1 Cell-Cell Communication

Cell-cell signaling is critical for the development of complex structures in every multicellular organism and is also important for the maintenance and homeostasis of adult tissues. The first experimental report implicating the importance of non-autonomous instructive signaling between cells was reported about 100 years ago by Mangold and Spemann in their famous cross-species grafting experiments in amphibian embryos (1924; Nobel Prize to Spemann 1934). When they grafted the blastopore dorsal lip from one gastrulating newt embryo onto an ectopic location of another host embryo of a different species, it induced ectopic gastrulation, resulting in two-headed tadpoles (Spemann and Mangold, 1924). As only cells originating from the blastopore could induce the host cells to achieve their new fates, Spemann and Mangold proposed that these cells create some "inducer" substance, such as a small, organic molecule that could freely diffuse between cells to mediate its instructive function to organize and influence the development of other cells and tissues. Research during the last four decades has identified almost all major pattern-inducing signaling proteins. Surprisingly, despite the amount of incredibly diverse patterns, the signaling proteins were found to be highly conserved throughout the animal kingdom. Further, they fall into only 11 main classes, which have been defined by the ligand or signal transducers involved: Notch, epidermal growth factor (EGF), fibroblast growth factor (FGF), Wnt/Wingless (Wg), Hedgehog (Hh), transforming growth factor β (TGFβ)/BMPs,

cytokines, Hippo, Jun kinase (JNK), NF-κB, and retinoic acid receptor (RAR). These pathways involve either cell-to-cell contact via surface proteins (juxtacrine signaling), or secreted growth and differentiation factors (paracrine signaling). Among these pathways, only Notch and Hippo are juxtacrine, whereas the others are paracrine (Perrimon et al., 2012). My thesis work focused on the local paracrine signaling mechanism and addresses one of the key regulatory steps in paracrine signaling - how the signal is controlled for release to ensure its target-specific dispersal through extracellular space.

The two most influential theories on how signal dispersion through a naive tissue might play an important role in inducing spatial tissue patterns were proposed long before the discovery of the first signaling molecules. In 1952, British mathematician Alan Turing, in his Chemical Basis of Morphogenesis (1952), coined the term "morphogen" for pattern-inducing chemicals that diffuse between cells to induce concentration-dependent responses. Turing established equations to model a “reaction-diffusion” mechanism where two morphogens with different diffusion capabilities form patterns (Turing, 1952). For instance, in his activator-inhibitor model, one morphogen acts as the “activator”, which diffuses slowly and elicits a response in a recipient cell if it surpasses a certain concentration in that cell. The other morphogen is produced in response to the first morphogen and acts as an “inhibitor” of the activator but diffuses further and faster than the activator. The counteracting balance of these morphogens along with their differential diffusivity could therefore elicit responses in a field of cells in periodic patterns. Later in the 1960’s, Lewis Wolpert proposed the theory of positional information to further explain how more complex patterns could

be established from simple prior asymmetries in the tissue. The concept of positional information proposes that cells acquire positional values as in a coordinate system, which they interpret by developing in particular ways to give rise to spatial patterns (Wolpert, 1971). He proposed that recipient cells within a developing tissue are sensitive enough to be able to detect very small differences in morphogen concentrations. Different positions within a tissue could be defined and established based on the difference in concentration of morphogen received. Thus, Wolpert's "French flag model" was created where cells in a recipient field respond differently to gradually lower concentrations of a morphogen with increasing distance from the morphogen source (Wolpert, 1969; 1971). This morphogen gradient induces recipient cells to exhibit threshold-dependent changes in behavior, such as gene expression differences, thereby endowing them with positional information within the tissue.

Although the theoretical models of both Turing and Wolpert can explain many of the signal and signaling patterns observed during pattern formation (Green and Sharpe, 2015), how a signal might move across a tissue to set up a concentration-dependent positional response remained highly controversial. For instance, four radically different mechanisms were proposed to explain the dispersion pattern of the TGFβ homolog Decapentaplegic (Dpp) in the *Drosophila* larval wing imaginal disc: 1) free diffusion through extracellular space (Teleman and Cohen, 2000; Hufnagel et al., 2006); 2) serial transfer between neighboring cells using transcytosis and endocytic trafficking (González-Gaitán, 2003; Kicheva et al., 2007); 3) extracellular transport within lipoprotein particles (Eaton, 2006; Panáková et al., 2005); and 4) direct transfer mediated by filopodial protrusions called cytonemes (Ramírez-Weber and Kornberg,

1999; Hsiung et al., 2005; reviewed in Kornberg and Guha, 2007) (Figure 1.1). Most biophysical and mathematical analyses supported a simple diffusion-based signal dispersion and gradient formation model over a single plane of cells (mechanism 1 above) (Yu et al., 2009; Müller et al., 2013). However, tissues in a developing embryo have complex contours and geography (Roy and Kornberg, 2015). Moreover, available published experimental evidence did not definitively establish any of these proposed mechanisms as operative or inoperative. It was unclear how these processes could be responsible for complex pattern formation in development until the recent demonstration of cytoneme-mediated Dpp dispersion (Roy et al., 2011; 2014) provided a new perspective on paracrine signaling (Figure 1.1).

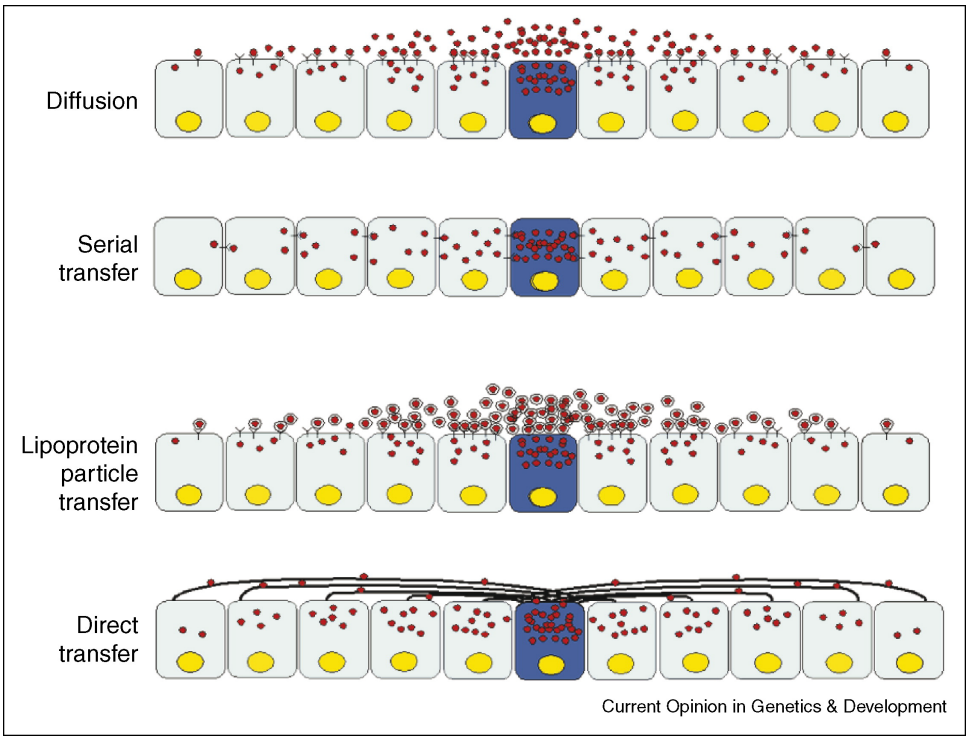

Figure 1-1: Proposed models of morphogen dispersal

Four mechanisms of morphogen distribution were proposed based on the distribution of Dpp in the wing disc. In the "Diffusion" model, signaling proteins are secreted from the producing cell and freely diffuse

through the extracellular environment. The "Serial transfer" model involves transcytosis and endocytosis of the signals to pass them between neighboring cells. The "Lipoprotein particle transfer" model involves the extracellular transport of signals that are contained within lipoprotein particles. In the "Direct transfer" model, signals are exchanged between cells via direct contact mediated by cytonemes that bridge the gap between the signal producing and recipient cells (adapted from Kornberg & Guha. *Curr Opin Genet Dev* 2007).

1.2 Discovery of cytoneme-mediated signaling

In 1999, a discovery from Tom Kornberg's lab (Ramírez-Weber and Kornberg, 1999) identified the existence of cytonemes in the *Drosophila* wing imaginal disc. They observed that Dpp-responding cells from the flanking region of the wing disc extended long, polarized filopodia or cytonemes towards the Dpp-expressing cells located in the center of the disc. These cytonemes were found to be ~200 nm in diameter and were only observed in live imaging conditions when GFP was over-expressed in the flanking wing disc region. Subsequent studies demonstrated that these cytonemes can respond to Dpp signaling and localize the Dpp receptor Thickveins (Tkv) (Hsiung et al., 2005). Although imaging and analyzing cytonemes was extremely challenging, in 2011 the wide-spread existence of cytonemes in many types of cells and tissues in *Drosophila* was first reported (Roy et al., 2011). In wing disc columnar cells, cytonemes were found to emanate from both the apical and basal membranes of cells. Furthermore, cytonemes from different locations within a single cell and in different tissues were shown to have different signaling specificities (Roy et al., 2011). Cytonemes from the apical part of the wing disc project towards the Dpp source cells in the wing disc, but their basal cytonemes do not. The use of a wing disc-associated tracheal branch called the Air-sac primordium (ASP) as a simple model system provided unique advantages that significantly advanced the cytoneme field (Figure 1-2, A). The ASP extends

cytonemes towards two different signal sources in the wing disc: FGF and Dpp (Figure 1-2, B). The finding that the receptors for FGF and Dpp (Breathless (Btl) and Tkv, respectively) independently sort into signal-specific cytonemes (Figure 1-2, D-F) strongly favored the idea that cytonemes mediate the transport of signals between cells. The first direct evidence that cytonemes are the conduits of signal exchange and transport came when the ASP cytonemes that orient towards the Dpp source were found to localize Tkv and receive Dpp in a receptor-dependent manner. Receptor-bound Dpp was shown to move toward the ASP cells in a retrograde manner (Figure 1-2) (Roy et al., 2014). Using a GFP-reconstitution experiment, Roy et al. (2014) also showed that the ASP cytonemes establish direct physical contact with the source and in absence of these contacts, Dpp cannot be received by the ASP cells that extended the cytonemes. Consequently, these cells could not activate signaling and the ASP developed abnormally. Importantly, genetic conditions that removed the source-ASP cytoneme contacts did not remove the inherent ability of the ASP cells to signal or to make cytonemes. If Dpp was expressed in cytoneme-deficient ASP cells, these cells could autonomously induce signaling. These experiments unequivocally established that cytonemes are responsible for signal exchange at their source cell contact sites and are essential for signaling. Since the discovery of cytonemes, there have been numerous reports on both invertebrate and vertebrate models demonstrating that cytonemes and cytoneme-like projections are associated with various signaling proteins such as EGF, Hh, Notch/Delta, Wnt, and FGF (Roy et al., 2014; Rojas-Ríos et al., 2012; Kornberg, 2014; Du et al., 2018a; Sanders et al., 2013; Huang and Kornberg, 2015; Stanganello

et al., 2015; Roy and Kornberg, 2015), suggesting a universal role for these specialized cellular structures (Kornberg and Roy, 2014). A recent study has provided strong

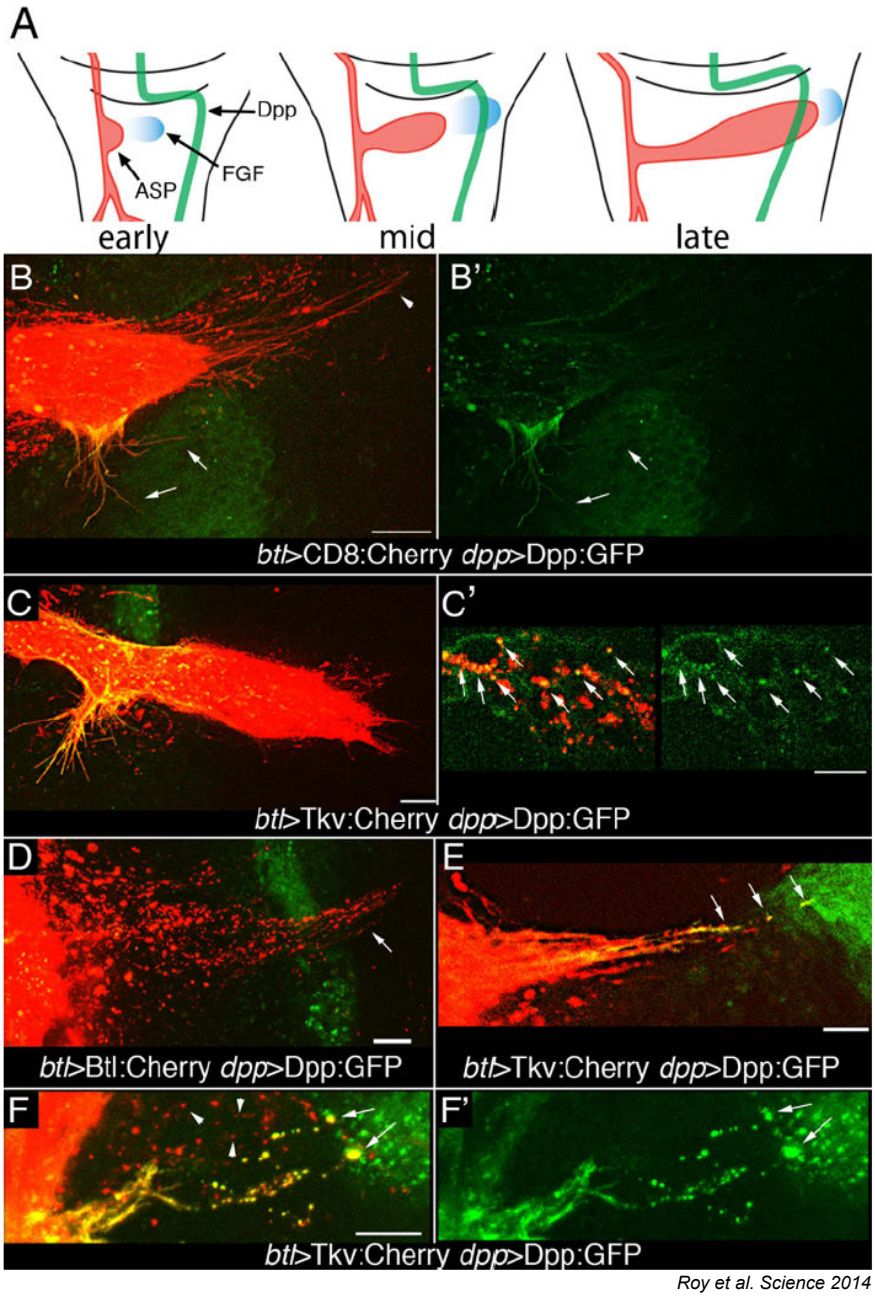

Figure 1-2: ASP cytonemes containing Tkv transport Dpp

(A) Drawings of different stages of 3rd instar larval wing discs that depict the growth of the ASP (red) and the relative positions of wing disc cells expressing Dpp (green) and FGF (blue). **(B, B')** Expression of CD8:Cherry in the ASP marks the ASP and ASP cytonemes (red) and expression of Dpp:GFP marks

the Dpp source cells in the wing disc (green). Dpp:GFP is seen in lateral cytonemes (arrows) that contact the Dpp source, but not tip cytonemes (arrowhead). Left panel (merge), right panel (GFP). **(C, C')** Expression of Tkv:cherry in the ASP and Dpp:GFP in the Dpp source cells shows that lateral Tkv-containing ASP cytonemes (red) receive Dpp:GFP (green). **(C)** Dpp:GFP and Tkv:Cherry colocalize in punctate form in the ASP (arrows in C'). **(D)** FGFR:Cherry expressed in the ASP (red) marks tip cytonemes that extend beyond Dpp:GFP in the Dpp-expressing wing disc cells (green). Dpp:GFP did not localize on cytonemes marked by FGFR:Cherry. **(E,F)** Only the cytonemes marked with Tkv:Cherry that make contact with Dpp-expressing cells localize Dpp:GFP. F, merge. F', GFP. Scale bars, 10 μm (adapted from Roy et al. *Science* 2014).

evidence with unprecedented resolution that ASP cytonemes also receive FGF in a contact-dependent manner (Du et al., 2018a). The signals are transported along the surface of the cytonemes in a receptor-bound form and are endocytosed in Rab7-bound vesicles within the ASP. This study also thoroughly revealed how cytoneme-mediated signaling can create an FGF morphogen gradient and tissue patterns (Du et al., 2018a). However, there has been no examination on how FGF-producing cells may regulate the signal in order to ensure that the cytoneme-mediated signaling of FGF is spatiotemporally regulated. Thus, although these studies have considerably helped advance the cytoneme field, there is still much to uncover about the foundational molecular mechanisms that control cytoneme-mediated signaling.

1.3 Fibroblast Growth Factors

Fibroblast Growth Factors (FGFs) are a family of signaling proteins that regulate the development of many tissues during embryogenesis and also function in adult tissues to regulate metabolism and to maintain and regenerate tissues (Nies et al., 2015; Itoh and Ornitz, 2011; Teven et al., 2014). In addition, defects in FGF have been implicated in several diseases, including cancer, asthma, and Alzheimer's (Mashayekhi et al., 2010; Turner and Grose, 2010; Volckaert and De Langhe, 2014; Bergwitz and

Jüppner, 2012). Despite their crucial role in development and disease, surprisingly little is known about how FGFs are exchanged between tissues or how FGF-producing cells control the release of the signal in order to maintain wild type spatiotemporal levels of signaling.

1.4 Mammalian FGFs

The first FGFs isolated, Fgf1 and Fgf2, were purified over 40 years ago from the bovine brain and pituitary gland (Gospodarowicz, 1974; Gospodarowicz et al., 1978). These proteins were found to induce growth and mitosis of fibroblast cells, and hence were named "Fibroblast Growth Factors". Thereafter, many more FGFs were discovered based on homology to Fgf1 and Fgf2. It is now known that the human and mouse FGF families are composed of 7 subfamilies with 22 total members (reviewed in Itoh and Ornitz, 2004). Of the 7 subfamilies, one subfamily comprised of the three Fgf15/19-like FGFs act as endocrine FGFs that travel over long distances to act on their targets. Members of the Fgf13-like subfamily act as intracrine FGFs, and are also referred to as fibroblast growth factor homologous factors (FHF), as they don't function in the same manner as the rest of the FGF family members (Goldfarb, 2005). Instead of traveling over distance to act on target cells, they act intracellularly in a receptor-independent manner to regulate the excitability of neurons and possibly other cell types by influencing voltage gated sodium channels (Goldfarb et al., 2007). The remaining 5 FGF subfamilies (Fgf4-, Fgf5-, Fgf8-, Fgf9-, and Fgf10-like) are comprised of canonical paracrine FGFs. The paracrine FGFs are secreted signaling proteins that travel locally between adjacent tissues and act on their target cells by binding to Fibroblast Growth Factor Receptor (FGFRs).

1.5 Mammalian FGF Receptors

FGFRs are Receptor Tyrosine Kinases (RTKs) that contain an extracellular portion with several immunoglobulin-like domains, a transmembrane domain, and a cytosolic portion that contains tyrosine kinase domains (Ornitz and Itoh, 2001). FGF binding to FGFR induces dimerization of two FGFRs and subsequent transphosphorylation of their cytosolic domains (Eswarakumar et al., 2005). This stimulates downstream events to activate one of several possible signaling pathways, including RAS-RAF-MAPK, PI3K-AKT, STAT, and PLCγ (Beenken and Mohammadi, 2009; Turner and Grose, 2010). In human and mouse, four FGFR genes (*Fgfr1-4*) have been identified, although alternative splicing of *Fgfr1-3* can create two different variants of each. Therefore, 7 major forms of FGFR can be generated, each with different spatiotemporal expression and ligand specificity (Zhang et al., 2006). Theoretically, over 70 different FGF/FGFR interactions are possible. The binding specificities of different FGF/FGFRs have been examined *in vitro*, but less is known about the actual pairings *in vivo.* Furthermore, the expression pattern of different FGFs or FGFRs are not fully understood and often overlap *in vivo* (Zhang et al., 2006). These complexities make it very difficult to reliably study FGF signaling in mammals.

1.6 Evolution the FGF family

The nematode *C. elegans* (*Caenorhabditis elegans*) has 2 *Fgf*-like genes (*egl-17* and *let-756*) (Huang and Stern, 2005), while *Ciona intestinalis* (a member of the Urochordata, the earliest-branching subphylum of Chordata), contains six *Fgf-like*

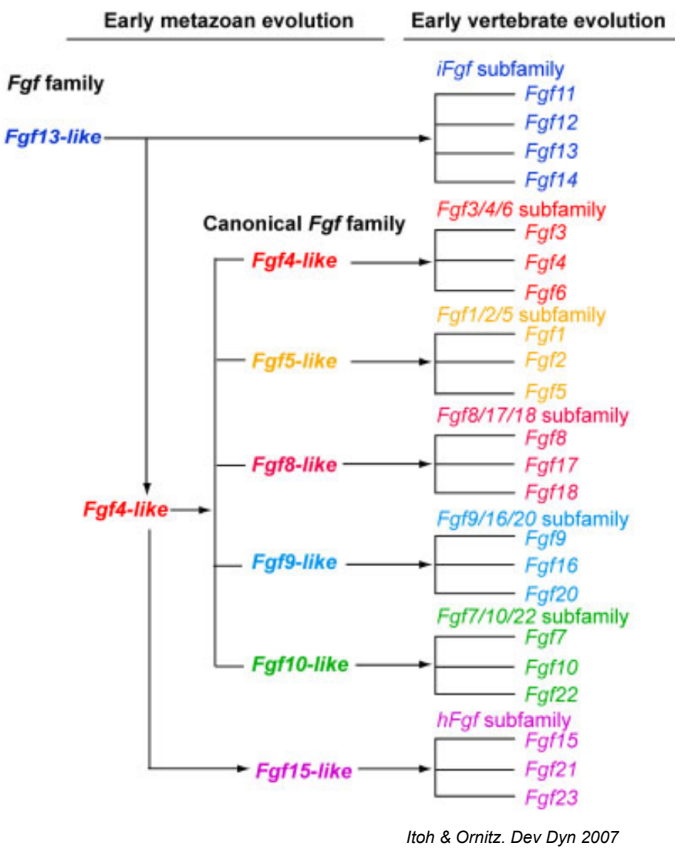

Figure 1-3: Proposed evolution of the *Fgf* gene family

Schematic showing the proposed evolution of the *Fgf* family. Gene duplication during early animal evolution created *Fgf4-like* from *Fgf13-like*. *Fgf4-like* is the common ancestor for the canonical paracrine *Fgf* subfamilies as well as the endocrine *Fgf15-like* subfamily. *Fgf13-like* is the ancestor of the intracrine *Fgf* subfamily (adapted from Itoh & Ornitz. *Dev Dyn* 2007).

genes, which are likely ancestors of the human/mouse FGF subfamilies (Itoh and Ornitz, 2011). This suggests that most members of the FGF subfamilies are a result of gene duplication after the divergence of protostomes (which include insects) and deuterostomes (which include mammals and other chordates). An evolutionary history of FGFs (proposed by Itoh and Ornitz (2007), Figure 1-3) starts with the single ancestral gene *Fgf13-like*, an intracrine-acting protein. Through gene duplication during early metazoan development, *Fgf4-like* was generated from *Fgf13-like*. *Fgf4-like* gained a signal sequence and the ability to be secreted and is likely the ancestral

gene of all paracrine FGFs. After the protostome/deuterostome divergence, the other paracrine FGF subfamily ancestral genes (*Fgf5-like, 8-like, 9-like,* and *10-like*) resulted from duplication of *Fgf4-like*. As no ancestral gene of endocrine *Fgfs* has been identified in *C. intestinalis* (an early deuterostome), the endocrine *Fgf* ancestral gene (*Fgf15/19-like)* may have arisen early in vertebrate evolution via duplication of *Fgf4-like*. During this period, *Fgf15/19* likely lost its affinity to proteins in the extracellular matrix (ECM) and therefore was able to act in an endocrine fashion. Finally, the members of each *Fgf* subfamily expanded into 3 or 4 members during two large genome duplication events during early vertebrate evolution.

1.7 *Drosophila* FGFs and FGFRs

In the fruit fly *Drosophila melanogaster*, there are three FGFs and two FGFRs (Muha and Müller, 2013). Pyramus (Pyr) and Thisbe (Ths), two of the *Drosophila* FGFs, share high sequence similarity in their core conserved FGF domain with the vertebrate Fgf8/17/18 subfamily (Gryzik and Müller, 2004). Pyr and Ths both function by binding to the *Drosophila* FGFR Heartless (Htl) (Muha and Müller, 2013). During gastrulation of the *Drosophila* embryo, signaling through Htl mediated by both Pyr and Ths is essential for the establishment of the mesoderm. Pyr and Ths are expressed in the neuroectoderm and signal to Htl-expressing mesoderm cells to give rise to several mesodermal lineages, including heart, somatic muscle, and fat body (Beiman et al., 1996; Gisselbrecht et al., 1996; Gryzik and Müller, 2004; Stathopoulos et al., 2004). FGF signaling through Htl is also essential for the morphogenesis of neuroectoderm-derived glia in the nervous system. In this context, Ths was shown to be responsible

for glial differentiation while Pyr was shown to be responsible for migration (Shishido et al., 1997).

Branchless (Bnl), the third *Drosophila* FGF, is functionally analogous to vertebrate Fgf10, which mediates the branching morphogenesis of the mammalian lung. Bnl functions by binding to the only other *Drosophila* FGFR Breathless (Btl) to fulfill its most well-studied role of regulating branching morphogenesis of the fly tracheal system (Sutherland et al., 1996). Recently, Bnl has been implicated in morphogenesis of the developing *Drosophila* eye disc (Mukherjee et al., 2012). It was shown that Bnl is responsible for restructuring eye disc cells to ensure that they properly form ommatidial clusters. Furthermore, Bnl regulates basal glia migration in the retina by signaling to Btl-expressing glial cells (Mukherjee et al., 2012). Bnl is also necessary in the developing *Drosophila* male genital disc to guide the migration of Btl-expressing mesodermal cells that eventually give rise to internal components of the male genitalia (Ahmad and Baker, 2002).

The *Drosophila* FGFRs Htl and Btl function as classical RTKs (Muha and Müller, 2013). Both contain two intracellular kinase domains for signal transduction, a transmembrane domain to anchor them in the membrane, and extracellular immunoglobulin (IG)-like domains to mediate ligand binding and dimerization. The intracellular kinase domains of Htl and Btl have high sequence homology with over 75% amino acid identity. However, the extracellular portions of Htl and Btl differ significantly, as Htl has two IG-like domains while Btl has five (Shishido et al., 1993). This, along with the differences in the *Drosophila* FGF ligand core domains, is likely

why Bnl cannot activate Htl and neither Pyr nor Ths can activate Btl (Kadam et al., 2009).

It is notable that human and mouse contain 22 FGFs each, while *Drosophila* contains only 3 FGFs. However, despite the large difference in number of FGF members in mammals and *Drosophila*, their functions are strongly conserved. FGF signaling in both the fly and vertebrates is implicated in similar cellular events such as survival, proliferation, differentiation, and migration. For example, branch formation of the mammalian lung and *Drosophila* trachea and air sacs are both mediated by FGFs: Bnl in fly, Fgf10 in mammals (Metzger and Krasnow, 1999). Additionally, Fgf8 directs the migration of epiblast cells at the primitive streak in the early mouse gastrula, (Ciruna and Rossant, 2001) while the Fgf8-like *Drosophila* ligands Pyr and Ths similarly guide mesoderm cells expressing Htl in the ectoderm (Klingseisen et al., 2009; Clark et al., 2011). Therefore, although there is a discrepancy in the number of FGFs across evolution, *Drosophila* is a very useful model for studying paracrine FGF signaling and provides several advantages over mammalian models, such as quicker generation times, cost effectiveness, and unique genetic tools. Furthermore, the presence of fewer FGFs in *Drosophila* and the exclusivity in Bnl/Btl signaling (one ligand, one receptor) also provide unique advantages to study FGF signaling.

1.8 FGF signaling pathway

In the classical FGF RTK signaling pathway (Figure 1-4), FGF binding to its receptor induces receptor dimerization and subsequent transphosphorylation of their cytoplasmic domains. This stimulates downstream events to activate one of several possible signaling pathways, including MAPK/ERK, PI3K-AKT, STAT, and

PLCγ (Beenken and Mohammadi, 2009; Turner and Grose, 2010). The *Drosophila* protein Stumps/Downstream of FGF (Dof), which constitutively binds to the intracellular domain of FGFR, is also phosphorylated upon ligand binding and receptor dimerization (Petit et al., 2004) (Battersby et al., 2003). In vertebrates, FGF receptor substrate-2 (FRS2) serves the same function as Dof, which is to provide a scaffold for recruitment of downstream signaling components. The Dof sequence contains binding sites for three proteins that have all been shown to contribute to the MAPK/ERK signaling pathway: Corkscrew (Csw)/Shp2, Grb2/Drk, and Src64b (Csiszár et al., 2010). Binding of Grb2/Drk recruits Son of sevenless (Sos), a guanine nucleotide exchange factor (GEF), which then activates the small GTPase Ras85D (Wassarman et al., 1995). Ras initiates the MAPK cascade by activating Raf (MAPKKK (Xia et al., 2008)), which results in the continued cascade by successive phosphorylation of Dsor (Downstream of Raf1), a MAPKK, and ERK (MAPK). Finally, ERK-mediated phosphorylation of erythroblast transformation-specific (ETS) transcription factors results in gene expression changes, such as activation of *eve, Mef2, pointed,* and *sprouty* (Muha and Müller, 2013).

Csw, one of the proteins that binds to the Dof scaffold, has also been shown to activate the Ras/MAPK pathway (Petit et al., 2004). Csw is the fly homolog of SHP2, which in mammalian cells interacts with Grb2 to form a complex to interact with the FRS2 scaffold. Therefore, it is possible that Csw and Dof form a similar complex to activate downstream signaling components in *Drosophila* FGF signaling. Negative feedback of FGF signaling via the protein Sprouty (Spry) is conserved in fly and

mammals (Hacohen et al., 1998; Tefft et al., 1999). Sprouty functions by binding to Grb2 and inhibiting the formation of the Grb2/Sos complex (Hanafusa et al., 2002).

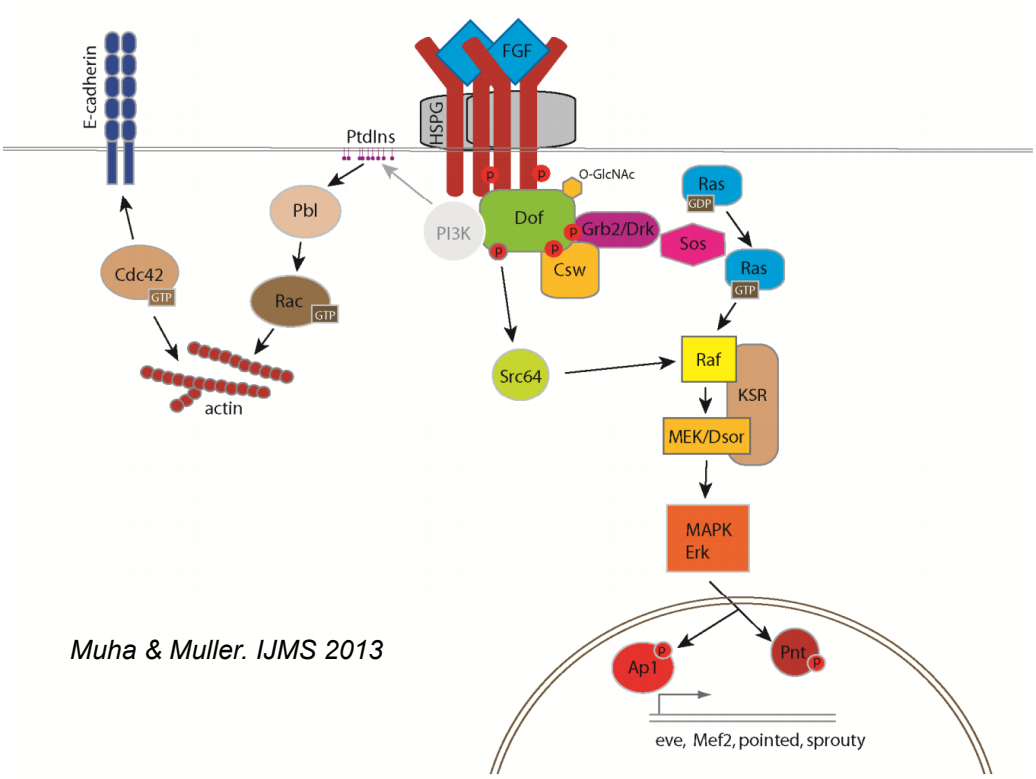

Figure 1-4: *Drosophila* FGF signaling pathway

Schematic of the FGF signaling pathway in *Drosophila*. FGF ligand binding to FGFR induces dimerization of the receptor and subsequent transphosphorylation of their intracellular domains, which can lead to activation of at least one of several signaling pathways, most notably the MAPK/ERK pathway (adapted from Muha & Muller. *IJMS* 2013).

FGF signaling also involves several MAPK-independent pathways to influence important cell activities. For example, FGF signaling induces the PI3-AKT pathway. GRB2 recruits the adaptor protein GAB1, which then activates the enzyme PI3K. PI3K phosphorylates the enzyme AKT, which has several functions including the activation of mTOR complex 1 by inhibiting TSC2 and phosphorylation of the FOXO1 transcription factor, causing it to exit the nucleus (Ornitz and Itoh, 2015). In addition,

FGF signaling can influence the activity of the Rho family of small GTPases, which are known to be involved in regulating the actin cytoskeleton. These GTPases are controlled mainly by GTPase activating proteins (GAPs and guanine nucleotide exchange factors (GEFs)) (Ridley, 2006). Recently, it was shown that RhoD, a small GTPase, is activated by FGF signaling in a MAPK-independent manner to produce actin-based filopodial cell protrusions (Koizumi et al., 2012). Similarly, it was shown that the PLCγ pathway induced by FGF signaling is responsible for cytoskeletal rearrangements that are critical for proper tissue morphogenesis (Sai and Ladher, 2008).

1.9 Branching Morphogenesis

Branching morphogenesis is a key developmental process that is also relevant in disease states. Branched tissue structures are conserved throughout evolution, and in vertebrates the branching morphogenesis process is critical for the shape and function of the kidney, mammary gland, vasculature, nervous system, and lung. Although the tissue types and locations are different, the general mechanism of branching morphogenesis is very conserved. Aside from nerve cells which only branch at the single-cell level, multicellular branches involve different cell fates and phenotypes within each growing branch. The leader of the growing branches adopts a tip cell fate and helps guide the growth and direction of the branch, while the follower cells adopt a stalk cell fate and are involved in maintaining the branch position and elongation of the branch (reviewed in Ochoa-Espinosa and Affolter, 2012).

Branching morphogenesis of all these organs is thought to involve an attractant that is expressed in the areas surrounding the tips of the growing branches and is

necessary for the directional outgrowth and patterning of the branch. For example, in the developing kidney, an epithelial cell layer forms the kidney collection ducts while a surrounding mesenchymal cell layer produces glial cell-line-derived neurotrophic factor (GDNF). GDNF signaling with its receptor Rearranged During Transfection (Ret) in the developing ducts is necessary for branch formation and outgrowth (Costantini, 2006). The mammary gland also exhibits branching morphogenesis during postnatal mammary development, where the end buds of the tips of growing ducts form a highly branched structure by growing into the surrounding fatty stroma (reviewed in Gjorevski and Nelson, 2011). This branching outgrowth of the duct end buds requires several growth factors, such as FGFs, Bmps, and EGFs (Hens and Wysolmerski, 2005; Mallepell et al., 2006; Hens et al., 2007; Brisken et al., 1998; Sternlicht, 2006).

1.9.1 Vasculature branching morphogenesis

The vasculature of vertebrate animals is formed by branching morphogenesis and is responsible for transporting critical nutrients and gases throughout the body. The initial generation of the most rudimentary vessels are formed by vasculogenesis, which create a simple circuit to and from the heart (Swift and Weinstein, 2009). These rudimentary vessels serve as the infrastructure from which smaller and finer vessels can branch throughout the body via branching morphogenesis. Vascular Endothelial Growth Factor (VEGF) is a key signaling protein that is involved in the sprouting and branching of new blood vessels. For example, in the mouse retina, tip cell migration and stalk cell proliferation of growing blood vessels depend on a gradient of VEGF-A. The vessels express VEGFR2 to receive the VEGF signal from adjacent astrocytes that produce and secrete the signal (Gerhardt et al., 2003). Similarly, other VEGF ligands

and their receptors have been shown to be involved in angiogenesis (Lohela et al., 2009).

Within growing vasculature branches, the tip cell selection of growing vessels is linked to Notch/Delta signaling. The ligand Delta-like 4 (*Dll4*) is a target of VEGF signaling, so cells that receive high levels of VEGF also have high levels of Delta. Delta then signals to adjacent cells to laterally inhibit their ability to become tip cells and influences them towards a stalk cell fate (Liu et al., 2003). Thus, differing levels of VEGF signaling helps establish the tip cell and stalk cell phenotypes in each growing branch through Delta/Notch signaling.

1.9.2 Lung branching morphogenesis

Another organ that relies on branching morphogenesis for its structure and function is the lung. Within the lung, numerous secondary and tertiary bronchi form a highly branched structure that allows for efficient and rapid exchange of gases with cells in the vasculature. During lung development, the formation of this highly branched respiratory tree relies mainly of Fgf10, which is expressed in groups of mesenchymal cells surrounding the growing epithelial lung buds (Bellusci et al., 1997; Sekine et al., 1999). The lung buds express Fgfr2b, to which Fgf10 binds and activates signaling. This interaction between Fgf10 and Fgfr2b is required for the lung buds to grow and form a branched network (De Moerlooze et al., 2000). Fgf10 signaling through its receptor activates several genes in the tip of the growing lung bud, including *sprouty2* (*spry2*), *BMP2*, *BMP4*, and *sonic hedgehog* (*shh*) to influence morphogenesis of the developing branches. (Bellusci et al., 1996; Lebeche et al., 1999; Tefft et al., 1999; Eblaghie et al., 2006).

1.9.3 Branching morphogenesis in disease

Defective branching morphogenesis is often associated with numerous diseases (Tímár et al., 2001). One example is angiogenesis, a process that involves branching morphogenesis and outgrowth of new blood vessels and is the underlying mechanism in the growth and metastasis of cancerous tumors (reviewed in Hoff and Machado, 2012). Cancer cells produce and release growth factors, including VEGF, to promote the branching morphogenesis of blood vessels towards the tumor (Kerbel, 2008). This not only supplies the oxygen and nutrients needed to support the rapidly growing tumor, but also supplies the infrastructure that is necessary for the tumor to metastasize and spread throughout the body via blood vessels. Thus, as branched tissue structures in organisms are so common and critical to both development and disease, it is necessary to understand more about the cellular and molecular mechanisms involved in branching morphogenesis.

1.9.4 Branching morphogenesis of the *Drosophila* trachea

The *Drosophila* tracheal system is an excellent model to study conserved mechanisms of branching morphogenesis. The tracheal system of *Drosophila* begins to form in the embryo where small groups of tracheal progenitor cells are present in each body segment (Manning and Krasnow, 1993). The *Drosophila* FGF Bnl is expressed in small groups of cells surrounding the tracheal placodes and each Bnl source induces budding and migration of a single branch from the placode. Bnl signals to its receptor Breathless (Btl), which is expressed in the recipient tracheal cells (Klämbt et al., 1992). The migrating tracheal cells eventually branch out to fuse and form additional secondary and terminal branches to create the entire branched tracheal network.

Traditionally, it was thought that an extracellular gradient of Bnl induces branch migration. In this model, the concentration of Bnl surpasses a threshold in the proximal tracheal tip cells to induce a signaling response, which includes the synthesis of secondary signals such as Sprouty or Delta to laterally inhibit stalk cells and specify their fates. The difference in tip or stalk cell phenotype in a growing branch endows the branch with polarity, and the migrating tip cells pull the stalk cells as they grow, causing them to intercalate and elongate to extend the branch following the tip cell leader (Caussinus et al., 2008).

1.10 Mechanisms of Bnl signaling during branching morphogenesis

The growth and migration of *Drosophila* tracheal branches during development requires the tight spatiotemporal regulation of Bnl expression and source cell localization, but the mechanisms by which these requirements are achieved were a

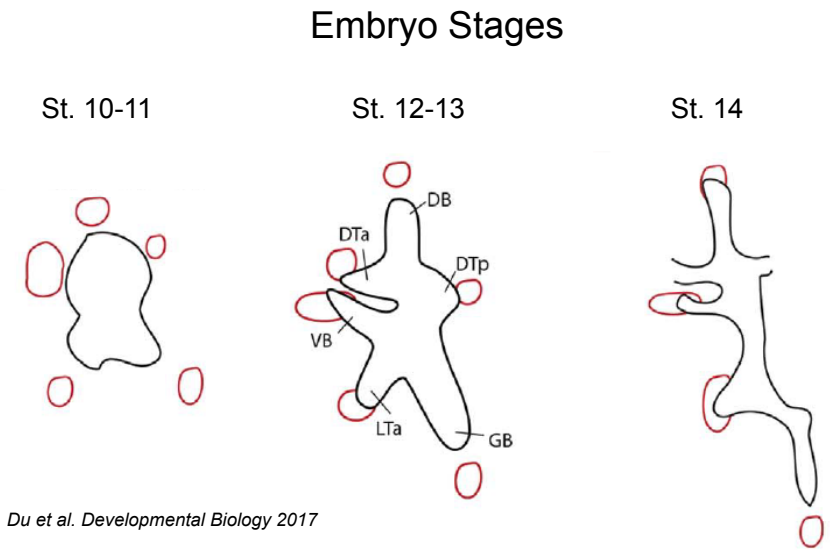

Figure 1-5: Early Bnl expression in *Drosophila* embryonic tracheal development

Schematic showing that small groups of Bnl source cells (red circles) surround a tracheal placode in Stage 10-11 embryos and remain just ahead of the migrating tracheal branches through later embryo stages to guide their growth (adapted from Du et al. *Developmental Biology* 2017).

mystery. For example, during early embryonic tracheal development, the six groups of Bnl expressing cells that surround a placode of tracheoblasts are situated within 2-3 cell diameters away from each other (Figure 1-5) (Sutherland et al., 1996) (Du et al., 2017). With the close proximity of the source cells, it was unclear how a soluble Bnl gradient could induce branch-specific signaling and migration. The source cells must have a way to regulate signal release and communicate with their cognate branch. To unravel the mystery, Du et al. (2017, 2018b), generated a *bnl-LexA* enhancer trap to reliably mark the signal source together with the recipient tracheal cells. Live imaging analyses showed that each Bnl source always remained closely associated with the migrating tracheal cells. This dynamism of Bnl-producing cells during tracheal migration was originally thought to be achieved by rapid activation/deactivation of *bnl* expression in cells along the tracheal branch's migratory path. Instead, Du et al. (2017) found that the same group of Bnl-expressing cells migrate in synchrony with the migrating trachea, and that dynamic transcriptional activation of *bnl* was not responsible for spatiotemporal activity of Bnl. During this co-migration, both the source and recipient cells establish direct cell-cell contacts with each other. This close association of the source and recipient cells raised doubt on the traditional model that branching morphogenesis is guided by an extracellular soluble signal gradient.

To visualize the Bnl gradient and determine how it is formed, Du et.al. (2018) generated an endogenous Bnl:GFP knock-in construct and used a larval wing disc-associated neotracheal branch called the air sac primordium (ASP), a precursor of the

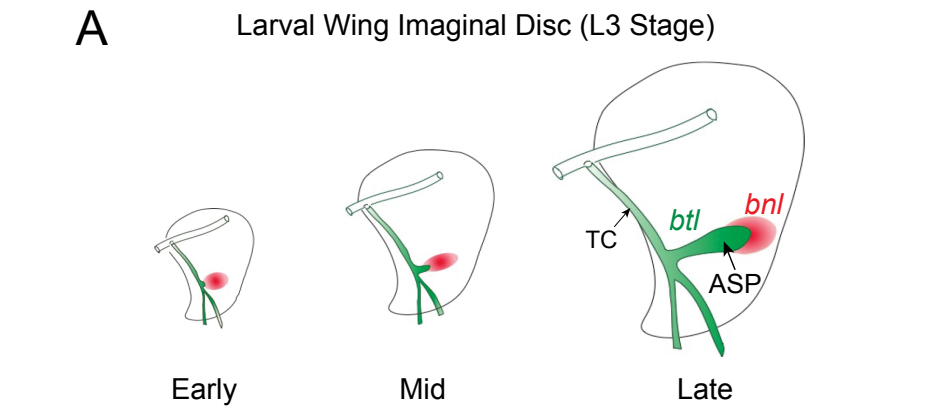

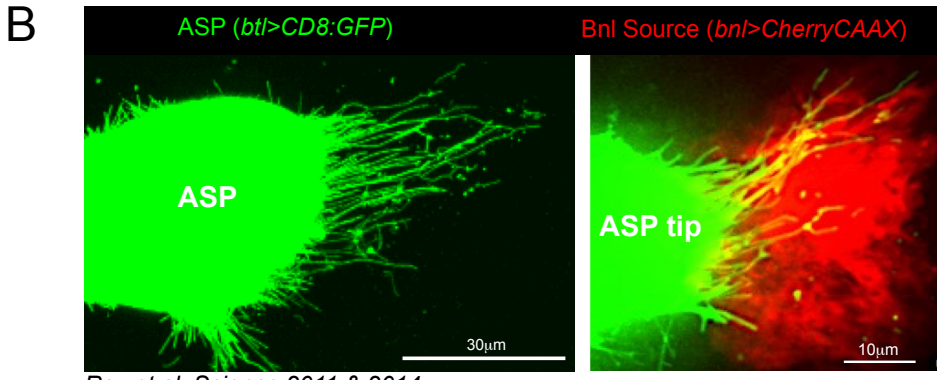

Roy et al. Science 2011 & 2014

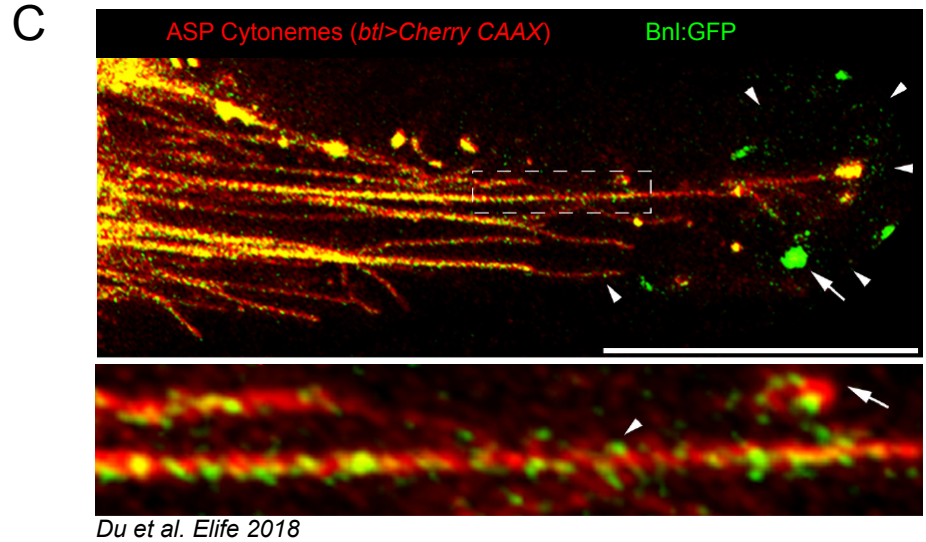

Du et al. Elife 2018

Figure 1-6: ASP morphogenesis and cytoneme-mediated Bnl transport

(A) The air sac primordium (ASP) buds out from the transverse connective (TC) tracheal branch in the early L3 larval stage and grows into a full-grown tubular structure by the late L3 larval stage. ASP growth and morphogenesis is guided Bnl (FGF), which is expressed in a small group of wing disc cells and signals to its receptor Btl (FGFR) expressed in the ASP cells. **(B)** ASP tip cells extend many cytonemes

(green, left and right image) that make contact with the Bnl-producing cells (red, right image) in the wing disc (adapted from Roy et al. *Science* 2011 & 2014). **(C)** Bnl:GFP (green) travels along ASP cytonemes (red) from the source cells to the ASP recipient cells to activate signaling and control its morphogenesis. The lower image is the inset from the upper image (adapted from Du et al. *Elife* 2018). Scale bar, 10 μm.

adult air sacs. In this system, a small group of cells in the wing imaginal disc epithelium express Bnl and signal to the ASP, which expresses Btl. The ASP buds out from the transverse connective (TC) in early stages of 3rd instar larval development (L3) and grows towards the wing disc Bnl source until it is fully grown in the late L3 larval stage (Figure 1-6, A). Use of this tissue system to study the inter-organ transport of Bnl revealed that Bnl does not diffuse freely to create an extracellular soluble gradient. Surprisingly, this study discovered that a Bnl gradient is formed, but only within the recipient ASP branch. ASP cells produce Btl-containing cytonemes that make contact with the Bnl-producing wing disc cells to receive the signal and transport it back to the ASP recipient cells where the signal is endocytosed and downstream signaling occurs (Figure 1-6, B and C) (Roy et al., 2014; Du et al., 2018a). This cytoneme-mediated target-specific signaling leads to the formation of a Bnl gradient within the ASP that adopts its shape. Different levels of FGF signaling in the ASP induce different target genes, indicating that Bnl functions as a morphogen to pattern the ASP epithelium. High to medium levels of Bnl in the tip region of the ASP induce the transcription factor Pointed-P1 (PntP1), which elicits positive feedback on Btl-containing cytoneme production (Figure 1-7) (Ohshiro et al., 2002; Du et al., 2018a). Further from the source cells, low levels of Bnl reception results in increased activity of the transcription factor Cut, which elicits negative feedback on Btl-containing cytoneme production (Du et al., 2018a). In addition, PntP1 and Cut antagonize each other's expression, resulting in a

graded number of ASP cytonemes based on Bnl reception levels that reinforces and maintains the Bnl gradient (Du et al., 2018a). This was the first demonstration of this novel mechanism underlying tracheal branching morphogenesis. It also, for the first time, showed how cytoneme-mediated signaling can create a morphogen gradient and tissue patterns.

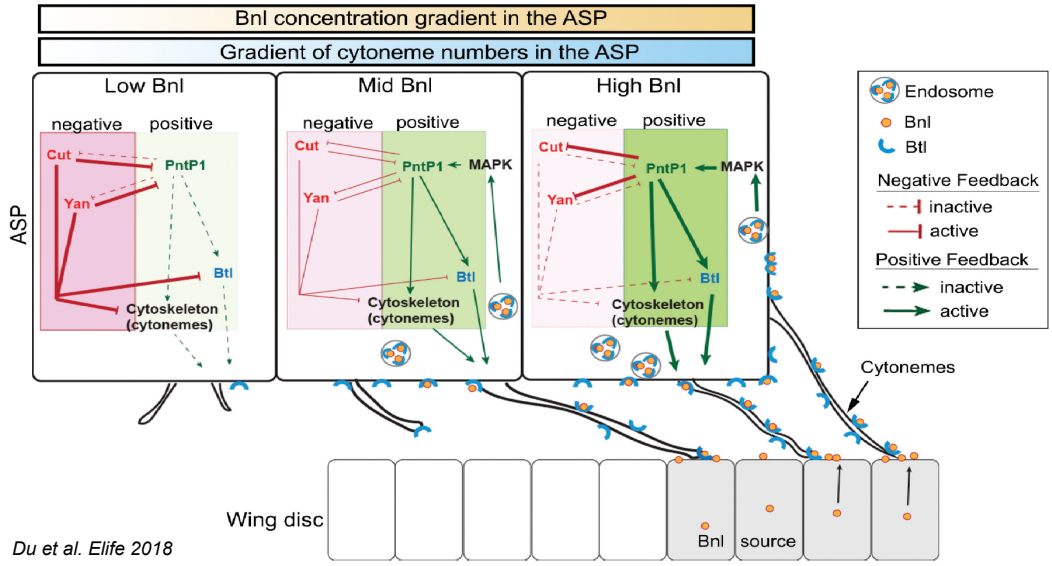

Figure 1-7: Bnl gradient formation in the recipient ASP

A schematic is shown representing how a Bnl gradient is formed and maintained in the ASP. Bnl is transported along Btl-containing cytonemes (arrow) extended by ASP cells. In the ASP, Bnl forms a gradient and activates different genes in a concentration-dependent manner. High levels of Bnl induce PntP1, which positively feedback controls Btl-containing cytoneme production. Low levels of Bnl induce Cut, which negatively feedback controls cytoneme production. PntP1 and Cut antagonize each other's expression, leading to a graded level of cytoneme production along the ASP which results in the maintenance of the Bnl gradient that adapts the ASP shape (adapted from Du et al. *Elife* 2018).

1.11 Important conceptual gaps, Aims, and Significance of this study

To initiate and maintain the type of self-regulated gradient formation mechanism described above, Bnl release from the source cells must be tightly controlled and restricted. If uncontrolled and unlimited Bnl protein were released from

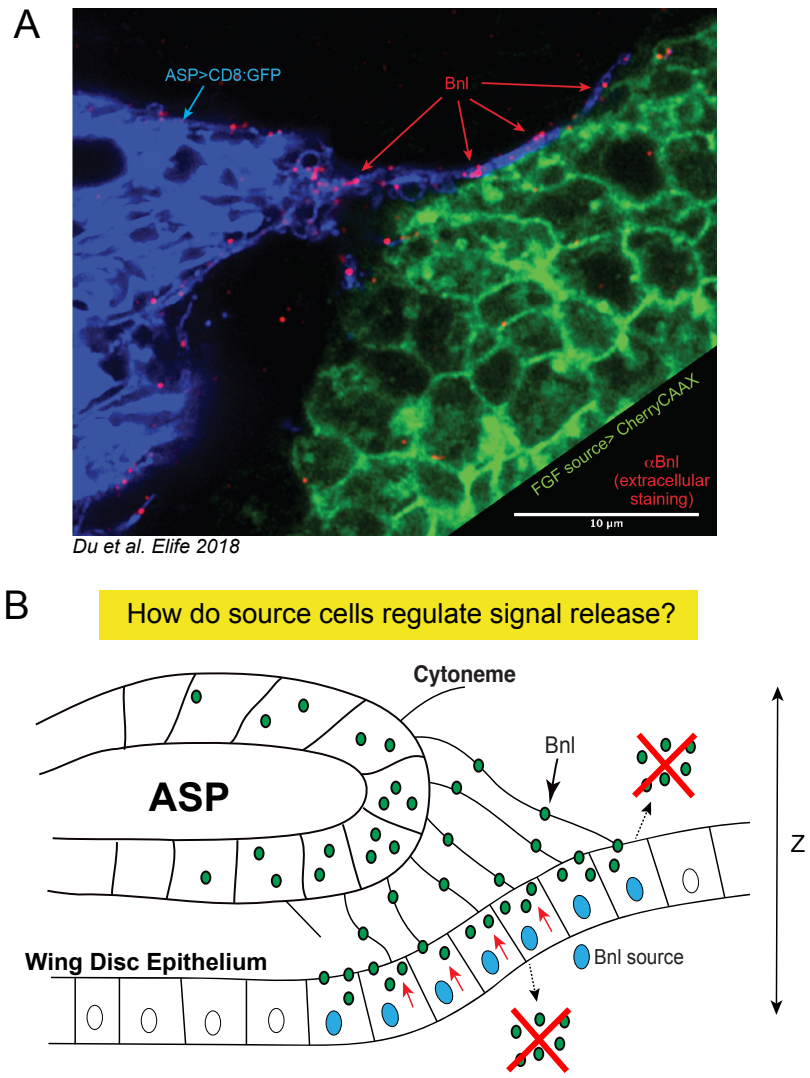

Figure 1-8: Restricted Bnl release

(A) Extracellular staining of Bnl using αBnl antibody (white puncta) reveals that the signal is only released from the source cells (green) where ASP cytonemes (blue) establish contact. The signal is not secreted from other regions of the source cells (adapted from Du et al. *Elife* 2018). **(B)** Schematic of a cross section of the ASP and wing disc representing restricted Bnl release only at the points of cytoneme contacts. Bnl is not secreted uncontrollably and appears to only be released from the surface that the cytonemes establish contact. So, how is Bnl release regulated within the source cells?

the source, establishment of the gradient and proper directional outgrowth in newly budding tracheal branches would be difficult to achieve. Furthermore, limited Bnl release is likely required to maintain the established gradient by ensuring that not all

recipient cells can receive the same amount of the signal. Consistent with this idea, marking both the Bnl source and recipient cells and staining externalized Bnl showed that the Bnl-producing cells only release the signal where cytonemes make contact with the source cells (Figure 1-8, A) (Du et al. 2018). These results leave several questions unanswered: How do the signal-producing cells ensure that the signal is spatiotemporally released at the sites of cytoneme contacts? As most morphogens are secreted signaling proteins, why doesn't the secreted signal simply diffuse away when the producing cells externalize it for cytoneme transport (Figure 1-8, B)? My thesis addressed these fundamental questions, advancing our overall understanding of cytoneme-mediated signaling and the cell biology underlying tissue development.

1.12 Model System

To study this aspect of cytoneme-mediated signaling in the branching morphogenesis process, *Drosophila melanogaster* was used as a model organism. *Drosophila* is ideal for studying basic, fundamental cellular processes for numerous reasons, such as the sophisticated genetic tools, high fecundity, short generation time, and well-established *in vitro* and *in vivo* systems and imaging methods. The wing disc/ASP is an ideal system to study FGF signaling because the *Drosophila* FGFR (Btl) is only expressed in the trachea and not in any surrounding wing disc cells. Therefore, manipulation of the FGF signal (Bnl) or of *bnl*-expressing cells does not affect the development of the wing disc and ASP phenotypes can be reliably interpreted as a direct result of a defect in Bnl signaling. This is a major advantage for unraveling the mechanisms within the source cells that regulate cytoneme-mediated signaling.

Chapter 2: Characterization and role of Bnl endo-proteolysis

2.1 Introduction

A general mechanism that occurs for almost all signaling protein families is the proteolytic cleavage of an initial proprotein form of the signaling protein, often mediated by members of the Proprotein Convertase (PC) family. This study revealed the role of PCs in FGF signaling and may provide insights into the role of proteolysis in other signaling systems.

2.1.1 Proprotein Convertases and Furin

The hunt for proteases that post-translationally modify other proteins for their maturation and/or activation began when it was shown that some hormones, such as insulin, were produced as larger prohormones and subsequently cleaved at doublets or clusters of basic amino acids (i.e. Lysine and Arginine) (Steiner et al., 1969; Chrétien and Li, 1967). These studies initiated decades of research that collectively found that most peptide hormones, growth factors, and even bacterial toxins and viral envelope glycoproteins all follow a very similar scheme of maturation that involves cleavage of a proprotein form (Seidah and Chrétien, 1999). The yeast endoprotease kexin, or Kex2, was the first enzyme discovered to catalyze these types of reactions in 1984 (Julius et al., 1984). Eventually, it was shown that Kex2 was actually just one enzyme within a much larger family of proprotein convertases (PCs) that served this proprotein-modifying function. Later, it was shown that Kex2 could process mammalian proproteins, which led to the hypothesis that mammalian PCs and Kex2 had similar

structural features and recognition sites (Thomas et al., 1988). Shortly thereafter, Furin was discovered in humans as the first Kex2 homolog (Fuller et al., 1989). Based on sequence homology, an additional six members of the mammalian PC family were isolated. Currently, it's been shown that PCs catalyze the maturation of many proteins that are involved in essentially every homeostatic and disease process (Thomas, 2002).

2.1.2 Furin structure and localization

The PC family belongs to the Subtilisin superfamily of serine endoproteases, which all share similarity within their subtilisin-like catalytic domains. The aspartate, histidine, and serine residues that constitute the catalytic triad within PCs are very conserved in the Subtilisin superfamily. Furin, the best-studied PC, is a Type 1 transmembrane protein that is found in all vertebrates and most invertebrates (Seidah et al., 1998; Thacker and Rose, 2000; Roebroek et al., 1991). It is an essential protein needed for proper development, as Furin knockout mice are embryonic lethal with death occurring at very early embryonic stages (Roebroek et al., 1998). Furin and the other PCs contain an N-terminal prodomain immediately downstream to their signal peptide. The prodomain acts as a chaperone to its guide the folding, transport, and activation, and is eventually cleaved off from the rest of protein via autocatalytic cleavage (Anderson et al., 2002). The mature Furin protein has a large extracellular/luminal domain that is homologous to similar regions of other PC family members and a P domain that functions to modulate pH and calcium requirements, as Furin activity is calcium-dependent (Zhou et al., 1998). The consensus cleavage site for Furin is -R-X-L/R-R-, and the minimal Furin cleavage site is -R-X-X-R- (R represents Arginine, L represents Lysine, X represents any amino acid), with cleavage

occurring immediately after the C-terminal Arginine (Molloy et al., 1992; Walker et al., 1994). Furin can localize in many parts of the cell and typically cycles through the trans-Golgi network, secretory vesicles, the cell surface, and endosomal vesicles (Molloy et al., 1999). The FI motif within Furin interacts with the adaptor protein AP-4 and results in it being predominantly basolaterally localized in polarized cells (Simmen et al., 1999; 2002). This diversity in Furin localization can partly explain how Furin can act on so many substrates in vivo, and why Furin is involved in numerous developmental and diseases processes.

2.1.3 Furin and disease

As Furin is involved in so many biological processes, it is unsurprisingly also associated with many disease states. Furin expression is upregulated in several types of cancer, including non-small-cell lung carcinomas, head and neck squamous-cell carcinomas, and glioblastomas (Mbikay et al., 1997). Increased levels of Furin in tumors is correlated with the aggressiveness of the tumor (Bassi et al., 2001a). Increased tumor aggression is associated with increased activation of membrane type 1-matrix metalloproteinase (MT1-MMP), one of Furin's substrates that it cleaves to activate (Bassi et al., 2001b). MT1-MMP cleaves and activates Mmp2, or pro-gelatinase, which can lead to tumor growth and vascularization by breaking down components of the extracellular matrix (Sounni et al., 2002). In mice, the Furin inhibitor α1-PDX leads to reduced activation of MT1-MMP and therefore reduced Mmp2 levels, which results in lower amounts of tumor metastasis (Bassi et al., 2001b; Aznavoorian et al., 2001). In colon, breast, prostate, and lung cancers, Insulin-like growth factor-1 (IGF1) and its receptor are both upregulated, and both are also substrates of Furin (Wu

et al., 2002). Inhibiting the Furin-mediated processing of IGF1 and IGF1R using α1-PDX significantly reduces the severity of tumor development and vascularization in mice (Khatib et al., 2001).

In individuals with rheumatoid arthritis, Furin and TGF-β act together in a positive feedback loop that increases the severity of the disease (Yamanishi et al., 2002). TGF-β is cleaved and activated by Furin, and autocrine TGF-β binding to its own receptor stimulates transcription of Furin through a SMAD2 and MAPK convergent pathway (Blanchette et al., 1997; 2001). The increased levels of both Furin and activated TGF-β lead to higher amounts of activated ADAMTS-4 (a disintegrin and metalloprotease with thrombospondin motifs-4). This metalloprotease degrades the cartilage protein aggrecan in joints and contributes to rheumatoid arthritis (Yamanishi et al., 2002; Tang, 2001).

Furin is also directly involved in the pathogenesis of different bacterial and viral diseases. For example, Furin on the cell surface can cleave and activate anthrax toxin (Molloy et al., 1992), aerolysin toxin, which causes food-borne illness (Abrami et al., 1998), and clostridium septicum alpha toxin, the causative agent of gas gangrene (Gordon et al., 1997). Furin in endosomal compartments can activate other bacterial toxins, like shiga toxin (ST), shiga-like toxin-1 (ST-1) and Pseudomonas exotoxin A (PEA) (Thomas, 2002). Inhibition of Furin activity using α1-PDX protects cells from the detrimental effects of these bacterial toxins (Jean et al., 1998). Several pathogenic viruses such as avian flu, HIV, measles, RSV, and some Ebola virus strains have envelope glycoproteins that must be cleaved by Furin to generate mature forms and aid

the virus in causing infection (Volchkov et al., 1998; Thomas, 2002; Molloy et al., 1999).

2.1.4 Proteolysis of signaling proteins

Most signaling proteins are known to require proteolytic maturation, many of which are cleaved by Furin. For example, Furin mediates the activation of members of the TGF-β/BMP family of signaling proteins, as both BMP4 and its *Drosophila* counterpart, Decapentaplegic (Dpp), are produced as proproteins and are cleaved multiple times by Furin (Kim et al., 2012; Künnapuu et al., 2009). Similarly, the *Drosophila* BMP5/6/7/8 type ligands Screw (Scw) and Glass bottom boat (Gbb) are also processed at several sites by Furin (Fritsch et al., 2012; Künnapuu et al., 2014). Furin also cleaves β-Nerve growth factor (β-NGF) to alter its activity in developing neurons (Lee et al., 2001b). In Notch/Delta signaling, maturation and membrane localization of Notch, the receptor for Delta, depends on Furin cleavage (van Tetering and Vooijs, 2011). Other signaling proteins that require cleavage include Hh, EGF, FGF, VEGF, Wnt, and peptide hormones such as insulin and Ghrelin (Lee et al., 1994; 2001a; Urban et al., 2001; Tulin and Stathopoulos, 2010; Shimada et al., 2002; Vempati et al., 2014; Zhang et al., 2012; Hook et al., 2008; Duckworth et al., 1979). Although proteolytic cleavage of signaling proteins appears to be a universal phenomenon, the precise role of this cleavage in the signaling process is often unclear.

2.2 Results

2.2.1 Bnl:GFP chimeras with different tag sites show different dispersion patterns

To identify various functional forms of GFP-tagged Bnl proteins, four different Bnl:GFP variants were generated and their signaling activities were examined (Figure 2-1, A-C). The Bnl protein is 770 amino acids long with an N-terminal 31-residue signal peptide and a conserved FGF domain spanning from amino acids 243 to 379 (Figure 2-1, C). Each of the four variants contained a GFP tag at a single internal site: at the 87^{th} (Bnl:GFP_1), 206^{th} (Bnl:GFP_2), 432^{nd} (Bnl:GFP_3), and 701^{st} (Bnl:GFP_4) amino acid residue. Transgenic *Drosophila* lines harboring these constructs were crossed to *bnl-Gal4* flies to drive their expression specifically in Bnl-producing cells and their activity was analyzed in 3^{rd} instar larval wing imaginal discs. In three-dimensional confocal stacks of wing discs, the lower Z sections revealed the Bnl-expressing cells in the wing disc columnar epithelium and the upper Z sections (close to the objective) showed the associated ASP (Figure 2-1, B and D-D').

When the Bnl:GFP variants were expressed under *bnl-Gal4* control, all of the variants were detected in disc Bnl source as bright fluorescent puncta (Figure 2-1, E-H). Overexpression of all four Bnl:GFP variants led to ASP overgrowth (Figure 2-1, E'-H'), which phenocopied Bnl overexpression (Sato and Kornberg, 2002). Thus, all of the Bnl:GFP variants were functional and could signal non-autonomously. Unlike a membrane-tethered CD8:GFP protein, the fluorescent puncta comprised of Bnl:GFP_2, Bnl:GFP_3, and Bnl:GFP_4 were detected in the recipient ASP, suggesting that the signals

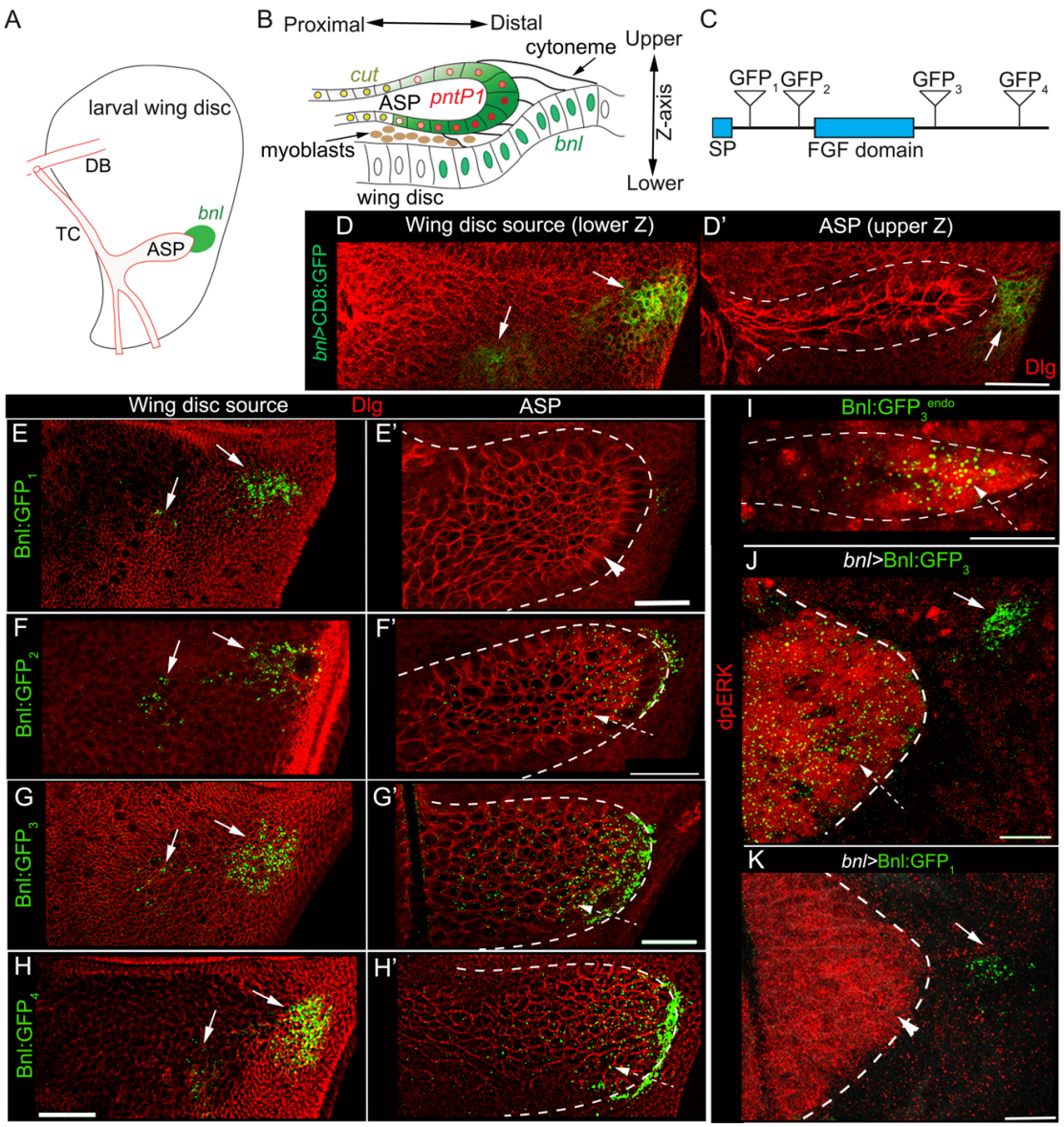

Figure 2-1: Separate GFP fusion sites in Bnl result in different distribution patterns

(A) Drawing depicting the organization of the ASP and *bnl*-expressing wing disc cells from 3rd instar larva; TC, transverse connective; DB, dorsal branch. **(B)** Drawing of a sagittal view showing the tubular ASP epithelium, upper-lower Z-axis, ASP cytonemes that contact the disc *bnl*-source (green nuclei), and the spatial domains of *pntP1* and cut induced by high-to-low Bnl levels (green) (Du et al., 2018a). **(C)** Schematic map of the Bnl protein backbone showing its conserved FGF domain, Signal Peptide (SP), and four different GFP insertion sites. **(D-H')** Representative images of maximum intensity projection of lower (wing disc source) and upper (ASP) Z-sections of 3rd instar larval wing-discs expressing CD8-GFP, Bnl:GFP1, Bnl:GFP2, Bnl:GFP3, or Bnl:GFP4 under *bnl-Gal4* as indicated; red, αDlg staining marking cell outlines. **(I-K)** Representative ASP images showing MAPK signaling (αdpERK, red) zones

when Bnl:GFP$_3^{endo}$ was expressed under native cis-regulatory elements (I), and when *bnl-Gal4* overexpressed Bnl:GFP$_3$ (J) or Bnl:GFP$_1$ (K). **(D-K)** White dashed line, ASP; white arrow, disc *bnl*-source; dashed arrow, Bnl:GFP puncta in the ASP; arrowhead, ASP without Bnl:GFP$_1$ puncta. Scale Bars: 30 µm.

moved from the source to the ASP (Figure 2-1, D-H'). Surprisingly, although Bnl:GFP$_1$ puncta were visible in the source cells and its overexpression induced ASP overgrowth, the fluorescent puncta were absent from the recipient ASP (Figure 2-1, E-E'; Figure 2-2, A-B'). Generally, as shown with an ASP derived from a genome edited *bnl*:*GFP$_3^{endo}$* larva that expressed the Bnl:GFP$_3$ at physiological levels (Du et al., 2018a), only the distal ASP cells with high-to-moderate levels of Bnl induce MAPK signaling (Figure 2-1, I). In contrast, overexpression of Bnl:GFP$_3$ or Bnl:GFP$_1$ in the source activated MAPK signaling in all of the ASP cells (Figure 2-1, J and K). Thus, Bnl:GFP$_1$, like Bnl:GFP$_3$, is an active signal but GFP fluorescence was undetectable in the recipient ASP.

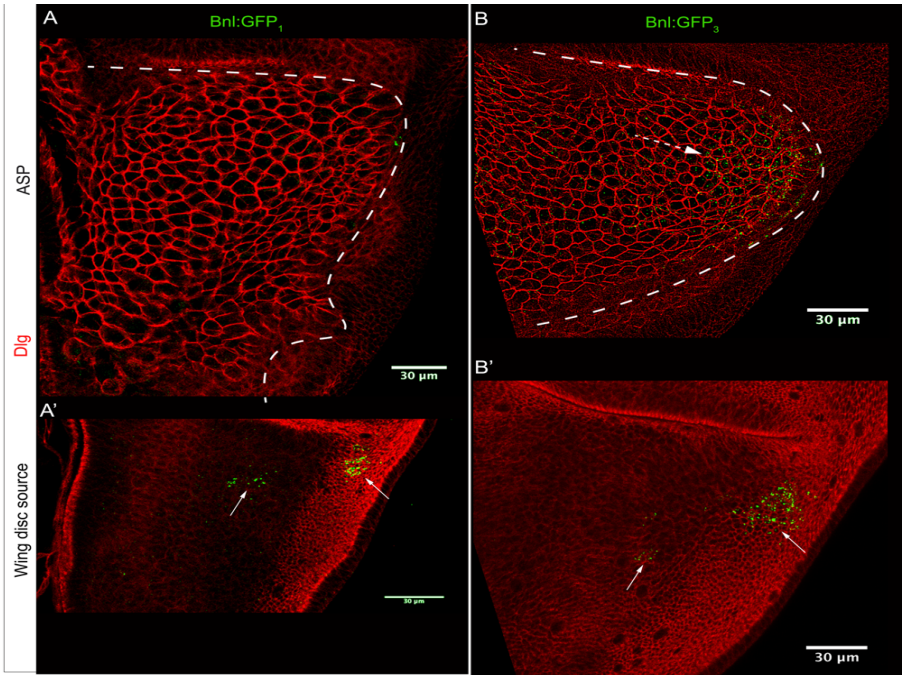

Figure 2-2: Comparison of Bnl:GFP$_1$ and Bnl:GFP$_3$ expression and dispersion

(A-B) Overexpression of both Bnl:GFP_1 (A) and Bnl:GFP_3 (B) under *bnl-Gal4* led to ASP overgrowth, but only Bnl:GFP_3 localized in the ASP (dashed arrow). (**A'-B')** Lower optical sections showing Bnl:GFP_1 (A') and Bnl:GFP_3 (B') expressed in the wing disc source cells (arrows) below the ASP. Cells marked with αDlg (red). Scale bars, 30 μm.

2.2.2 Bnl is cleaved prior to its transport to the recipient ASP

One possibility for Bnl:GFP_1 being functional, yet undetectable in the ASP, could be that the protein was cleaved downstream of tagging site-1 prior to the inter-organ transport of its untagged C-terminal fragment (Figure 2-1, C). To test this possibility, a double-tagged Bnl chimera was generated with HA inserted at site 1 and GFP inserted at site 3 (Figure 2-3, A). Western Blot analyses were performed on total protein lysates of cultured S2 cells that were transfected with either the *bnl:GFP_1*, *bnl:GFP_3*, or *bnl:HA_1GFP_3* constructs. An αGFP antibody recognized a common 150 kDa band, which likely represented the full-length protein (Figure 2-3, B). Although the molecular weight of full length Bnl:GFP was predicted to be ~113 kDa, a larger size could be due to post-translational modifications. Similar observations were reported earlier for the other two *Drosophila* FGFs, Pyramus and Thisbe (Tulin and Stathopoulos, 2010). Bnl:HA_1GFP_3 and Bnl:GFP_3 had similar size profiles, but multiple variant-specific bands were detected for Bnl:GFP_1 and Bnl:GFP_3 (Figure 2-3, B). The detection of unique smaller bands (~37 and 60 kDa) for N-terminally tagged Bnl:GFP_1 and unique larger bands (>100 kDa) for C-terminally tagged Bnl:GFP_3 and Bnl:HA_1GFP_3 was consistent with a cleavage near tagging-site 1. These biochemical analyses suggested a cleavage in the Bnl backbone, but it was difficult to estimate the actual molecular size of the cleaved products. Furthermore, the intracellular and

intercellular fates of the cleaved products cannot be directly visualized in tissues using biochemical assays.

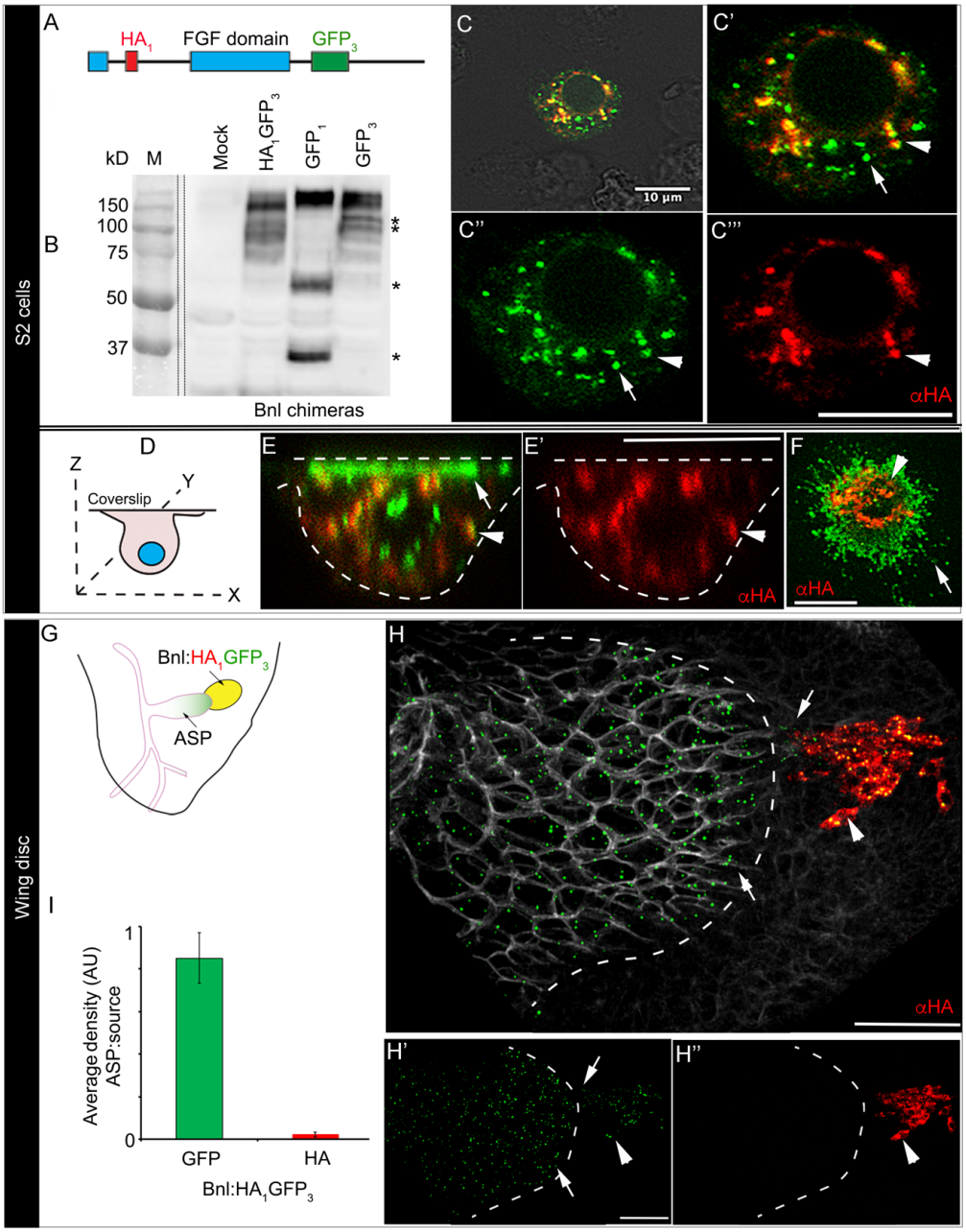

Figure 2-3: Bnl is cleaved in producing cells prior to its transport to the recipient ASP

(A) Schematic map of a dual-tagged Bnl:HA_1GFP_3 construct containing an HA-tag at site 1 and a GFP-tag at site 3. **(B)** An αGFP Western Blot showing differential bands (*) obtained from S2 cell lysates containing Bnl:HA_1GFP_3, Bnl:GFP_1, and Bnl:GFP_3; mock, lysates from untransfected cells. **(C-F)** Representative images of αHA-immunostained (red) S2 cells expressing Bnl:HA_1GFP_3; examples from

adherent cells grown on coverslip (D-F): XZY section (E,E') and XYZ section near coverslip (F); merged bright field and fluorescent (C), merged fluorescent (C',E,F), and split channels shown (C",C"',E'). **(G)** A schematic drawing showing the expected localization pattern of the uncleaved Bnl:HA_1GFP_3 (yellow) and truncated Bnl:GFP derivative (green) in the αHA-stained (red) discs/ASP. **(H-I)** A representative image of an αHA-stained (red) wing disc and ASP (dashed line) when *bnl-Gal4* expressed Bnl:HA_1GFP_3 (*UAS-bnl:HA_1GFP_3*); white, αDlg; split channels (H',H''); a graph (I) comparing the fractions of GFP and HA (αHA) signal in the recipient ASP relative to that of the wing disc source (n=14) under this condition. **(C-H)** arrowhead, uncleaved Bnl:HA_1GFP_3; white arrow, truncated Bnl:GFP_3 derivative of Bnl:HA_1GFP_3. Scale bars: 10 μm; 30 μm (H-H").

Therefore, a fluorescence microscopy-based assay was employed to simultaneously visualize both the HA- and GFP-tagged parts of Bnl in cells. Immunostaining with αHA in S2 cells harboring uncleaved Bnl:HA_1GFP_3 molecules was expected to show both HA_1 and GFP_3 localizing together. On the other hand, a cleavage in the molecules would separate the HA_1 tag from GFP_3. Indeed, in transfected S2 cells, Bnl:HA_1GFP_3 was present in two distinct spatially separated forms (Figure 2-3, C-F). An internal perinuclear zone showed colocalized GFP and HA signal, suggesting that the zone contained uncleaved Bnl. In addition, there were a number of exclusively GFP-positive puncta that localized more towards the periphery of the S2 cells. Cells that were cultured and allowed to adhere to a coverslip contained peripheral lamellipodial and filopodial projections at the adherent surface. These peripheral lamellipodial/filopodial projections contained only a truncated Bnl:GFP portion (Figure 2-3, D-F). Spatial separation of the C-terminal GFP-tagged portion from the rest of the Bnl:HA_1GFP_3 molecule suggested Bnl cleavage.

To further test the peripheral distribution of the truncated C-terminal fragment, two additional constructs were generated: *bnl:HA_1GFP_4* and *bnl:GFP_1HA_4*, where the HA and GFP tags were interchanged between sites 1 and 4. Although the tag positions

were changed in these constructs, irrespective of the tags and tagging sites the cleaved N and C terminal Bnl fragments showed consistent subcellular localization patterns (Figure 2-4, A and B). These results showed that Bnl is cleaved and a truncated C-terminal portion is trafficked toward the cell periphery, probably for release. To test inter-organ dispersion of cleaved/uncleaved forms of Bnl, transgenic *Drosophila* lines harboring the *bnl:HA$_1$GFP$_3$* construct were generated. When *bnl-Gal4* overexpressed Bnl:HA$_1$GFP$_3$ in the wing disc source, the N-terminal HA-tagged portion of Bnl remained in the signal producing cells and a truncated GFP-tagged C-terminal portion of Bnl (Bnl:GFP$_3$) localized only in the recipient ASP cells (Figure 2-3, G-I). These results strongly suggested that Bnl is cleaved in the source and only a truncated Bnl derivative is received by the ASP.

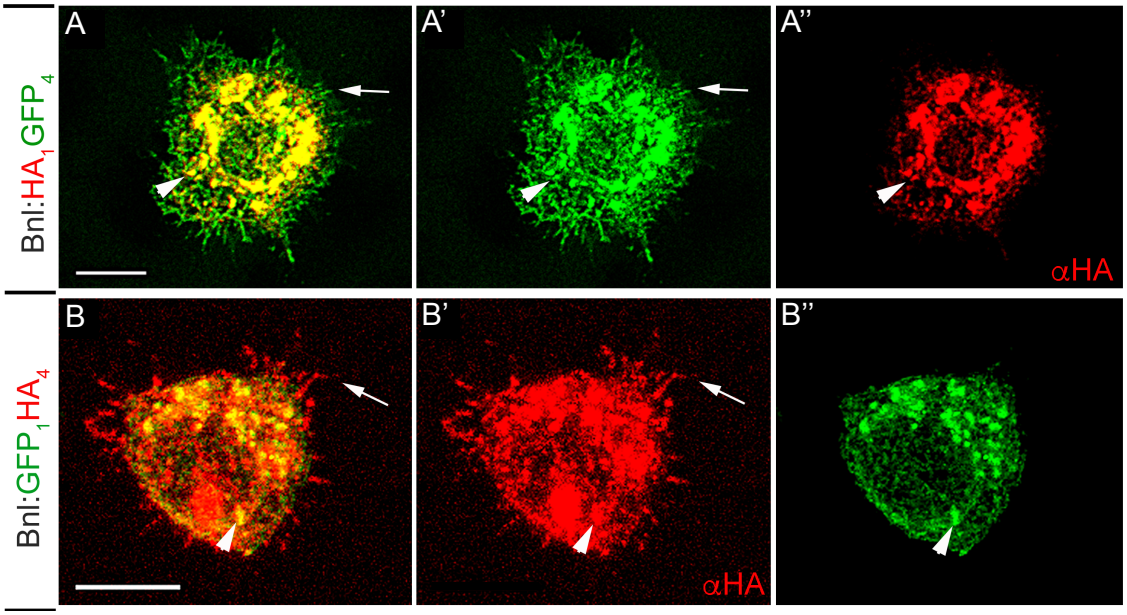

Figure 2-4: Switching tags between sites 1 and 4 does not alter cleavage

(A-B") αHA immunostained S2 cells cotransfected with *act-Gal4* and either *UAS-bnl:HA$_1$GFP$_4$* (A-A") or *UAS-bnl:GFP$_1$HA$_4$* (B-B"); arrow, truncated C-terminal tagged part of Bnl; arrowhead, uncleaved Bnl; A',B', channel of tag at site 4 for A and B, respectively; A'',B'', channel of tag at site 1 for A and B, respectively. Scale Bars: 10 μm.

2.2.3 Bnl is cleaved at a single endoproteolytic site in the Golgi network

Evolutionarily conserved serine proteases, namely the pro-protein convertases (PCs) that include Furins, cleave many growth factors and hormones that are synthesized in the form of pro-ligands (Thomas, 2002). With an artificial neural networks-based *in silico* PC site (PCS) prediction tool (Duckert et al., 2004), three putative PC sites (PCS1-3) were identified in the Bnl backbone. Among them, PCS1 was Furin-specific with a core R–X–[R/K]–R domain (Figure 2-5, A-A'). Coincidentally, the four selected tagging sites in the Bnl backbone were perfectly structured for testing the putative cleavage sites (Figure 2-5, A). To test for cleavage at PCS3 (Figure 2-5, A), a chimeric Bnl:GFP_3HA_4 construct was generated where the GFP and HA tags were inserted at sites 3 and 4, respectively. Immunostaining with an αHA antibody on S2 cells transfected with *bnl:GFP_3HA_4* showed colocalization of GFP_3 and HA_4 (Figure 2-5, B). Based on this cell biological assay, PCS3 is an unlikely cleavage site. However, the possibility of potential PCS3 cleaved products remaining closely associated during their intracellular trafficking was not investigated. In contrast, a cleavage at either PCS1 or PCS2 could explain the observed differential distribution of the N and C portions of Bnl:HA_1GFP_3 (Figure 2-3, C-H).

To test PCS1 and PCS2, their Arginine (R) residues were replaced with Glycine (G) to generate *bnl:HA_1GFP_3-M1* (henceforth referred as M1), a construct with mutations in PCS1 ($(R/G)_{161}TE(R/G)_{164}$^SI$(R/G)_{166}$), and *bnl:HA_1GFP_3-M2* (henceforth referred as M2) with mutations in PCS2 $(R/G)_{233}NE(R/G)_{236}$^) (Figure 2-5, A). R to G substitutions in PC sites were shown to successfully block PC

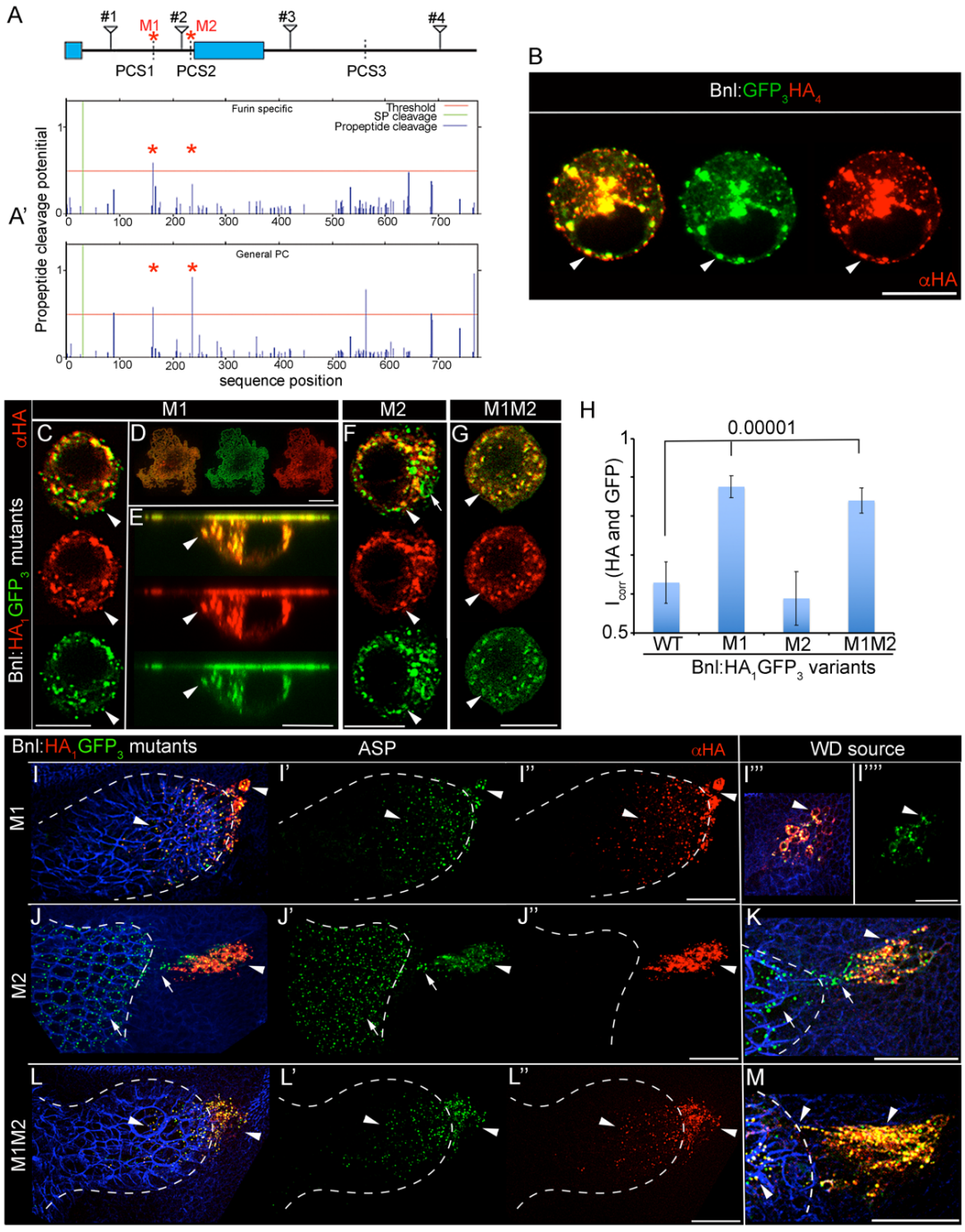

Figure 2-5: Bnl is cleaved at a single endoproteolytic site

(A) Location of putative PCS1-3 in the Bnl backbone; #1-4: GFP insertion sites; *, point mutations generated at PCS1 (M1) and PCS2 (M2). (A') In-silico predictions of PC sites; upper panel, Furin-specific; lower panel, for General PC; green line, SP cleavage site; red line, a set threshold above which the sequence is predicted to be a PCS. **(B-G)** Examples of αHA immunostained (red) S2 cells expressing Bnl:GFP_3HA_4 (B) and Bnl:HA_1GFP_3 mutants as indicated (C-G); XYZ section near coverslip (D) and

XZY section (E) of M1-expressing adherent cells. **(H)** Graphs comparing colocalization index (I_{corr}) of the HA- and GFP- tagged parts of Bnl:HA_1GFP_3 (WT), M1, M2, and M1M2 in αHA-stained (red) S2 cells; n=15 (WT), 13 (M1), 9 (M2 and M1M2); p values: ANOVA followed by Tukey HSD. **(B-H)** S2 cells cotransfected with *act-Gal4* and *UAS-X, X*= constructs as indicated. **(I-M)** Maximum intensity projections of the wing-disc source (I"'-I"",K,M) expressing Bnl:HA_1GFP_3 mutants as indicated (*bnl-Gal4* x *UAS-X*, *X*= M1, M2, or M1M2) and the recipient ASPs (I-I",J-J",L-L"); blue, αDlg; white dashed line, ASP. **(B-M)** arrow, truncated Bnl:GFP_3 derivative; arrowhead, uncleaved Bnl:HA_1GFP_3. Scale bars: 10 μm (B-G); 30 μm (I-M).

cleavage (Künnapuu et al., 2009). In transfected S2 cells, PCS1 mutation rendered the M1molecules uncleavable, as HA and GFP colocalized together in the intracellular compartments (Figure 2-5, C-E). However, M2 molecules were cleaved like wild type proteins (Figure 2-5, F). To compare the cleavage efficiency among the Bnl mutants, the fraction (index of correlation, I_{corr}) of colocalized pixels of HA and GFP channels was measured from 3D images (Jaskolski et al., 2005). The average I_{corr} value was significantly higher for M1 and M1M2 than either the control Bnl:HA_1GFP_3 or M2 cells, suggesting that the PCS1 mutation inhibited cleavage (Figure 2-5, H). Transgenic flies harboring the M1, M2, or M1M2 constructs were also generated and their distribution in the wing disc and ASP was analyzed. When the M1 and M1M2 mutants were expressed in the wing disc source, the recipient ASPs received co-localized HA-GFP puncta comprised of the uncleaved full-length Bnl molecules (Figure 2-5, I-I"'' and L-M). In contrast, only the GFP-tagged C-terminal part of M2 was distributed within the ASP (Figure 2-5, J-K). Collectively, these results suggest that Bnl:HA_1GFP_3 molecules are cleaved at PCS1 prior to their delivery from the disc source to the ASP.

Bnl cleavage could be intracellular or, alternatively, could occur on the surface of the source cell plasma membrane where the signal is delivered to the recipient ASP cytonemes (Figure 2-1, B). To test this possibility, a detergent-free αGFP-based

immunostaining protocol (henceforth referred to as αGFP^{ex}) was employed, which was previously used to detect surface-exposed Bnl:GFP (Du et al., 2018a). The αGFP^{ex} assay detected only Bnl:GFP$_3$ on the expressing source cell surface, but not Bnl:GFP$_1$, indicating that the cleaved Bnl prodomain never reached the cell surface (Figure 2-6, A and B). Thus, Bnl cleavage occurs within the source cells and only the truncated C-terminal Bnl portion is displayed on the basal surface of the source cells. To determine the subcellular location of Bnl cleavage, standard immunostaining with αGM130 antibody, a cis-Golgi probe, was performed on discs expressing Bnl:GFP$_1$, Bnl:HA$_1$GFP$_3$, or Bnl:HA$_1$GFP$_3$–M1. In the wing disc source, 100% of either Bnl:GFP$_1$ or uncleaved Bnl:HA$_1$GFP$_3$ puncta were localized in the GM130-marked cis-Golgi (Figure 2-6, C-D'). In contrast, the truncated Bnl:GFP$_3$ derivative (GFP-only puncta) localized in many small uncharacterized intracellular vesicles, some of which were enriched with Syntaxin16, a target-SNAP receptor for intra/trans-Golgi sorting (Charng et al., 2014) (Figure 2-6, D-D' and F-F'). On the other hand, uncleaved M1 puncta were seen in all of the vesicular compartments, indicating their routing through the secretory pathway (Figure 2-6, E-E' and G-G'). Similar intracellular distribution profiles of the cleaved and uncleaved portions of Bnl were observed in cultured S2 cells (Figure 2-6, H-J'). Since the cleaved N-terminal Bnl prodomain did not make it past the Golgi, these results collectively showed that Bnl is cleaved during its trafficking through the Golgi network.

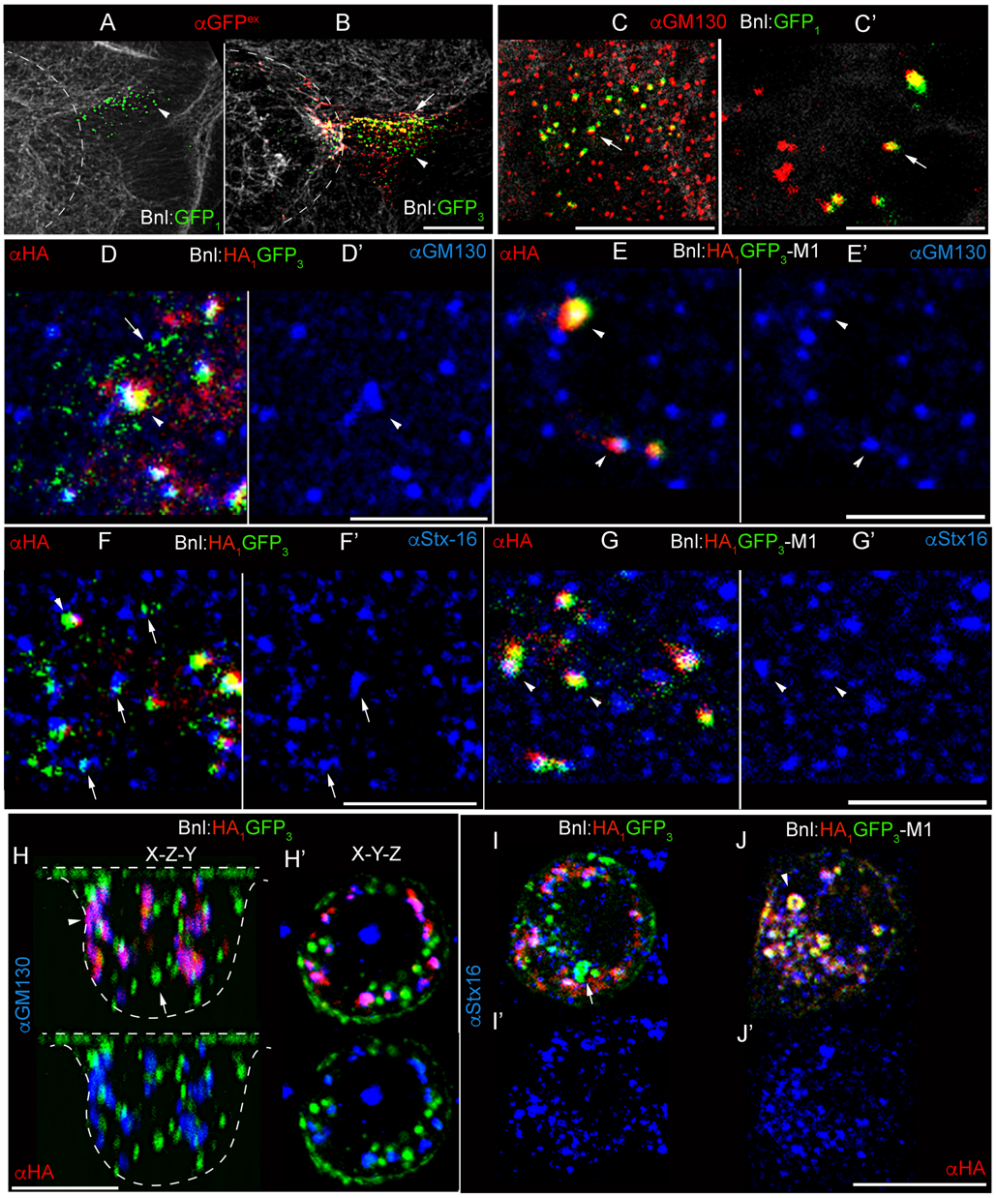

Figure 2-6: Bnl is cleaved in the Golgi network of Bnl-producing cells

(A-B) Projection images of lower Z-stacks of the disc *bnl* source showing detergent-free αGFP immunostaining (αGFP^{ex}; red) when *bnl-Gal4* expressed Bnl:GFP$_1$ (A) and Bnl:GFP$_3$ (B); white, phalloidin:Alexa-647 to mark actin-rich cell outlines; arrowhead, intracellular molecules (only green); arrow, surface-localized molecules (green+red); dashed line, ASP in the upper Z-stacks (not shown). **(C-C')** αGM130-stained (red) optical sections of wing disc *bnl*-source expressing Bnl:GFP$_1$. **(D-J')** Single optical sections of αHA-immunostained (red) disc *bnl*-source (D-G') and S2 cells (H-J') expressing either Bnl:HA$_1$GFP$_3$ or M1 and marked with α-Stx-16 or αGM130 (blue) as indicated; arrow, truncated Bnl:GFP$_3$ derivative; arrowhead, uncleaved Bnl:HA$_1$GFP$_3$ or M1 mutant; merged (D-J) and split blue channels (D'-J') shown. Scale Bars: 20 μm (A-C); 5 μm (C'-G'); 10 μm (H-J').

2.2.4 Bnl is cleaved by Furin1 in the wing disc *bnl* source

Intracellular Bnl cleavage at PCS1, which is Furin-specific, indicated that Bnl is likely cleaved by a Furin. To identify the specific protease, *RNAi*-mediated knockdown was performed on two *Drosophila furin* genes, *Dfurin1* (*fur1*) and *Dfurin2* (*fur2*) in cell culture. The role of *amontillado* (amon), a mammalian PC2 ortholog, was not investigated since it is expressed only in neurons and neuroendocrine cells (Künnapuu et al., 2009; Roebroek et al., 1992; 1993). In S2 cells, RNAi treatment of either *fur1*, *fur2*, or both significantly reduced Bnl:HA_1GFP_3 cleavage in comparison to a non-specific control RNAi (Figure 2-7, A-E). Thus, Bnl cleavage is Fur1 and Fur2-dependent in cell culture.

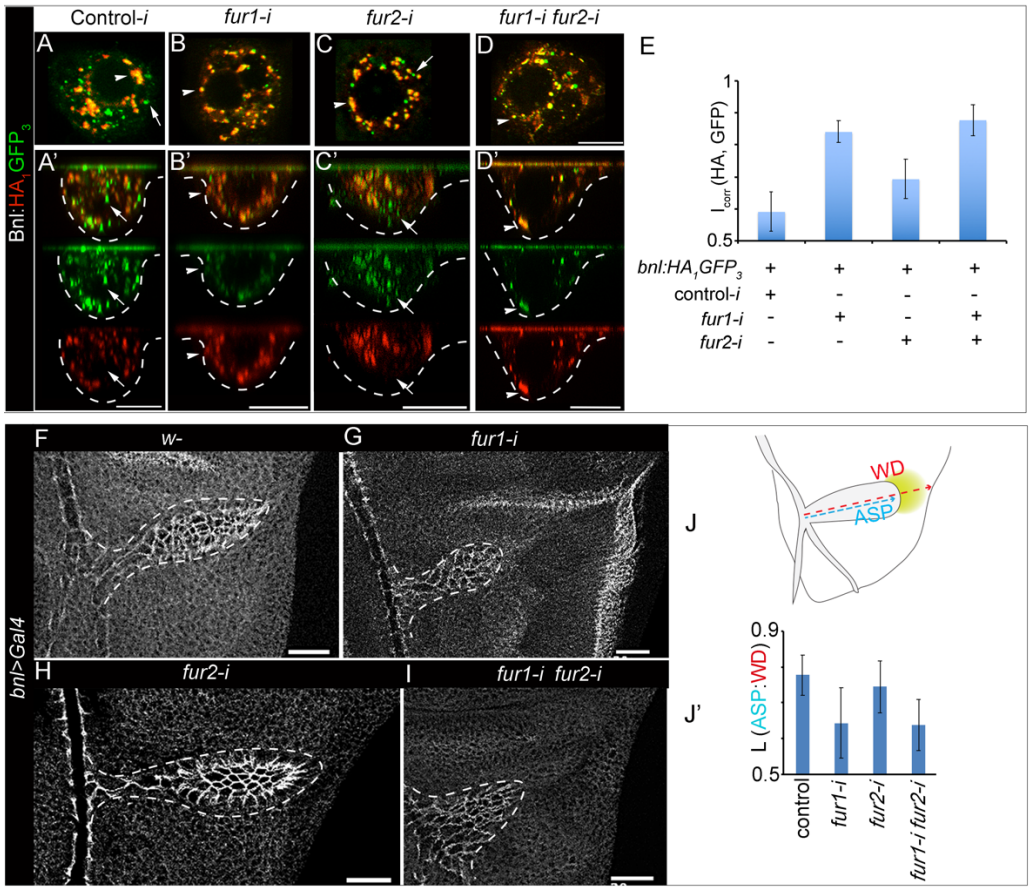

Figure 2-7: Knockdown of *furin* expression affects Bnl cleavage

(A-D') Images of αHA-immunostained (red) S2 cells co-transfected with *act-Gal4*, *UAS-bnl:HA$_1$GFP$_3$*, and the synthesized *RNAi* as indicated; control-*i*, non-specific dsRNA; XYZ (A-D) and XZY (A'-D') views; arrow, truncated Bnl:GFP$_3$ derivative; arrowhead, uncleaved Bnl:HA$_1$GFP$_3$. **(E)** Graph comparing Bnl:HA$_1$GFP$_3$ cleavage under various *furin* knockdown conditions in S2 cells; I_{corr}: index of HA and GFP colocalization, with lower values indicating cleavage and color separation; n=13 (control), 11 (*fur1i*), 12 (*fur2i*), 14 (*fur1-i fur2-i*); p-values (ANOVA followed by Tukey HSD): *fur1-i* vs *fur1-i fur2-i*, p=0.347, all other groups, p<0.001. **(F-I)** αDlg-immunostained (white) wing disc and ASP (white dashed line) from larvae where *bnl-Gal4* expressed *furin RNAi* as indicated; control, *bnl-Gal4* x *w*$^-$. **(J and J')** Drawing depicting the scheme (J) of allometric measurement of ASP length (L) relative to the corresponding wing disc (WD); graph (J') comparing the length (L) ratio of ASP to wing-disc (WD) under conditions indicated; n=48 (control), 95 (*fur1-i*), 86 (*fur2-i*), 102 (*fur1-i,fur2-i*); p-values (ANOVA followed by Tukey HSD): all groups vs *fur1-i*, p<0.001, all groups vs *fur1-i fur2-i*, p<0.001. Scale Bars, 30 μm; 10 μm (A-D).

However, *in vivo*, only *fur1* knockdown in the wing disc *bnl* source resulted in stunted ASP development, which phenocopied a *bnl* knockdown condition (Figure 2-7, F-I and Figure 2-8, A-D). Measurement of the allometric ratio of the recipient ASP length along its major Distal-Proximal (D-P) axis to the width of the wing disc confirmed that the growth abnormality was ASP-specific and was not due to a systemic developmental delay (Figure 2-7, J and J'). Lack of *a fur2* knockdown phenotype in the ASP is likely due to the absence of *fur2* expression in the *bnl* source, as expression analyses of *fur1* and *fur2* showed only *fur1* expression in the *bnl* source (Figure 2-8, E-K). Thus, although both Fur1 and Fur2 could cleave Bnl in S2 cells, their substrate-specificity might depend on their tissue-specific expression.

The RNAi analyses provided correlative evidence of Furin's role in Bnl cleavage. For direct evidence, larval wing discs expressing Bnl:HA$_1$GFP$_3$ in the *bnl* source were *ex vivo* cultured either in the presence or absence of Furin inhibitors. In spite of prolonged (up to 16 h) *ex vivo* culture conditions, Bnl:HA$_1$GFP$_3$ was cleaved in the absence of inhibitors and the truncated Bnl:GFP$_3$ moved to the growing ASPs

(Figure 2-9, A-C"). In the presence of inhibitors (Figure 2-9, D-F'), Bnl cleavage in the disc source was blocked and the amount of uncleaved puncta received by the ASP gradually increased with longer incubation times (Figure 2-9, G). The time-dependent inhibition of Bnl cleavage by Furin inhibitors confirmed Furin-dependent Bnl cleavage.

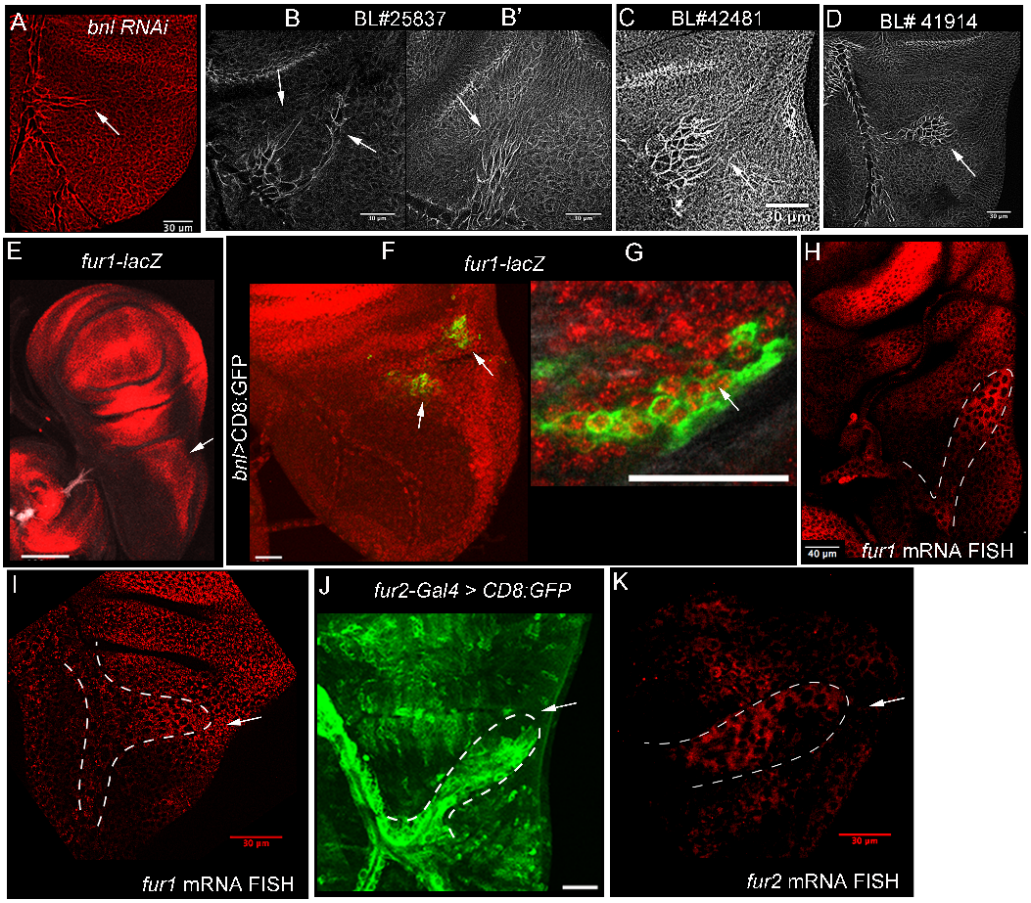

Figure 2-8: Furin-dependent Bnl cleavage

(A) An example of stunted ASP growth (arrow) due to the expression of *bnl RNAi* under *bnl-Gal4.* **(B-D)** Examples of stunted ASPs (arrow) generated by three separate *fur1 RNAi* lines (BL# 25837, 42481, 41914) expressed under *bnl-Gal4.* **(A-D)** αDlg immunostaining marked ASP and disc cell outlines: red for A, white for B-D. (**E)** Expression of *fur1-LacZ* in the α-βGal immunostained (red) wing disc source (arrow). **(F-G)** Zoomed-in images of an α-βGal immunostained (red) wing disc expressing both *fur1-LacZ* and *bnl-Gal4*-driven CD8-GFP (green, arrow) (F,G); arrow, Bnl expression domain. **(H-I)** Fluorescent *in-situ* hybridization (red) of *fur1* mRNA in the wing disc source (arrow) and ASP (white dashed line). **(J)** *fur2-Gal4*-driven CD8-GFP. **(K)** Fluorescent in situ hybridization of *fur2* mRNA (N, red); arrow, Bnl source cells, white dashed line, ASP. Scale Bars: 30 μm; 40 μm (H); 100 μm (E).

Importantly, these results, together with the M1 mutant analyses, showed that when Bnl cleavage is blocked the uncleaved signals can still move from the disc to the ASP. These results indicated that cleavage might not be essential for molecular activation of the Bnl protein and led us to examine the physiological roles of Bnl cleavage.

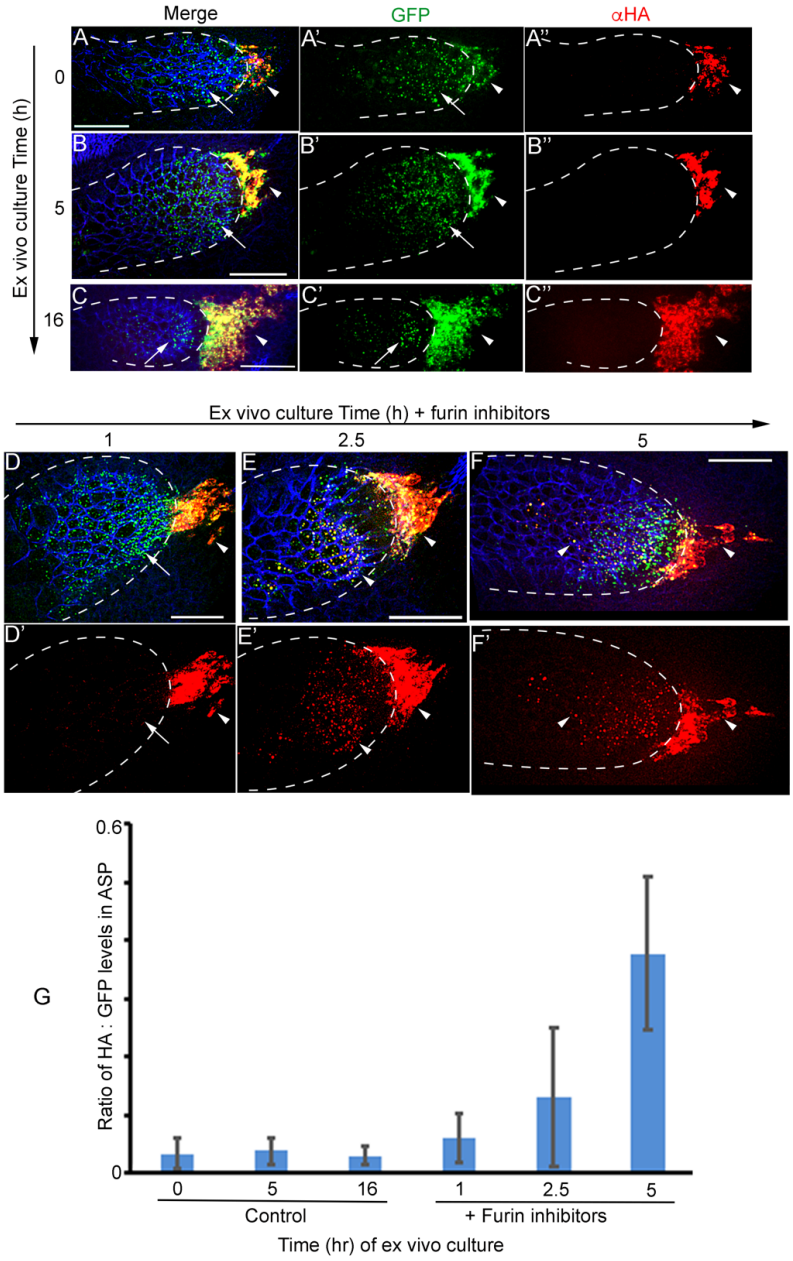

Figure 2-9: Furin-dependent Bnl cleavage in the wing disc

(A-F') αHA-stained (red) wing discs that expressed Bnl:HA_1GFP_3 under *bnl-Gal4* were *ex vivo*-cultured for 0 (pre-treat) -16h in the absence and 1-5h in the presence of Furin inhibitors as indicated; arrow, truncated Bnl:GFP_3 derivative; arrowhead, uncleaved Bnl:HA_1GFP_3; blue, phalloiden-Alexa-647 marking cell outlines; merged (A-D) and either split green, red (A'-C") or only red (D'-F') channels were shown. **(G)** Graphs comparing average levels of colocalized HA and GFP in the ASP grown in presence and absence of Furin inhibitors; samples were harvested at different time points from the continuous culture; n=11 (0h), 11 (1h), 10 (2.5h), 9 (5h control), 12 (5h test), 5 (16h); p-values (ANOVA followed by Tukey HSD): p=0.0001 for 5h vs either 0h, 1h, or 2.5h. Scale Bars, 30 μm.

2.2.5 Uncleaved Bnl can signal and is dispersed by cytonemes, but only within a narrow range.

To examine M1 distribution and activity at its physiological levels of expression, a previously reported *bnl:GFP_3^{endo}* allele was modified into *bnl:$HA_1GFP_3^{endo}$* (henceforth referred as *wt^{endo}*) and corresponding *bnl:HA_1GFP_3-$M1^{endo}$* mutant alleles (henceforth referred as *$m1^{endo}$*) by employing genome-editing (see Chapter 5, section 5.3; Figure 2-10, A). Consistent with earlier observations for *bnl:GFP_3^{endo}* (Du et al., 2018a), *wt^{endo}* flies were homozygous viable and had normal tissue morphology. Although *bnl* is an essential gene, *$m1^{endo}$* mutant flies were homozygous viable, indicating that the PCS1 mutation was non-lethal. As expected, the endogenous Bnl:$HA_1GFP_3^{endo}$ (WT^{endo}) molecules were cleaved and ASPs received only the truncated Bnl:GFP_3 portion (henceforth referred as t-WT^{endo}; Figure 2-10, B and Figure 2-11, A). The *$m1^{endo}$* ASPs received uncleaved Bnl:HA_1GFP_3-$M1^{endo}$ (henceforth referred as $M1^{endo}$) puncta containing both HA and GFP (Figure 2-10, C and Figure 2-11, B). Furthermore, *ex vivo* cultured *wt^{endo}* wing discs grown in the presence of Furin inhibitors had uncleaved Bnl:$HA_1GFP_3^{endo}$ puncta in the ASP (Figure 2-10, D and E). Thus, in the absence of cleavage, uncleaved Bnl could move to the ASP and sustain tracheal growth.

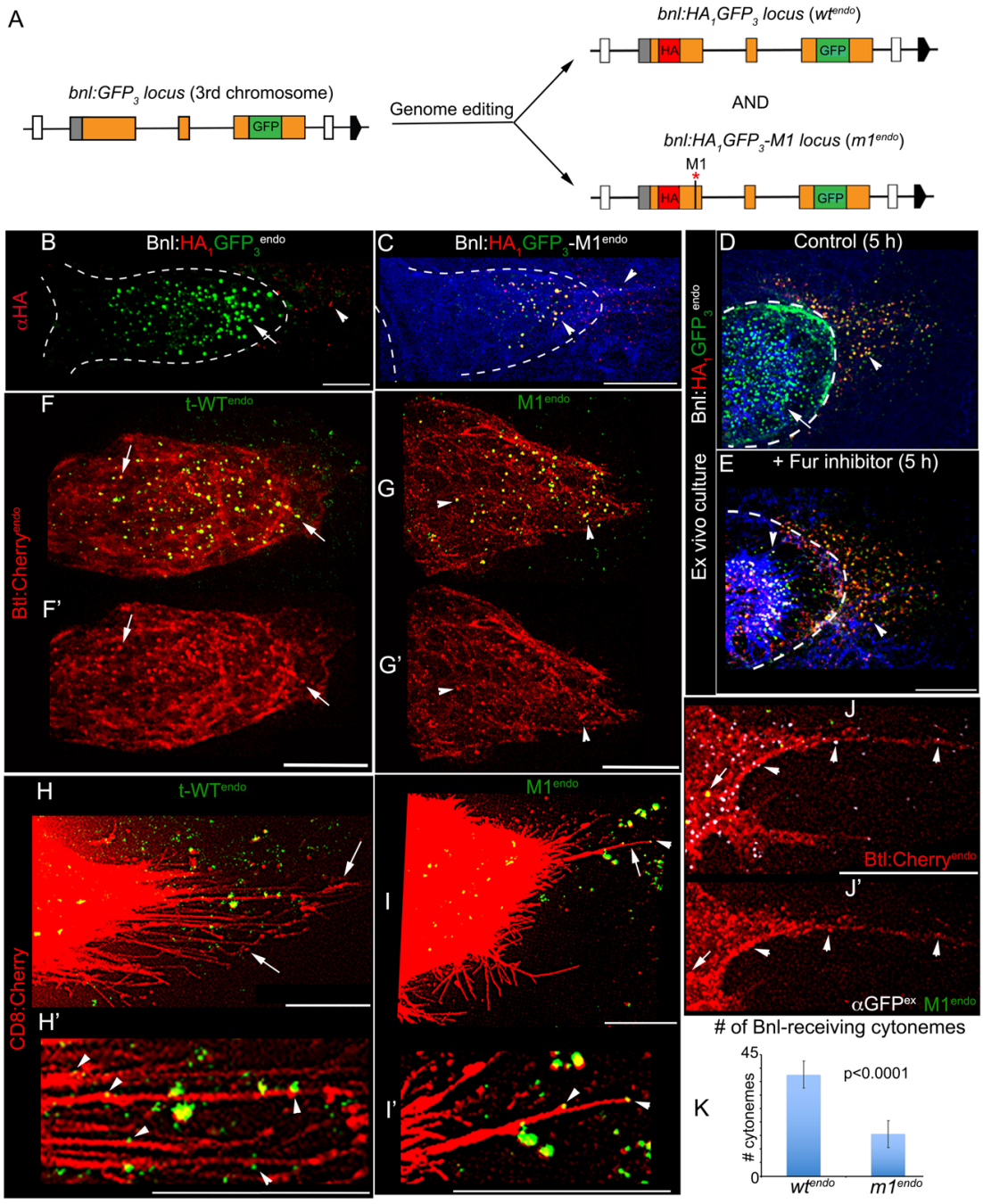

Figure 2-10: Comparison of activities of endogenously expressed cleaved and uncleaved Bnl

(A) Schematic map of the genomic *bnl:gfp*^{endo} locus and the products of its subsequent CRISPR/Cas9-based editing; orange box, coding exon; grey box, non-coding exon; line, introns; red star, M1 mutation. **(B-C)** Representative images of αHA-stained (red) ASP and wing disc from homozygous *wt*^{endo} (n=85) and *m1*^{endo} (n=79) larvae. **(D-E)** Representative images of αHA-immunostained (red) ASP and wing disc from *wt*^{endo} larvae after five hours (h) of *ex-vivo* culture in the absence (control; n=18) and presence

(n=29) of Furin inhibitors. **(B-E)** white dashed line, ASP; blue, phalloidin-Alexa-647; arrow, t-WT^{endo}; arrowhead, uncleaved WT^{endo} or M1^{endo}. **(F-G')** Receptor-colocalized t-WT^{endo} and M1^{endo} puncta (arrow) in trans-heterozygous *btl:Cherry^{endo}/ wt^{endo}* (F,F') and *btl:Cherry^{endo}/ m1^{endo}* (G,G') ASP; split red channels (F',G'). **(H-I')** Live images of CD8:Cherry-marked ASPs showing the long (>15 μm) oriented ASP cytonemes (arrows) containing t-WT^{endo} (H,H') and M1^{endo} (I,I') puncta (arrowheads). **(J and J')** Surface αGFP^{ex} immunostaining (white) detecting M1^{endo} on the ASP cytoneme surfaces of *btl:cherry^{endo}/m1^{endo}* larvae; arrow and arrowhead, receptor-colocalized intracellular (bright green) and surface M1^{endo}, respectively. **(K)** Graph comparing the number of cytonemes (>15 μm long) counted from a 60 μm perimeter centering the ASP tip (Materials and methods) in *wt^{endo}* (n=28) and *m1^{endo}* (n=38). Scale Bars: 20 μm; 10 μm (H-I').

When either *wt^{endo}* or *m1^{endo}* were genetically combined with a *btl:cherry^{endo}* allele, which expressed endo-tagged Btl:Cherry (Du et al., 2018a), both t-WT^{endo} and M1^{endo} puncta colocalized with the receptors in the ASPs (Figure 2-10, F-G'). As reported earlier (Du et al., 2018a), the distal ASP tip, which is closest to the disc *bnl* source, had a high concentration of the receptor-colocalized t-WT^{endo} or M1^{endo} puncta. With increasing distance from the source their concentration gradually decreased. Bnl is known to be transported by cytonemes to form a receptor-associated gradient (Du et al., 2018a). To examine cytoneme-mediated transport, CD8:Cherry-marked ASPs were live-imaged in homozygous *wt^{endo}* or *m1^{endo}* larvae (>30 discs/genotype). In both conditions, ASPs extended long (>15 μm) polarized cytonemes toward the source cells and received GFP-tagged fluorescent puncta comprised of either t-WT^{endo} or M1^{endo} (Figure 2-10, H-I' and Figure 2-11, C-D). Surface αGFP^{ex} immunostaining showed that both M1^{endo} and t-WT^{endo} colocalized with Btl:Cherry^{endo} on the recipient cytoneme surfaces prior to their endocytosis (Figure 2-10, J-J' and Figure 2-11, E-F'). Therefore, the pattern of tissue-specific dispersion of M1^{endo} was comparable to that of t-WT^{endo}.

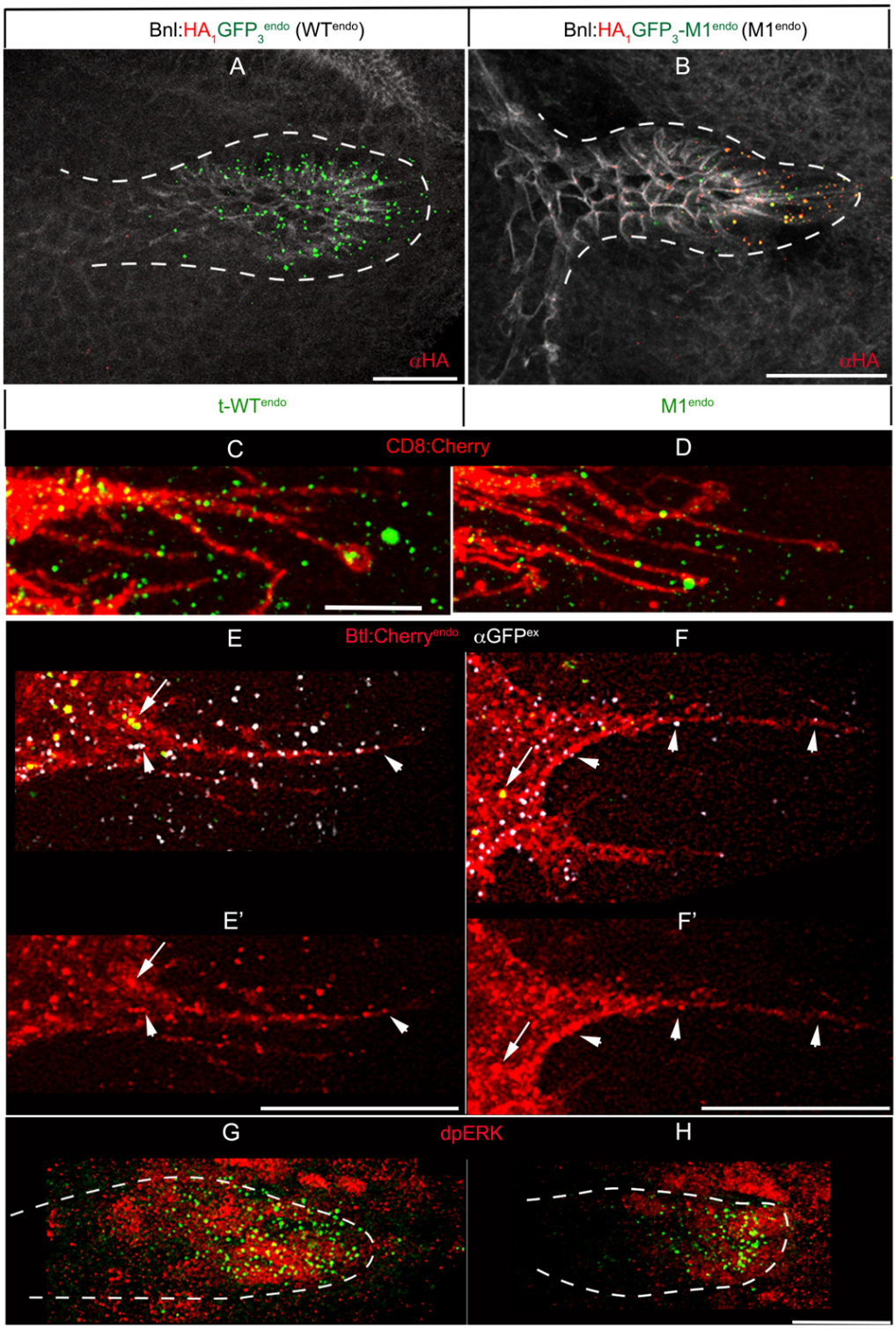

Figure 2-11: Localization and signaling of WT^{endo} and $M1^{endo}$ in the ASP

(A-B) Examples of αHA immunostained (red) ASPs (white dashed outline) and wing discs from homozygous wt^{endo} (A) and $m1^{endo}$ (B) larvae. **(C-D)** High-gain Airyscan (Zeiss LSM 800, 60X) images

of fixed CD8:Cherry-marked ASP cytonemes that localized either t-WT^{endo} (C) or M1^{endo} (D). **(E-F')** Detergent-free αGFP surface staining (white) of t-WT^{endo} and M1^{endo} on ASP cytonemes from *btl:cherry^{endo}/wt^{endo}* (E) and *btl:cherry^{endo}/m1^{endo}* (F) larvae; arrowhead, receptor-colocalized t-WT^{endo} or M1^{endo} on the cell and ASP surface; arrow, receptor-colocalized intracellular (bright green) t-WT^{endo} or M1^{endo} in the ASP; merged (E,F) and red channels (E',F') were shown. **(G-H)** ASPs from homozygous *wt^{endo}* (G) and *m1^{endo}* (H) larvae showing correlation of zones of MAPK signaling (αdpERK, red) with t-WT^{endo} and M1^{endo} uptake (green puncta). Scale Bars: 5 μm (C,D); 20 μm (A,B), 30 μm (G,H).

However, a thorough scrutiny revealed that the *m1^{endo}* allele produced hypermorphic phenotypes due to a reduced signaling range. The distal tip area of *m1^{endo}* ASPs had significantly fewer long (>15 μm) signal-receiving cytonemes than the *wt^{endo}* ASPs (Figure 2-10, K). All of the cells (~6-7 cells in Z-projected images) within a 60 μm periphery surrounding the tip of *wt^{endo}* ASPs extended long signaling cytonemes. In contrast, only 1-2 distal tip cells in the comparable region of the *m1^{endo}* ASPs extended M1^{endo}-receiving cytonemes. A restricted zone of M1^{endo}-receiving cytonemes is reflected in the narrow gradient range and attenuated *m1^{endo}* ASP growth (Figure 2-12, A-E). While t-WT^{endo} formed a long-range gradient along the ~10-12 cells-long ASP D-P axis, M1^{endo} formed a narrow, steeper gradient along the ~5-6 cells-long D-P axis (Figure 2-12, D and E). Accordingly, the *m1^{endo}* ASPs had a reduced zone of nuclear dpERK in comparison to the *wt^{endo}* ASPs. Thus, M1^{endo} had a narrow distribution and signaling range compared to t-WT^{endo} (Figure 2-11, G-H and Figure 2-12, G-I). Nevertheless, normalization of either the signal concentration or the signaling zone with recipient ASP length showed comparable scaling of the t-WT^{endo} and M1^{endo} gradients and signaling zones in relation to the recipient ASP size (Figure 2-12, F and I). Previous work suggested that the Bnl gradient adopts recipient ASP-specific shapes due to two counteracting Bnl signaling feedbacks on cytonemes (Du et al., 2018a).

Thus, scaling of the M1^{endo} gradient to the recipient-specific shape indicated normal M1^{endo} signaling, but within a limited range.

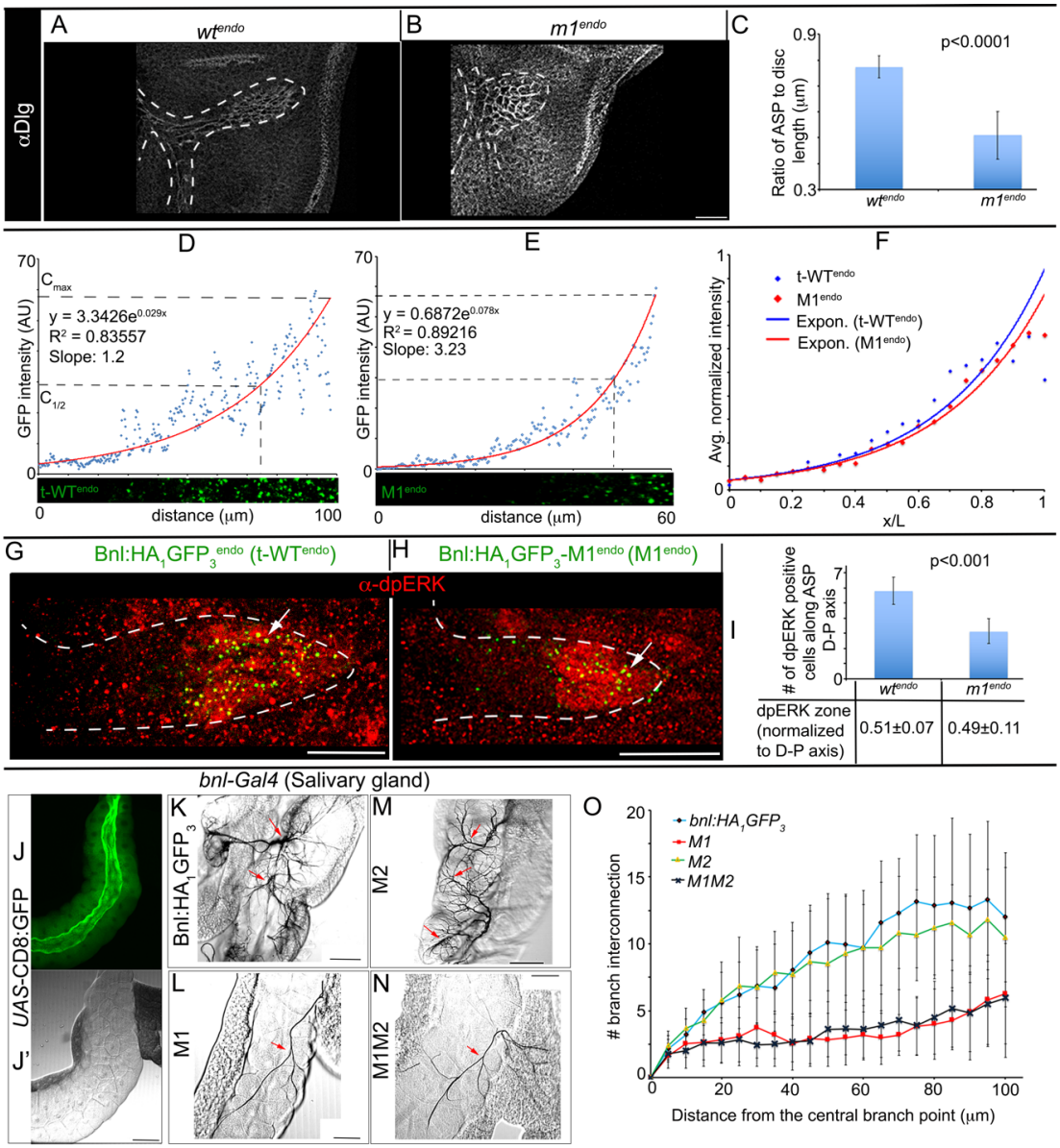

Figure 2-12: Bnl cleavage determines the range of gradient distribution and signaling

(A-C) Images of αDlg immunostained (white) ASPs (white outline) and wing discs from homozygous *wt^{endo}* (n=52) and *m1^{endo}* (n=64) larvae (A,B); a graphical comparison (C) of their ASP length relative to the wing disc size. **(D-E)** Average intensity profiles of t-WT^{endo} (D, n=3) and M1^{endo} (E, n=5) along the ASP D-P axis; lower panels, examples of signal distribution along the ASP D-P axis; red line, exponential fit trend line; C_{max}, maximum average intensity; $C_{1/2}$, ½ C_{max}; slope for the trend line between C_{max} and $C_{1/2}$. **(F)** Average intensity profiles of t-WT^{endo} (n=9) and M1^{endo} (n=12) normalized with

recipient ASP length (D-P axes) (Materials and methods). **(G-I)** Images of αdpERK-stained (red) ASPs from homozygous wt^{endo} (n=16) and $m1^{endo}$ (n=20) larvae (G,H) and graphical comparison (I) of their nuclear dpERK positive zones along the D-P axes; lower chart: average ratio (± standard deviation) of number of dpERK positive cells along the D-P axis to the total number of cells in the D-P axis. **(J-N)** Larval salivary glands expressing CD8:GFP, Bnl:HA_1GFP_3 (18), M1 (11), M2 (20), and M1M2 (18) under *bnl-Gal4* as indicated; red arrow, central branch point. **(O)** A quantitative assessment of the frequency of terminal branching on salivary gland determined by Sholl analysis under the conditions indicated. Scale Bars: 30 μm; 100 μm (J-N).

Ectopic Bnl expression in the salivary gland, a non-tracheated organ that does not normally express *bnl* (Jarecki et al., 1999), consistently showed a limited spatial distribution of M1 signaling. Since Bnl expression is known to induce tracheal invasion toward source cells, active Bnl expression in the salivary gland was expected to induce easily scorable tracheal invasion. Non-specific expression of *bnl-Gal4* (Du et al., 2017) in the salivary gland was used to express the Bnl mutants. Except for a CD8:GFP control, equivalent levels of expression of Bnl:HA_1GFP_3 (WT), M1, M2, or M1M2 all induced tracheal invasion into the salivary gland, confirming their non-autonomous signaling (Figure 2-12, J-N). Thus, M1 is an active signal. However, the salivary glands expressing WT and M2 had a significantly higher number of terminal branches ramifying throughout the gland surface. In contrast, glands expressing M1 or M1M2 showed poor terminal branching frequencies and surface coverage (Figure 2-12, K-O). Thus, M1 induced a spatially restricted response on the source cell surface. Since Bnl distribution pattern on a producing cell surface determines the spatial coverage of terminal branching on it (Peterson and Krasnow, 2015), attenuated terminal branching on the M1-expressing salivary glands suggested a reduced availability of M1 on the exposed basal cell surface of the salivary gland.

2.2.6 Bnl cleavage ensures its trafficking to the basal cell surface.

To examine this possibility, the surface αGFP^{ex} assay was performed on salivary glands expressing the M1 or WT constructs. As expected, a significantly lower fraction of total M1 molecules were externalized on the basal surface of the salivary gland cells in comparison to WT (Figure 2-13, A-D). Strikingly, while the WT protein covered the entire basal surface of the giant-sized salivary gland cells, most of the externalized M1 molecules were restricted to the cell junctions (Figure 2-13, B and B'). Such abnormality in spatial distribution might suggest mispolarized M1 trafficking, reducing its availability at the basal surface. Indeed, confocal sections through the salivary glands showed that most M1 signals were selectively enriched at the apical luminal sides of the cells that were inaccessible to the external trachea (Figure 2-13, E-H). Notably, although salivary gland cells do not express Bnl, they do contain the Bnl

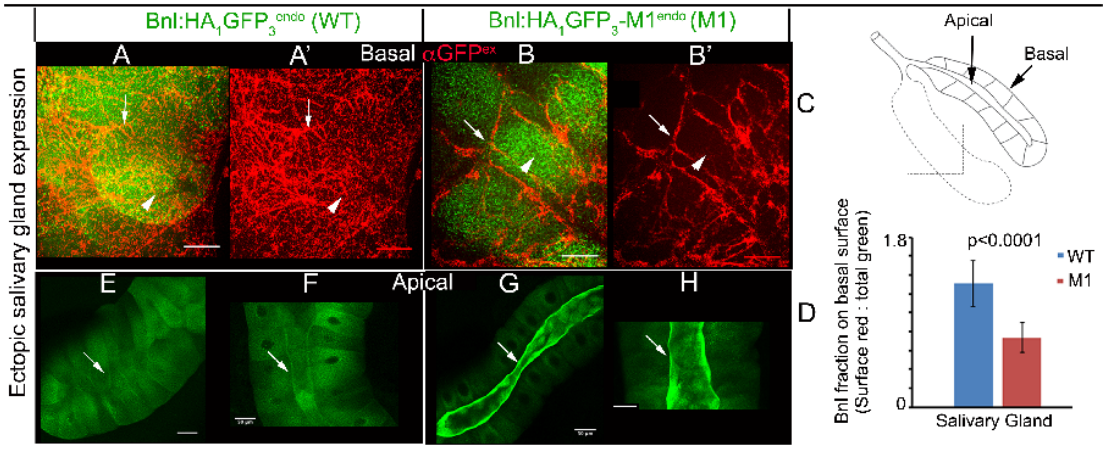

Figure 2-13: The M1 mutant has reduced basal surface localization in salivary gland cells

(A-C) High-magnification (40X) images of the exposed basal surfaces (arrowhead) of salivary glands expressing WT or M1 under *bnl-Gal4* from an area schematically shown in C; red, surface αGFP^{ex} immunostaining; arrow, cell junction. **(D)** Graph comparing fractions (red surface stain/total GFP) of overexpressed WT (n=12) and M1 (n=10) that got externalized on the salivary gland surface. **(E-H)** Images of sagittal sections of salivary glands expressing WT and M1 under *bnl-Gal4*; arrow, apical lumen. Scale bars, 20 μm; 50 μm (E-H).

cleavage machinery. Bnl:HA_1GFP_3 (WT) driven by *bnl-Gal4* was cleaved leading to clear spatial separation of the HA- and GFP-tagged fragments (Figure 2-14, A and A'). Therefore, these results suggested that Bnl cleavage promotes efficient polarized trafficking to the basal signaling surface from where tracheal cells can receive the signal.

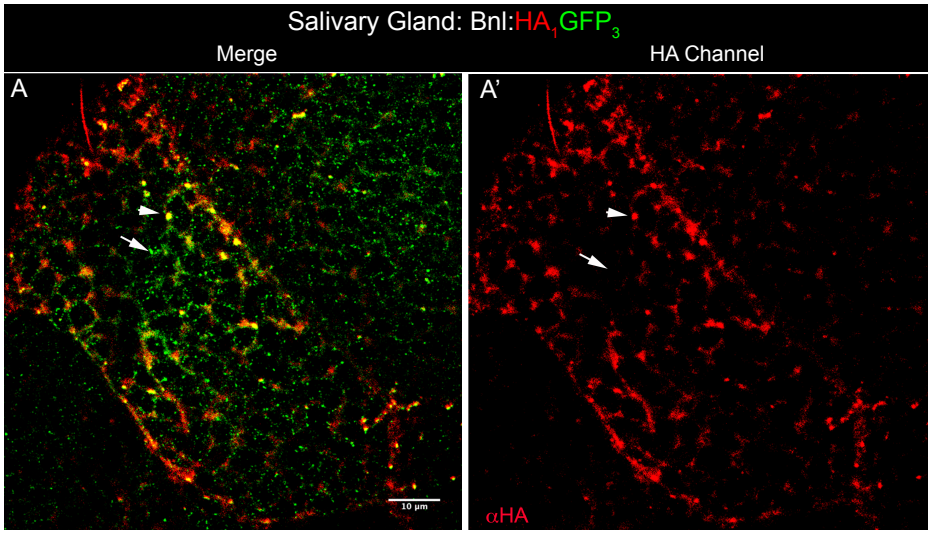

Figure 2-14: Bnl is cleaved in salivary gland cells

(A and A') An αHA (red) stained salivary gland (a single giant cell in center focus) expressing Bnl:HA_1GFP_3 under *bnl-Gal4*, showing signal cleavage; while the truncated Bnl:GFP_3 portion localized likely in secretory granules (green), the uncleaved HA-GFP colocalized signal remained in a separate subcellular compartment; B', red channel of B; arrowhead, uncleaved Bnl:HA_1GFP_3; white arrow, truncated Bnl:GFP_3 derivative of Bnl:HA_1GFP_3.

To confirm polarized Bnl sorting in the wing disc source, X-Z-Y sections of the wing disc-ASP tissue complex were acquired along the ASP D-P axis (Figure 2-15, A-E). In the CD8:Cherry-marked disc *bnl* source, overexpressed M1 molecules preferentially populated the apical luminal and lateral sides of the columnar epithelial cells. In contrast, the truncated WT molecules had relatively higher density toward the basal side of the source cells (Figure 2-15, B-D). In αHA-immunostained discs that

expressed the Bnl:HA$_1$GFP$_3$ construct under *bnl-Gal4*, the truncated Bnl:GFP$_3$ signal was clearly polarized toward the basal surface of the columnar epithelial cells facing the overlying ASP (Figure 2-15, E). Indeed, examination of genome-edited *wt*^{endo} and *m1*^{endo} larvae revealed that the basal surface of the disc source and recipient ASP had significantly higher t-WT^{endo} density in comparison to M1^{endo} (Figure 2-15, F-H). Thus, Bnl cleavage in the source cells directs efficient polarized sorting of the signal to the basal signaling surface, thereby affecting intercellular signaling range and tissue morphogenesis.

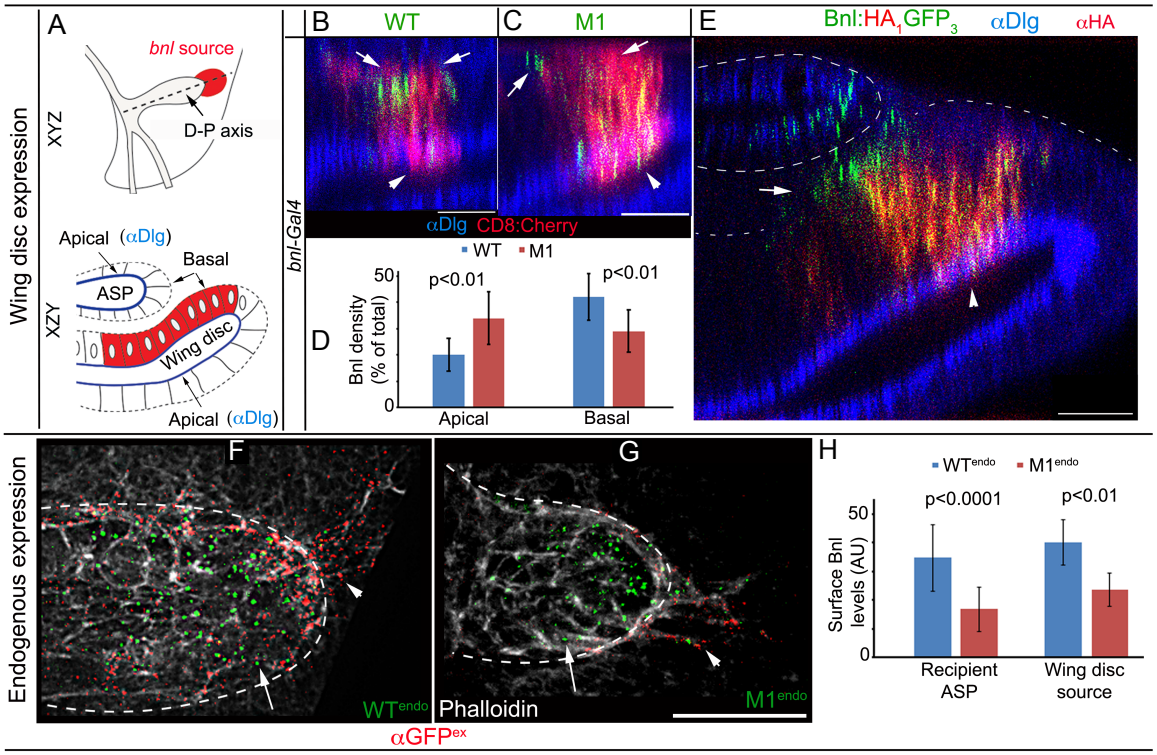

Figure 2-15: Cleavage ensures polarized Bnl sorting to the basal cell surface for signaling

(A) Drawings depicting the ASP D-P axis (dashed line; upper panel) and an XZY section along the D-P axis (lower panel) showing the tubular ASP and disc epithelia as shown in J-M. **(B-C)** Sagittal sections of αDlg immunostained (blue, sub-apical marker) wing disc and ASP when the disc *bnl* source coexpressed CD8:Cherry with either the WT or M1 construct under *bnl-Gal4*; arrow, basal side; arrowhead, apical side. **(D)** A graph comparing apical and basal percentage of WT and M1 relative to the total amount in the disc source; n=24 (WT), 32 (M1). **(E)** Maximum projections of mid- and para-

sagittal sections within ~3 μm of mid-Y of an αDlg (blue) and αHA (red) stained wing-disc/ASP, where *bnl-Gal4* expressed Bnl:HA_1GFP_3; arrow, truncated Bnl:GFP_3; white dashed line, ASP and wing disc. **(F-H)** Comparison (graph in H) of levels of t-WT^{endo} (F, n=17) and $M1^{endo}$ (G, n=33) on the surface of the disc source and ASP (dashed line); red and arrowhead, detergent-free αGFP-staining; arrow, intracellular puncta; white staining, phalloidin-Alexa-647. Scale bars, 20 μm.

2.2.7 Biochemical analysis of Bnl:GFP_1 cleavage mutants reveals possible alternative Bnl cleavages

The N-terminal prodomain of Bnl is fairly small, about 14 kDa after signal peptide removal. This made it difficult to accurately examine the cleavage product using Western Blotting of Bnl:GFP_3 or Bnl:HA_1GFP_3 while probing for GFP, since full length Bnl:GFP is >150 kDa. On the other hand, examination of Bnl:GFP_1 using Western Blot and probing for GFP provided clearer visualization of Bnl cleavage since the inclusion of the GFP insertion in the N-terminal prodomain of Bnl:GFP_1 resulted in further separation of the cleavage products from the full length Bnl:GFP protein. Therefore, to further examine the cleavage of Bnl from a biochemical perspective, the same PCS1 and PCS2 cleavage site mutations (M1, M2, and M1M2) were generated in the Bnl:GFP_1 background.

The full-length form of all of these proteins is seen just above the 150 kDa marker, which is an indication of post-translational additions to the Bnl protein as full-length Bnl:GFP is predicted to be just 112 kDa (Figure 2-16, A and B). This phenomenon is consistent with the other *Drosophila* FGFs Pyr and Ths, whose full-length forms are also much larger than their predicted size (Tulin and Stathopoulos, 2010). Furthermore, Bnl does contain several predicted N- and O-glycosylation sites that would increase the molecular weight of the protein, although these sites have not

been tested (Tulin and Stathopoulos, 2010). Consistent with possible glycosylation is the observation that the Bnl proteins, both full-length and cleavage forms, are present in doublets on the Western Blot when viewed at lower exposure (Figure 2-16, A). It has been shown that variable glycosylation of proteins can result in double bands that are only slightly different in size, similar to what we see for Bnl (Moriconi et al., 2015). If Bnl is variably glycosylated, inhibiting glycosylation should result in the loss of the double bands and/or decreased size of the bands such that they are closer to their predicted molecular weight.

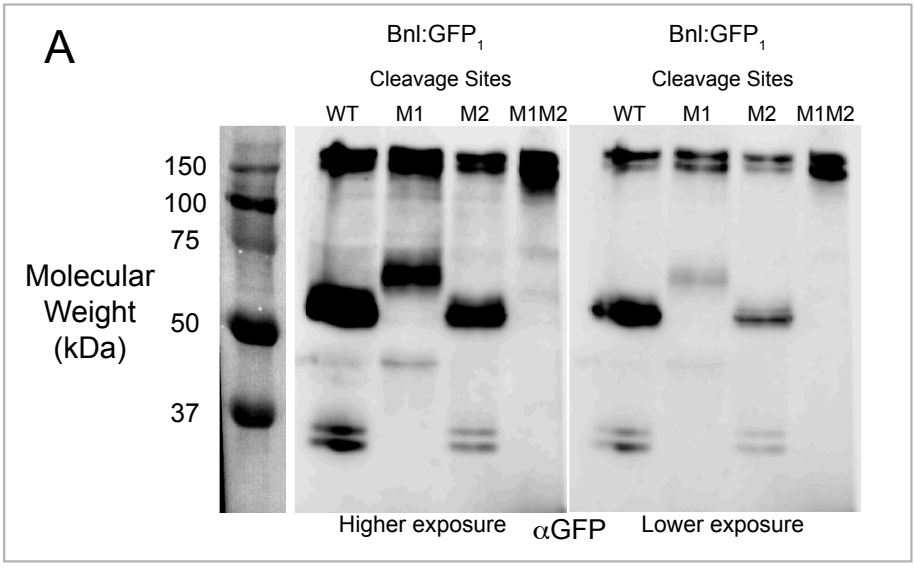

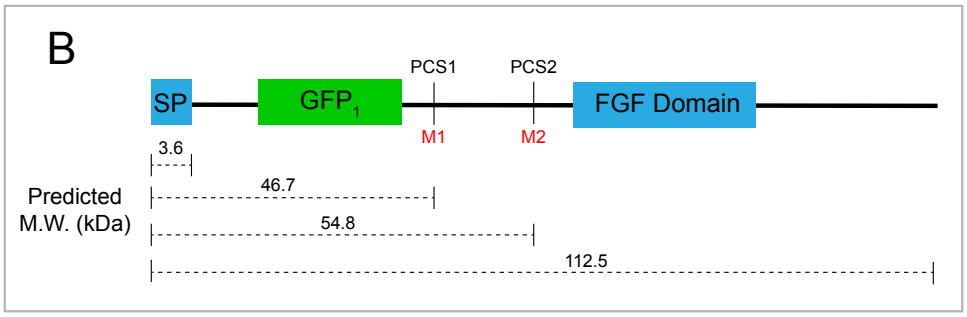

Figure 2-16: Biochemical M1 and M2 mutant analysis

(A) Western blot probing with αGFP on proteins isolated from S2 cells expressing Bnl:GFP$_1$, Bnl:GFP$_1$-M1, Bnl:GFP$_1$-M2, and Bnl:GFP$_1$-M1M2. A higher exposure image (left) and a lower exposure image

(right) of the gel are shown. All lanes show full-length Bnl:GFP around 150 kDa. In addition to the full-length band, Bnl:GFP$_1$ with wild type cleaved sites (WT) has two additional bands, one just above 50 kDa and one just below 37 kDa. These bands shift upwards in the M1 mutant and are not present in the M1M2 mutant. **(B)** Schematic of Bnl:GFP$_1$ showing relative locations of the GFP insertion, cleavage sites, and conserved FGF domain. Predicted sizes of the protein for different cleavage events are shown below the schematic.

For Bnl:GFP$_1$ with wild type (WT) cleavage sites, the full-length form migrates just above 150 kDa and two additional forms of Bnl migrate below the full-length protein, one just below 37 kDa and the other just above 50 kDa (Figure 2-16, A). Cleavage of Bnl:GFP$_1$ at PCS1 is predicted to produce a 46 kDa fragment (Figure 2-16, B), so the band above 50 kDa could be produced by cleavage at PCS1 in addition to other post-translational modifications. However, the band below 37 kDa cannot be explained by cleavage only at PCS1 or PCS2 in Bnl:GFP$_1$. It is possible that there are additional active cleavage sites that cut the Bnl protein upstream of the GFP$_1$ insertion that results in a smaller band fragments in S2 cells.

The two lower Bnl bands that are present in Bnl:GFP$_1$ with WT cleavage sites are no longer detected for the Bnl:GFP$_1$-M1 mutant, suggesting that these bands are PCS1-specific. However, the Bnl:GFP$_1$-M1 mutant contains a new band slightly larger than the upper PCS1 cleavage band, of approximately 65 kDa (Figure 2-16, A). As Bnl:GFP$_1$-M1 contains an unaltered PCS2 site, cleavage at PCS2 in the M1 mutant background could result in the appearance of this new product. Although cleavage of Bnl:GFP$_1$ at PCS2 is predicted to only produce a 54 kDa product (Figure 2-16, B), post-translational modifications such as glycosylation could explain the size difference. Further evidence that this band is a result of PCS2 cleavage is the observation that it is

no longer present when PCS2 is mutated in the Bnl:GFP_1-M1M2 double mutant (Figure 2-16, A).

When PCS2 alone is mutated in the Bnl:GFP_1-M2 mutant, the band profile looks identical to Bnl:GFP_1 with WT cleavage sites. This is consistent with the *in vivo* data that suggests PCS2 is not normally an active cleavage site and is likely not involved in the typical proteolytic maturation of Bnl (Figure 2-5, F, H, and J-K). However, it is interesting that PCS2 appears to be active when PCS1 cleavage is blocked in cell culture. It is possible that when an active Furin site is blocked, cleavage at a normally unutilized additional site can occur. For example, the *Drosophila* BMP Glass Bottom Boat (Gbb) has 3 Furin sites and can exhibit relatively normal activity as long as at least one of the sites remains functional (Fritsch et al., 2012), suggesting that cleavage at multiple sites can be used to compensate for blockage at other sites.

The finding that cleavage at PCS2 can occur in S2 cells is very interesting. It is possible that cleavage does normally occur at PCS2, but that subsequent PCS1 cleavage occurs so rapidly that the PCS2-specific cleavage band is difficult to detect. However, if this occurs, initial cleavage at PCS2 is not required for cleavage at PCS1, because in the Bnl:GFP_1-M2 mutant the cleavage products are the same as in Bnl:GFP_1 with WT cleavage sites. Although this shows that cleavage at PCS1 can still occur if PCS2 is blocked, there could be a temporal or quantitative difference in cleavage at PCS1 in this scenario. Another intriguing possibility for an active PCS2 site is represented by findings for BMP4, in which cleavage at an optimal Furin site adjacent to the mature ligand domain separates the prodomain from the mature ligand, but the prodomain remains non-covalently attached to the mature domain until a second cleavage within

the prodomain frees the mature ligand from the prodomain (Degnin et al., 2004). Our *in vivo* results showing that cleavage at PCS1 is required for complete separation of the prodomain and mature ligand do not necessarily rule out the possibility that cleavage of PCS2 could result in the prodomain remaining non-covalently attached to the rest of the mature signaling domain. In this scenario, Bnl:HA_1GFP_3-M1 could still appear as a full-length, uncleaved protein even though it had been cleaved at PCS2. Additional biochemical analyses from *in vivo* samples and an endogenous PCS1/PCS2 double mutation in Bnl could be used to further examine this possibility.

2.2.8 Lifespan of *bnl:HA_1GFP_3-$M1^{endo}$* flies is slightly reduced

It was somewhat surprising that *bnl:HA_1GFP_3-$M1^{endo}$* flies are homozygous viable, which indicated that Bnl cleavage at PCS1 is not essential for development and survival. To test if there was any difference in lifespan between *bnl:$HA_1GFP_3^{endo}$* and *bnl:HA_1GFP_3-$M1^{endo}$*, a survival assay was performed in which groups of flies of each genotype were transferred to fresh food every other day and scored for how long they lived (Figure 2-17). Wild-type (*wt*) males and females (without any insertion in the *bnl* locus) survived similar lengths compared to *bnl:$HA_1GFP_3^{endo}$* flies, as 50% death occurred after ~55 days, and 100% death occurred after at least 86 days. On the other hand, for *bnl:HA_1GFP_3-$M1^{endo}$* flies, 50% death occurred after ~50 days and 100% death occurred after just 77 days. Thus, the lifespan of flies that contain the M1 mutation in Bnl is slightly shorter. It is possible that in the wild, where conditions such as habitat and food are not as optimal or readily available, this reduction in lifespan could be even further exacerbated. However, this study did not thoroughly examine the flight, mating behavior, or other activities of the M1 mutant flies.

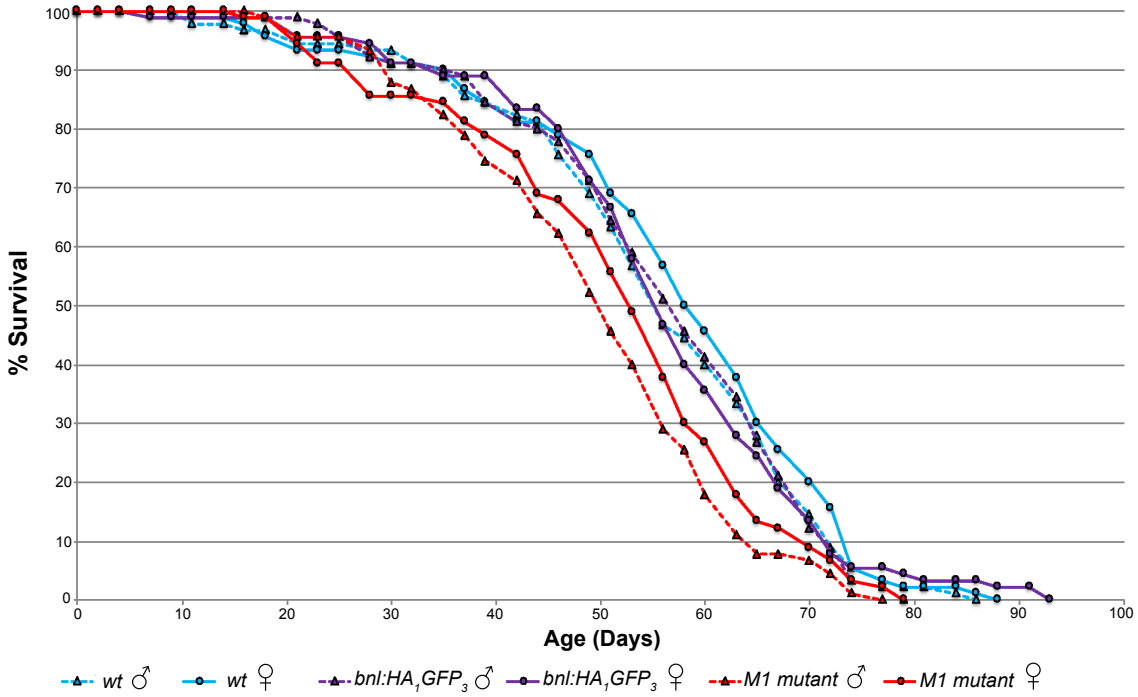

Figure 2-17: Survival Assay of the M1 mutant

A survival curve is shown for males and females of the following homozygous genotypes: *wt, bnl:HA$_1$GFP$_3^{endo}$*, and *bnl:HA$_1$GFP$_3$-M1^{endo}*. Flies harboring the endogenous M1 mutation (*bnl:HA$_1$GFP$_3$-M1^{endo}*) did not live as long as *wt* or *bnl:HA$_1$GFP$_3^{endo}$* flies.

2.2.9 Bnl is cleaved during embryonic development

The regulation of Bnl cleavage may differ spatiotemporally throughout development. Bnl expression is critical in the early embryo for formation of the initial tracheal system. To test if Bnl is cleaved in the embryo, *LexO-bnl:HA$_1$GFP$_3$* was expressed in the embryonic Bnl source cells using an endogenous *bnl-LexA* fly that was created by Du et al. (2017). When viewing stage 14 embryos, full-length Bnl (HA and GFP together) is seen in clusters of cells while only truncated Bnl (GFP only) is transported to adjacent recipient cells, suggesting that Bnl is cleaved for embryonic tracheal development as well (Figure 2-18). However, overexpression of Bnl led to abnormal embryonic tracheal development, consistent with findings in larval tissues.

Further experiments need to be performed with the tracheal cells marked to confirm that the cleaved Bnl is in fact being transported to developing tracheal branches. Moreover, endogenous constructs, although very poorly detected in the embryo, can also be examined. As Bnl is expressed in many sources such as leg discs, eye discs, the gut, and neurons (Du et al., 2017), it will be valuable to know if Bnl cleavage occurs in these other signal-producing cells. If Bnl is cleaved in other types of sources, it will be interesting to examine the regulation of the cleavage and whether it modulates Bnl trafficking and activity in the same way that it does in the wing disc source cells.

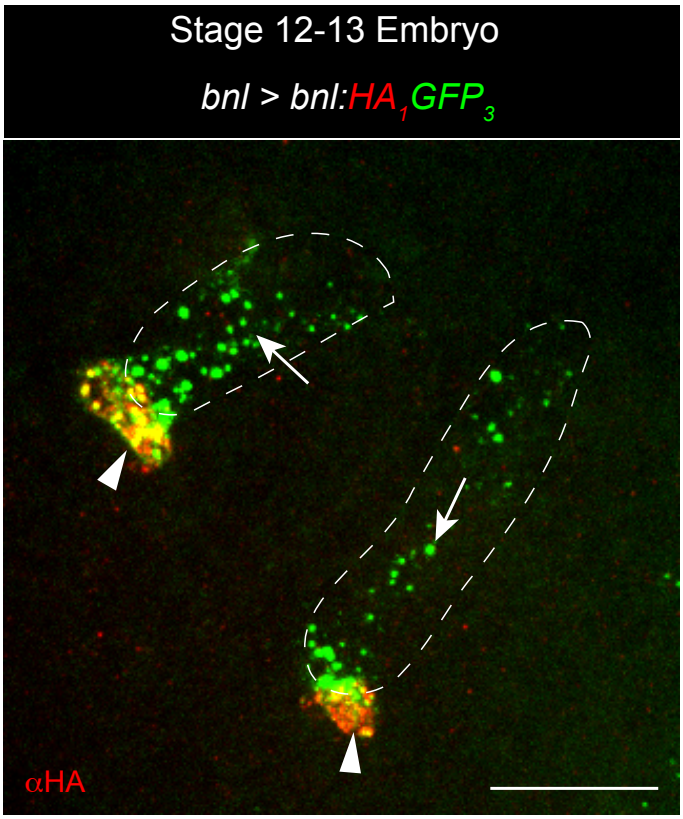

Figure 2-18: Bnl cleavage in embryonic tracheal development

Representative fluorescent image from a stage 14 embryo expressing Bnl:HA_1GFP_3 in the source cells (*bnl-LexA x LexO-bnl:*HA_1GFP_3). Bnl source cells (arrowheads) are seen with both HA and GFP fluorescence, but only GFP is located adjacent to the source cells likely in growing recipient tracheal branches (arrows). Scale bar: 10 μm.

2.3 Discussion

In conclusion, this study showed that the FGF family protein Bnl is synthesized as a proprotein and subsequently endoproteolytically cleaved at a single site by Furin1 in the Golgi network. The cleavage ensures efficient polarized intracellular sorting of a truncated C-terminal fragment of Bnl containing the FGF domain to the signaling site where the signal is received by ASP cytonemes for intercellular dispersal and signaling.

Limited proteolysis is one of the versatile posttranslational mechanisms that activates most, if not all, developmental signals (LeMosy, 2006). Signals including Hedgehog (Hh); Dispatched; EGF; Trunk; the TGF-β/BMP family proteins Decapentaplegic (Dpp), Screw, and Glass bottom boat (Gbb); two Drosophila FGFs, Pyr and Ths; and human FGF7 were all shown to be cleaved (Lee et al., 1994; Schweitzer et al., 1995; Porter et al., 1996; Künnapuu et al., 2009; 2014; Wharton and Serpe, 2013; Constam, 2014; Johnson et al., 2015; Anderson and Wharton, 2017; Stewart et al., 2018). Although signal cleavage usually activates the signal and affects the range of signaling response (Künnapuu et al., 2009; 2014; Wharton and Serpe, 2013), full-length uncleaved ligands were also found to activate receptors and were shown to be secreted when expressed in cultured cells (Künnapuu et al., 2009; Sopory et al., 2010; Tokhunts et al., 2010; Tulin and Stathopoulos, 2010; Constam, 2014). Therefore, why are signals synthesized as proproteins and subsequently cleaved for their activity or dispersion?

This study showed that Bnl cleavage acts as a catalytic switch that ensures its efficient polarized sorting to the basal signaling surface from where it can be taken up by the recipient cytonemes (Figure 2-19). The uncleavable mutant Bnl can activate

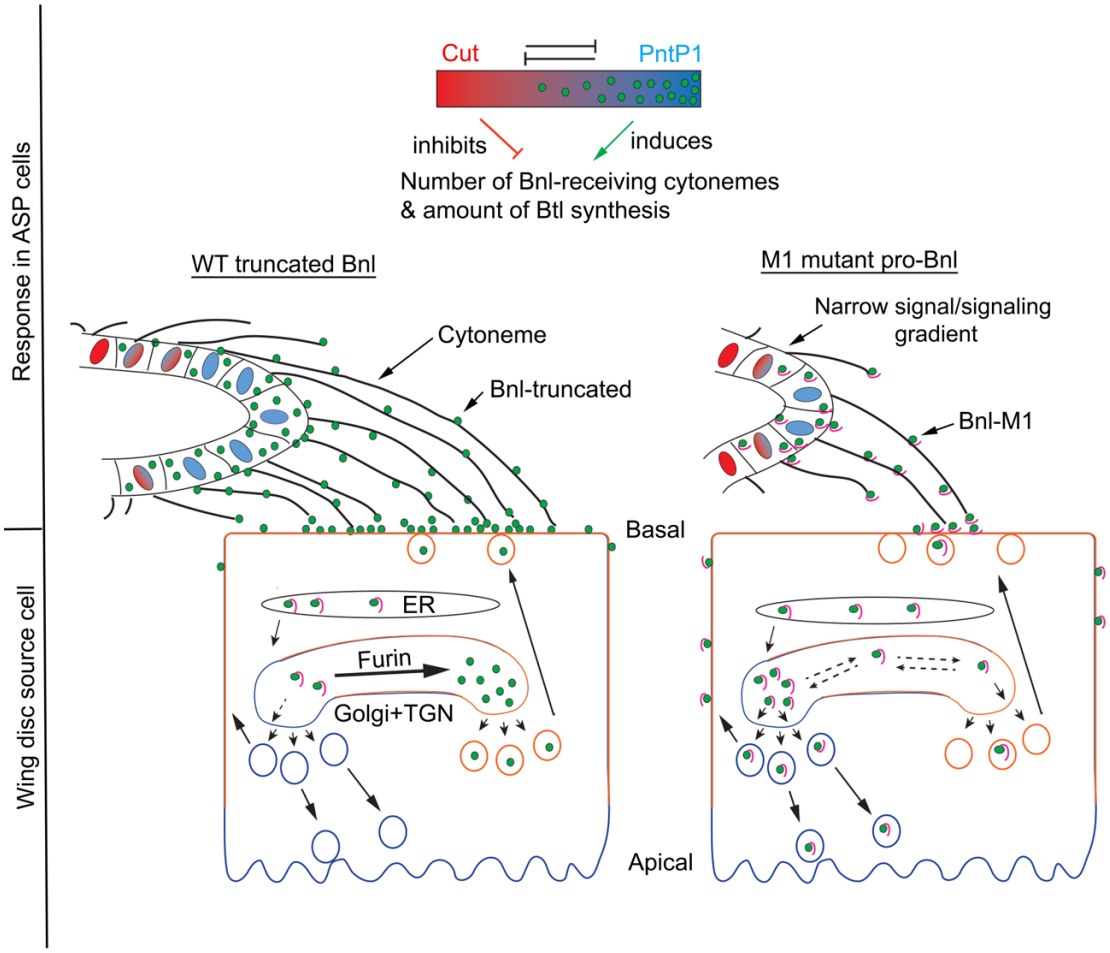

Figure 2-19: Proposed model for the role of Bnl cleavage in determining signaling range

Pro-Bnl is cleaved by Furin1 in the Golgi into a truncated form of Bnl, which, through an unknown process, is asymmetrically sorted to the basal surface of the source cells. In the absence of cleavage, mutant Bnl-M1 molecules traffic randomly and are mostly sequestered at a distant apical domain, reducing their basal availability. The ASP, which is located near the basal side of the source cells, extends cytonemes to directly receive Bnl from the basal surface of the source cells. High Bnl levels/signaling in the ASP induce PntP1, which induces Bnl-receiving cytoneme formation. Lower Bnl uptake in cells further from the source induces Cut, which suppresses Bnl-receiving cytoneme formation. Cut and PntP1 feedback-inhibit each other's expression, thereby generating a Bnl gradient that adopts recipient ASP-specific shapes (Du et al., 2018a). Consequently, reduced Bnl-M1 availability results in only a few ASP cells extending Bnl-receiving cytonemes, leading to a restricted range of signal distribution and stunted ASP growth.

receptors but is presented on the basal surface at low levels (Figure 2-13, A–D and Figure 2-15, F-H). The reduced basal presentation of uncleavable Bnl is due to its

mistargeting to a far apical domain of the source cells, which is inaccessible to recipient tracheal cytonemes. Therefore, it is likely that pro-Bnl cleavage activates a delivery barcode for efficient target-specific intercellular dispersal. Conceptually, the cleavage ensures a signaling polarity that is relayed from within the source cells to the recipient ASP through cytonemes. Such signal barcoding for determining intercellular destination might be conserved for all signals. Consistent with this view, a similar cleavage-dependent polarized sorting mechanism was reported for Hh in *Drosophila* retinal photoreceptor neurons (Huang and Kunes, 1996; Chu et al., 2006; Daniele et al., 2017). A complex choreography of apical and basal localization followed by the basal cytoneme-dependent dispersion of Hh was also described in *Drosophila* wing imaginal disc cells (Guerrero and Kornberg, 2014; Kornberg, 2011).

Interestingly, the efficiency of intracellular and intercellular Bnl trafficking depends on the enzymatic activity of Fur1 (Figure 2-7, G and Figure 2-8 A–D). Although Bnl expression is spatially restricted in tissues, the molecular machinery that cleaves Bnl exists even in salivary glands that do not normally express Bnl (Figure 2-14). This might reflect the broad range of Fur1 expression, as reported in several studies (Roebroek et al., 1992; 1993; Künnapuu et al., 2009; van Tetering and Vooijs, 2011; Johnson et al., 2015). Alternatively, different types of cells might express different furin/PC genes that can act redundantly. Furins are known to be regulated enzymes that autoactivate in a Ca^{2+}-dependent manner during their intracellular trafficking (Thomas, 2002). How and when the Furin activation pathway might intersect with the pro-Bnl sorting itinerary is unknown. It is also not known why truncated Bnl is targeted only to the basal cell surface. Recently, the trans-Golgi cargo receptor AP-1γ, a component of

the Clathrin AP-1 complex, was shown to be necessary for Bnl trafficking to the basolateral membranes of bnl-expressing flight muscle cells (Peterson and Krasnow, 2015). It is possible that Bnl cleavage is somehow involved in interaction with a cargo-receptor binding site. The current knowledge of intracellular Bnl/FGF targeting is rudimentary and needs to be elucidated in the future.

These findings revealed that although Bnl cleavage is intracellular, it plays an important role in determining the range of cytoneme-mediated intercellular Bnl dispersal. Insights on how this intracellular event might influence the range of cytoneme-dependent dispersal came from an earlier study (Du et al., 2018a). As illustrated in Figures 1-7 and 2-19, high-to-low levels of Bnl signaling activate two counteracting feedback loops operating from the opposite poles of the ASP, which help to establish the zones of corresponding high-to-low number of Bnl-receiving cytonemes along the ASP epithelium. The consequence is a systemic self-regulatory process where the number of Bnl-receiving cytonemes produced by ASP cells is determined by the amount of Bnl received by the cells through cytonemes, which gives rise to the recipient ASP-specific Bnl gradient shapes. Therefore, the intracellular cleavage and polarized sorting pathway that modulate Bnl availability on the basal surface of source cells can determine the spatial range of cytoneme formation, signal dispersion, and signaling. These results suggest an intricate coordination of the intracellular events in the source and recipient cells with the intercellular cytoneme-mediated dispersal, which together precisely shape signal gradients and tissue patterns.

Chapter 3: Lipid modification of Bnl

3.1 Introduction

Despite characterization of the basal sorting of Bnl activated by Furin-dependent intracellular cleavage, it remained unclear why Bnl is not freely released once it is exposed to the surface of the source cells. Lipid modifications could render signals insoluble and restrict their dispersion through the extracellular matrix (Resh, 2006), but most signaling proteins, as described below, are known to be lipidated and/or directly interact with lipidated proteins such as proteoglycans. Despite the wide-spread occurrence, the exact cell biological and developmental role of signal lipidation remained a mystery. Here I show that Bnl is lipid modified, which ensures cytoneme-dependent signaling. This is the first report of any direct lipid modification to an FGF protein.

3.1.1 Lipidation of signaling proteins

Hedgehog (Hh) is a common morphogen that functions to pattern tissues during development and must travel over long distances to target cells to activate signaling. However, Hh is lipid-modified by both a cholesterol and a palmitate, a 16-carbon saturated fatty acid (Porter et al., 1996; Chamoun et al., 2001). The cholesterol modification to Hh requires autocatalytic activity of the Hh protein. An intein domain within its C-terminus catalyzes the proteolysis of the N-terminal signaling domain and subsequent Cholesterol addition to the C-terminal end of the signaling domain (Porter et al., 1996). The palmitate molecule is added to the N-terminal cysteine residue by the *Drosophila* membrane-bound O-acyl transferase (MBOAT) protein, Rasp (aka

Sightless, Skinny Hedgehog, and Central Missing) (Chamoun et al., 2001). Human Sonic Hedgehog (Shh) is also palmitoylated by the Rasp homolog Hhat (Pepinsky et al., 1998; Buglino and Resh, 2008). Due to its lipid modifications, Hh localizes in lipid rafts (Chen et al., 2004; Rietveld et al., 1999). This organization and clustering of Hh on the surface of the producing cells appears to be important for its long-range signaling (Vyas et al., 2008). Interestingly, Hh can still be secreted from producing cells when Rasp is mutated or when mutations in Hh block the addition of either lipid modification (Lee and Treisman, 2001; Micchelli et al., 2002; Chamoun et al., 2001; Chen et al., 2004). However, unlipidated Hh travels further in the *Drosophila* wing imaginal disc but is less potent in activating its target genes (Callejo et al., 2006). Therefore, the lipid modifications to Hh are required for precise control of Hh signaling.

The Wnt family of signaling proteins also contain two separate lipid modifications. Mouse Wnt3a has a palmitate molecule attached to its conserved cysteine C77 (Willert et al., 2003) as well as a monounsaturated palmitoleate molecule attached to its conserved serine S209 (Takada et al., 2006). Palmitoylation of Wingless (Wg), the *Drosophila* Wnt protein, by the MBOAT protein Porcupine (Por) is necessary for Wg localization to lipid rafts and proper secretion of the protein (Kadowaki et al., 1996; Zhai et al., 2004; van den Heuvel et al., 1993). Intriguingly, as palmitoleate is an unsaturated fatty acid, it is predicted to be excluded from lipid rafts, which typically contain highly ordered and saturated lipids. The interplay between these two lipid modifications on Wnt could play a role in its trafficking and release from the Wnt-producing cells. One finding consistent with the idea that Wg trafficking relies on lipid raft localization is that the palmitoylated cysteine residue in Wg is

required for normal secretion of the protein *in vivo* (Franch-Marro et al., 2008). Similar to Hh, lipidation of Wnt reduces its range of action and is necessary for the tight regulation of its signaling (Galli et al., 2007).

The *Drosophila* EGF Spitz (Spi) is palmitoylated by Rasp, the same MBOAT enzyme responsible for palmitoylation of Hh. The palmitate addition to the N-terminal cysteine of Spi results in it being stably attached to the outer membrane of cultured cells. When this cysteine residue is mutated, Spi is instead released into the media and is no longer attached to the surface of cultured cells. Similar to loss of Hh lipidation, loss of Spi palmitoylation results in an increased range of activation of its target genes *in vivo*, but a weakened signaling response as the target genes are activated at lower levels (Miura et al., 2006).

An interesting case of signaling protein lipidation is with Ephrins. Ephrin signaling is involved in organ boundary formation, axon guidance, and vasculature organization, and is also implicated in tumor malignancy (Pasquale, 2008; Wykosky and Debinski, 2008). Ephrins are ligands for Eph receptors, the largest family of Receptor Tyrosine Kinases (RTKs), and are categorized into two different classes, A and B, depending on how they are anchored in the membrane (Gale and Yancopoulos, 1997). Ephrin A1-A5 are tethered to the membrane by a glycosylphosphatidylinositol (GPI)-anchor, while Ephrin B1-B3 are anchored in the membrane by a transmembrane domain followed by a cytosolic domain (Gale and Yancopoulos, 1997). Interestingly, due to the membrane anchoring of Ephrin ligands either by a GPI-anchor (Eph A1-A5) or a transmembrane domain with a cytosolic domain (Eph B1-B3), Ephrins can participate in reverse signaling, meaning they can relay signals back into the Ephrin-

producing cells after ligand-receptor interactions (Pasquale, 2008). Although they have typically been thought of as membrane-bound, juxtacrine signaling proteins, it was shown that Ephrins can be released from the membrane by metalloproteases and function in soluble forms (Janes et al., 2005; Beauchamp et al., 2012).

3.1.2 Intercellular transport of lipidated signaling proteins

Since these lipidated proteins predominantly localize in the membrane due to their hydrophobic modifications, it remains somewhat of a mystery how they signal over long distances. One study found that Wg and Hh copurify from cultured cells with lipophorin, the protein scaffold of lipoprotein particles. The function of lipoprotein particles is to transport hydrophobic molecules within vesicles through the extracellular space. Furthermore, this study found that Hh and Wg also colocalize with lipophorin in the developing wing disc and that reduction of lipophorin levels also reduced the range of Hh and Wg signaling (Panáková et al., 2005). It has also been shown that lipoprotein receptor-related proteins can act as coreceptors for Wnt and Hh (He et al., 2004; Fisher and Howie, 2006). Some GPI-anchored proteins, such as parasite coat proteins, can travel through the body on lipoprotein particles (Neumann et al., 2007), so transport of lipid-modified proteins by lipoprotein particles has been shown before. However, direct evidence of lipid-modified signaling protein transport via lipoprotein particles has not been provided and colocalization of some lipidated signaling proteins with lipoprotein particle components does not rule out other modes of transport. In fact, somewhat contradicting the lipoprotein particle transport model, it was shown that Hh can be cleaved and shed from the membrane by matrix metalloproteases (Dierker et al., 2009).

Recently, increasing evidence has been surfacing that cytonemes, or thin actin-based filopodia, play a critical role in the transport of most, if not all paracrine signaling proteins, including ones that are lipid-modified (Yamashita et al., 2018). Wnt and its receptor, Frizzled (Frz), were shown to be transported along cytonemes to mediate patterning of tissues in embryogenesis of both vertebrates and invertebrates (Stanganello et al., 2015; Huang and Kornberg, 2015; Sagar et al., 2015). Hh transport is also mediated by cytonemes. In the *Drosophila* wing imaginal disc, anterior compartment cells extend cytonemes containing the Hh receptor Patched (Ptc) to contact the Hh-producing posterior compartment cells (Chen et al., 2017). The Hh source cells also extend cytonemes that contain the Hh ligand and the signal is exchanged where the receiving-cell and producing-cell cytonemes contact each other (González-Méndez et al., 2017). Furthermore, Shh is transported by cytonemes to pattern the limb bud in chick embryos (Sanders et al., 2013). In the developing *Drosophila* eye disc, cells that express EGFR to receive EGF extend cytonemes to contact the EGF-producing cells and EGF signaling in the EGF-recipient cells is required for the production of cytonemes (Roy et al., 2011). These findings strongly suggest that cytonemes are used to transport EGF as well. Overall, there is mounting evidence that many signaling proteins are both lipid modified and are also transported via cytonemes, although there is still much to be learned about how these two properties of signaling proteins are connected.

3.1.3 GPI anchor structure

A common type of post-translational lipid modification to a protein that results in the protein being tethered to the outer membrane of cells is a

glycosylphosphatidylinositol (GPI) anchor. The most common type of GPI anchor consists of a phosphatidylinositol (PI) lipid moiety, four glycan molecules (one glucosamine and three mannoses), and a terminal phosophoethanolamine that is amide-bonded to the GPI-anchored protein (Figure 3-1, reviewed in (Kinoshita, 2016)).

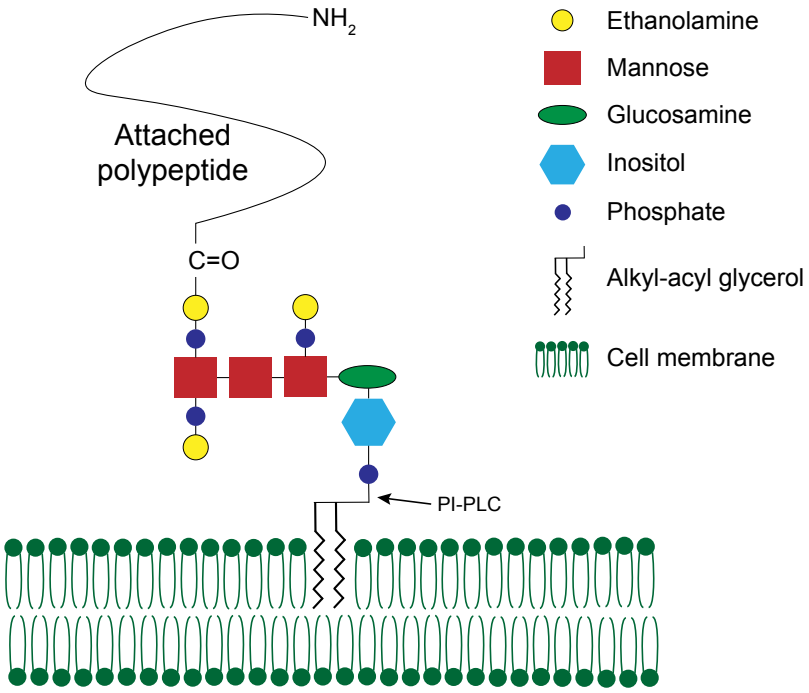

Figure 3-1: GPI anchor structure

Schematic of the GPI anchor structure is shown. Location of phospholipase C (PI-PLC) cleavage within the GPI anchor to release the tethered protein is indicated (arrow).

Depending on many factors, such as the organism or cell type, the GPI anchor can differ with various glycan side chains or modified lipid moieties. The GPI anchor is assembled in the ER by a series of enzymatic reactions to covalently attach the glycans and phosphoethanolamine to the PI lipid portion. Hydrophobic signal sequences in the C-terminus of GPI-anchored proteins induce the addition of the fully assembled GPI anchor in the endoplasmic reticulum (ER). During this process, the C-

terminal hydrophobic portion of the protein is cleaved off and concomitantly replaced with the preassembled GPI anchor via a transamidation reaction. Once added to the protein, the glycan and lipid portions of the GPI-anchor can be further remodeled in the ER and Golgi. GPI-anchored proteins are tethered to the outer surface of the cell membrane and often localize in membrane microdomains, or lipid rafts. They can be released from the membrane via phospholipase cleavage that occurs within the lipid portion of the GPI anchor (Figure 3-1).

3.2 Results

3.2.1 Additional predicted cleavage sites in the Bnl C-terminus

In addition to PCS1 and PCS2, which were tested using the BnlHA_1GFP_3-M1 and -M2 mutants, respectively, the Proprotein Convertase (PC) site prediction software (Duckert et al., 2004) indicated that there were additional potential cleavage sites downstream of tagging site 3 in the C-terminus of the Bnl protein (Figure 3-2, A). "General PC" prediction indicated that there were 2 sites in the C terminus that had a high probability of being cleavage sites, which were referred to as PCS3 and PCS4. PCS3 was located after R565 in the native protein, which is between tagging sites 3 and 4, and PCS4 was located after R767 in the native protein, which is just 3 amino acids upstream from the C-terminus. Previous experiments with Bnl:GFP_3HA_4 in S2 cells ruled out the possibility of an intracellular cleavage at PCS3 (Figure 2-5, B). However, the four original GFP tagging sites (Bnl:GFP_{1-4}) could not provide any information on possible cleavage at PCS4, which is downstream of Bnl:GFP_4. Therefore, to test for any cleavage event downstream of tagging site 3, an mCherry tag

was attached to the C-terminus of the Bnl:GFP$_3$ protein, creating Bnl:GFP$_3$Cherry$_c$ (Figure 3-2, B).

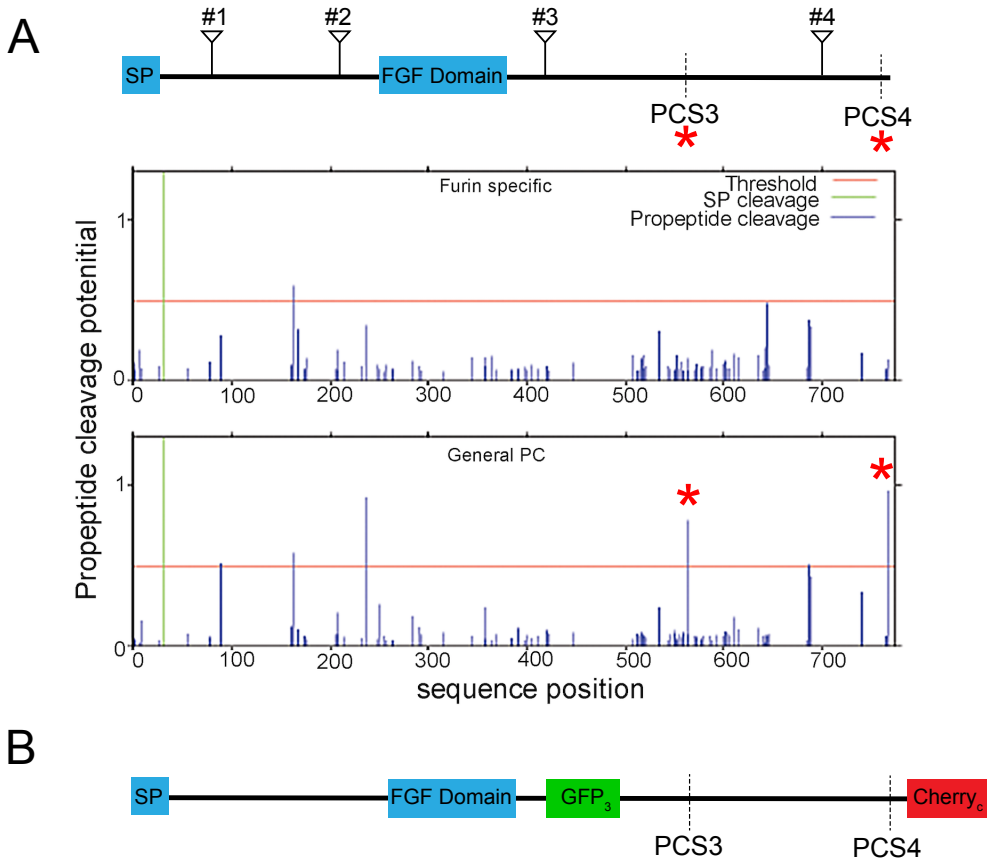

Figure 3-2: Putative C-terminal cleavage sites in Bnl

(A) Schematic of the Bnl protein with the relative locations of the original 4 GFP tagging sites (top). Prediction of General Proprotein Convertase (PC) sites (Duckert et al., 2004) in the Bnl protein revealed 2 putative sites, PCS3 and PCS4 (red stars), in the C-terminal region of Bnl. **(B)** To test for any cleavage in the C-terminus of Bnl, the construct Bnl:GFP$_3$Cherry$_c$ was created by fusing a Cherry tag onto the C-terminal end of Bnl:GFP$_3$.

When the Bnl:GFP$_3$Cherry$_c$ protein was expressed in S2 cells, GFP puncta consistently separated from Cherry puncta, suggesting a possible cleavage at PCS4 in the extreme C-terminal portion of Bnl (Figure 3-3, A). Furthermore, GFP puncta that were on the surface of the cells, as shown by an extracellular αGFP stain, were not colocalized with Cherry (Figure 3-3, A). Thus, the C-terminal fragment of Bnl

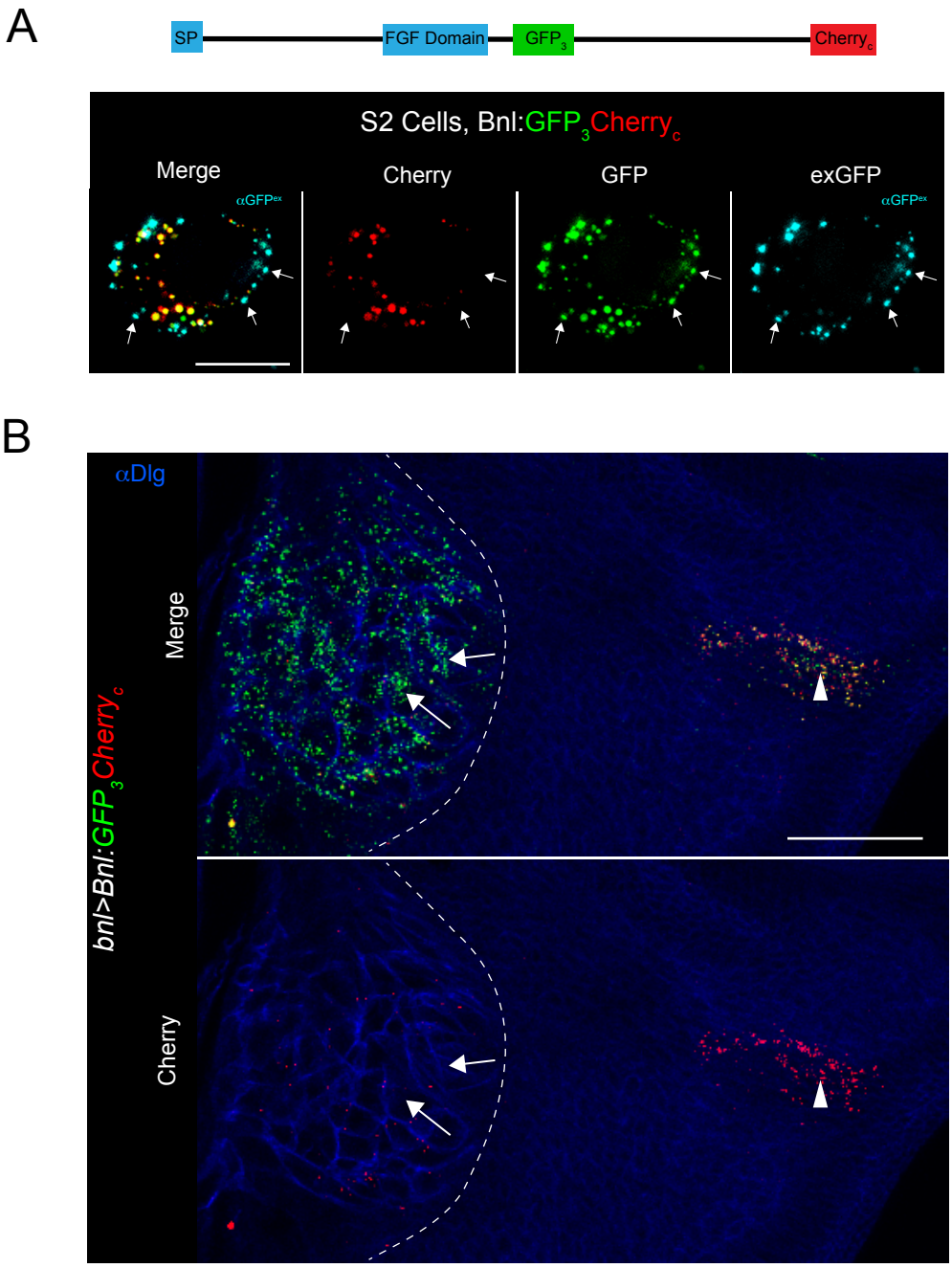

Figure 3-3: Separation of GFP and Cherry from Bnl:GFP$_3$Cherry$_c$

(A) S2 cells expressing the Bnl:GFP$_3$Cherry$_c$ protein (schematic shown above images) and stained with an αGFP extracellular stain (αGFP^{ex}). Merged and each individual channel are shown separately. Many GFP puncta (green) are seen without colocalization of Cherry fluorescence (red), including externalized Bnl:GFP, as viewed with αGFP^{ex} staining (blue, arrows). This indicates possible intracellular cleavage within the C-terminal region of Bnl that results in separation of GFP$_3$ and Cherry$_c$. **(B)** Wing disc from transgenic flies expressing Bnl:GFP$_3$Cherry$_c$ driven by Bnl-Gal4 (*bnl-Gal4 x UAS-bnl:GFP$_3$Cherry$_c$*).

Bnl:GFP (green) in the ASP recipient cells is predominantly absent of Cherry fluorescence (red, arrows), which instead remains behind in the Bnl source cells (arrowhead), indicating that somehow the $Cherry_c$ tag is separated from the rest of the Bnl protein *in vivo*. All cells marked with αDiscs-large (Dlg). Merged and Cherry channels are shown. Scale bars: 10 μm (A), 30 μm (B).

remained inside the cells while the rest of the signaling protein was externalized. To test if the cleavage also occurred *in vivo*, transgenic flies harboring the *UAS-bnl:GFP$_3$Cherry$_c$* construct were generated and the protein was expressed in the wing disc source cells using *bnl-Gal4*. Consistent with the *in vitro* S2 cell data, the Cherry tag remained in the wing disc source cells while the GFP_3 tag was transported to the recipient ASP cells (Figure 3-3, B), confirming that these tags are separated from each other, possibly by proteolysis or another mechanism.

3.2.2 Bnl localization on the extracellular surface of producing cells

Interestingly, previous results investigating the cleavage of Bnl at PCS1 showed that Bnl is present on the extracellular surface of the source cells (Figure 2-13, A-D; Figure 2-15, F-H). As these assays probing for extracellular Bnl involved many wash steps (see Chapter 5, section 5.9), it indicated that Bnl is firmly anchored in the membrane or extracellular matrix by some mechanism. Using an extracellular αGFP stain in non-permeabilized conditions, high levels of Bnl:GFP_3 were observed on the extracellular surface of S2 cells (Figure 3-4, A), confirming that Bnl:GFP_3 is anchored on the outer surface of the cell membrane. Extracellular staining of endogenous Bnl, either transfected by itself or cotransfected with CD8:GFP, using αBnl antibody gave similar results, indicating that membrane localization is not an artifact of the GFP insertion in Bnl:GFP_3 (Figure 3-4, A). Although membrane localization of Bnl might indicate that the protein contains a transmembrane domain that results in it being

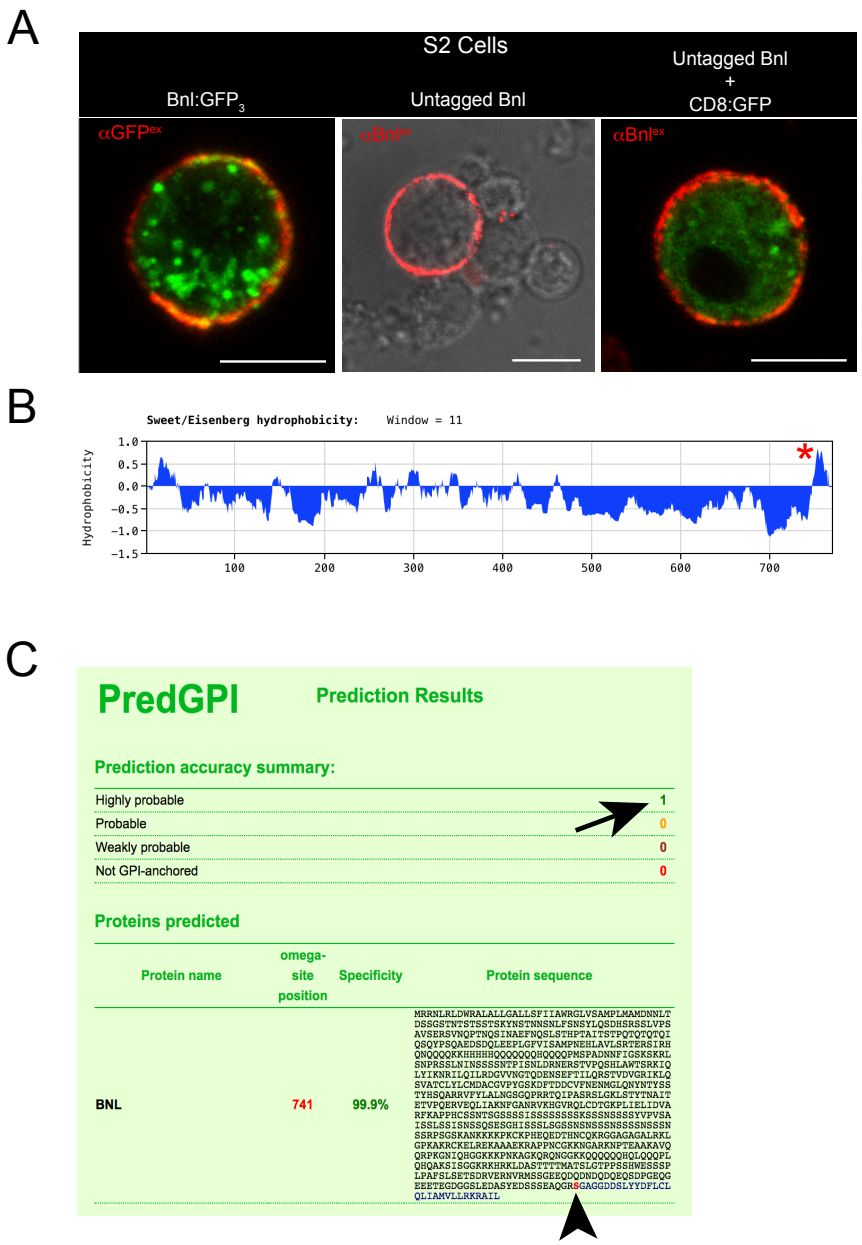

Figure 3-4: Surface localization of Bnl and GPI anchor prediction

(A) S2 cells transfected with Bnl:GFP$_3$ (left cell), untagged Bnl (middle cell), or cotransfected with untagged Bnl and CD8:GFP together (right cell). Extracellular staining using either αGFP antibody (left) or αBnl antibody (middle and right) showed that Bnl is firmly localized on the outer surface of S2 cells and is not an artifact of the GFP$_3$ insertion. **(B)** Sweet/Eisenberg Hydrophobicity plot of the Bnl protein showing a highly hydrophobic stretch of amino acids at the C-terminus of the protein (red star), an indication that Bnl could be GPI-anchored. **(C)** GPI anchor prediction software showing that GPI anchor modification to the Bnl protein is highly probable (arrow), with the modification occurring at residue S741 (ω site, arrowhead). Scale bars: 10 μm.

anchored in the membrane, there are no strongly predicted transmembrane domains in the Bnl protein. However, according to the Sweet/Eisenberg hydrophobicity scale, Bnl does contain a short hydrophobic stretch of amino acids 24 residues in length at its C-terminus (Figure 3-4, B). Intriguingly, a short stretch of amino acids near the C-terminus of a protein is a strong requirement and characteristic of proteins that are modified with a glycosylphosphatidylinositol (GPI) anchor (Galian et al., 2012). Furthermore, an online software called PredGPI (Pierleoni et al., 2008) that predicts if proteins are GPI-anchored found it highly probable that Bnl is modified with a GPI anchor (Figure 3-4, C). This software predicted that the ω site, the amino acid at which the GPI anchor is attached, is located at residue S741 of the 770 amino acid long Bnl protein. The addition of a GPI anchor to a protein results in it being tethered to the outer leaflet of the plasma membrane (Kinoshita, 2016), which could explain why Bnl is present on the outer membrane of producing cells. Moreover, GPI anchor modification results in the C-terminus of the target protein being cleaved off at the ω site with concomitant covalent addition of the GPI anchor (Kinoshita, 2016). Since Cherry was fused downstream of the predicted ω site, this could explain how the GFP and Cherry tags from Bnl:$GFP_3Cherry_c$ separated in cell culture and *in vivo*. Notably, the Cherry fusion onto the C-terminus of Bnl after the GPI anchor signal sequence did not disrupt the ability of Bnl to localize on the membrane due to possible GPI anchor modification (Figure 3-3, A). This is consistent with previous studies reporting that C-terminal fusions onto known GPI-anchored proteins do not affect their ability to be modified with a GPI anchor (Caras, 1991). Since the predicted GPI anchor modification could explain both observations that Bnl is tethered to the surface of the producing cell

plasma membrane and also the distribution of the tags from Bnl:GFP$_3$Cherry$_c$, it was hypothesized that Bnl is post-translationally modified with the addition of a GPI anchor.

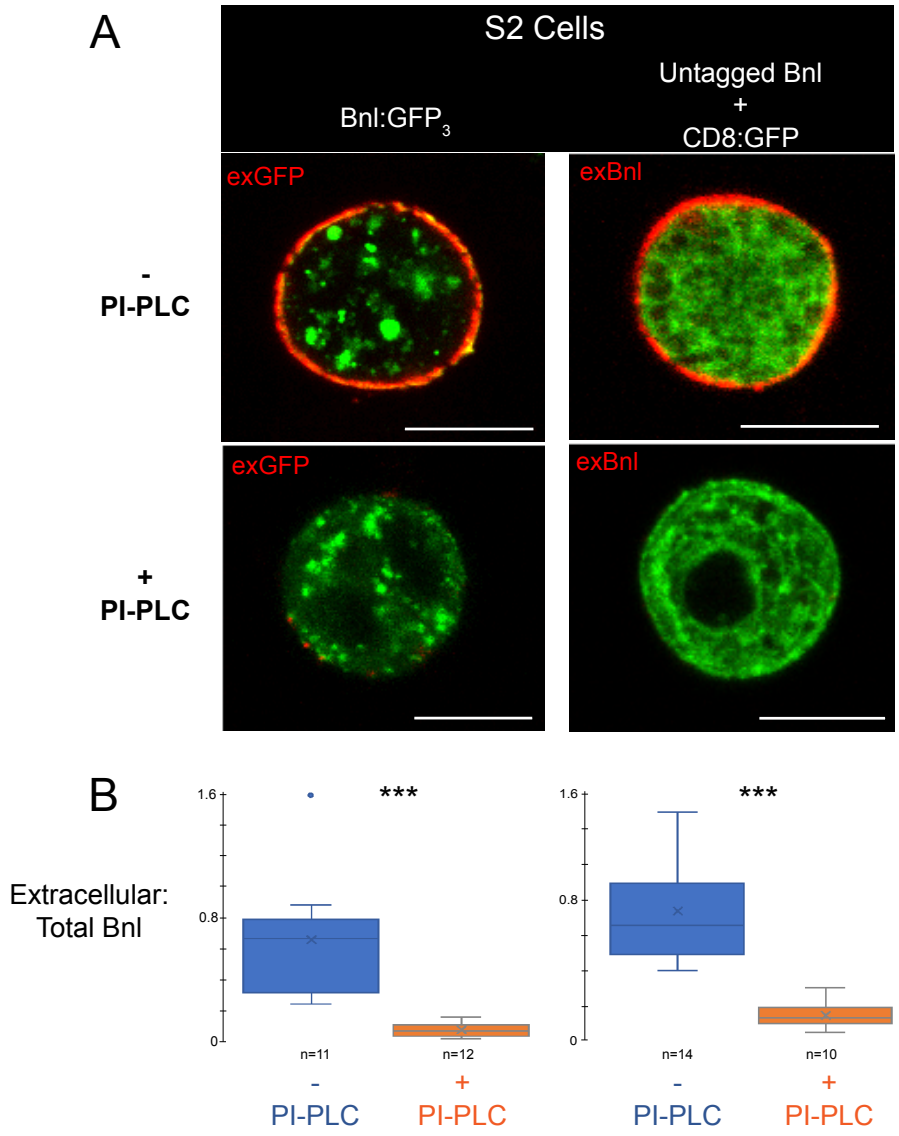

Figure 3-5: PI-PLC-mediated Bnl removal from S2 cell surface

(A) S2 cells transfected with Bnl:GFP$_3$ (left cells) or cotransfected with untagged Bnl and CD8:GFP (right cells). The cells were incubated in the absence (top cells) or presence (bottom cells) of PI-PLC and were extracellular stained with αGFP (left) or αBnl (right). Following PI-PLC treatment, both Bnl:GFP$_3$ and untagged Bnl appear to be removed from the surface of the cells. **(B)** Graph depicting the significant loss of extracellular Bnl following PI-PLC treatment. Scale bars: 10 μm. p values < 0.001.

3.2.3 PI-PLC treatment removes Bnl from the surface of S2 cells

The standard test to determine if a protein is GPI-anchored is to treat cells or tissues with phosphatidylinositol-specific phospholipase C (PI-PLC), which cleaves within the lipid portion of GPI anchors and releases the tethered protein from the membrane (Paulick and Bertozzi, 2008). Treatment of S2 cells expressing Bnl:GFP_3 or endogenous, untagged Bnl with PI-PLC followed by extracellular staining showed that PI-PLC treatment decreased Bnl levels on the extracellular surface of the cells (Figure 3-5, A). Obtaining a ratio of the surface:total Bnl levels quantitatively showed that PI-PLC significantly reduced the levels of Bnl:GFP_3 and endogenous Bnl from the surface of the cells (Figure 3-5, B).

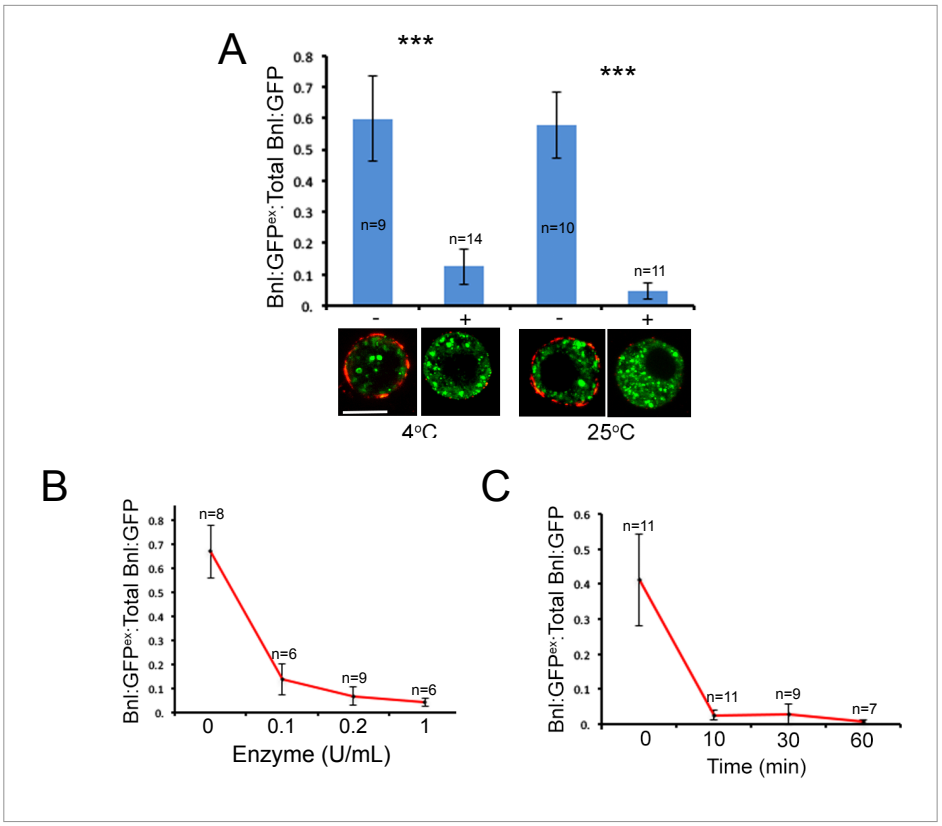

Figure 3-6: Standardization of PI-PLC treatment

(A-C) S2 cells transfected with Bnl:GFP_3 treated with or without PIPLC at different conditions and stained with αGFP^{ex}. All graphs represent the extracellular:total Bnl ratios. **(A)** Treatment with PI-PLC at 4°C and 25°C both significantly reduced surface levels of Bnl (both p values < 0.001), with no significant difference between 4°C and 25°C groups. (B-C) Different concentrations of enzyme were tested for 30 minutes each **(B)** and different times were tested using 0.2U/mL of enzyme **(C)**. Scale bar: 10 μm.

After it was found that PI-PLC treatment reduced extracellular Bnl surface levels on S2 cells, the PI-PLC treatment process was standardized by determining the optimal time, temperature, and concentration of enzyme to use in the assays (Figure 3-6). It was determined that the optimal conditions for PI-PLC treatment were: 30 minutes, 25°C, 1U/mL PI-PLC Enzyme. These optimized conditions were used for the rest of the experiments that involved PI-PLC treatment.

3.2.4 PI-PLC treatment controls

To ensure that the PI-PLC-mediated shedding of proteins from the membrane is specific to GPI-anchored proteins in S2 cells, the PI-PLC assay was performed on the *Drosophila* EGF Spitz (Spi), which is known to localize on the extracellular surface of cells due to palmitic acid lipid modification. PI-PLC treatment should not be able to directly release palmitoylated proteins from the membrane. As expected, PI-PLC treatment of S2 cells expressing Spi:GFP did not alter the extracellular levels of Spi (Figure 3-7, A and B), indicating that PI-PLC treatment is specific to GPI-anchored proteins. Alternatively, the construct GFP:mGPI was used as a positive control for PI-PLC treatment. The GFP:mGPI protein is composed of GFP flanked upstream and downstream by the signal sequence of rabbit lactase-phlorizin hydrolase (LPH) and a known mouse GPI signal sequence from the CD58 protein, respectively (Greco et al.,

2001). When GFP:mGPI was expressed in S2 cells, the extracellular-localized GFP:mGPI was efficiently removed after PI-PLC treatment (Figure 3-7, A and B),

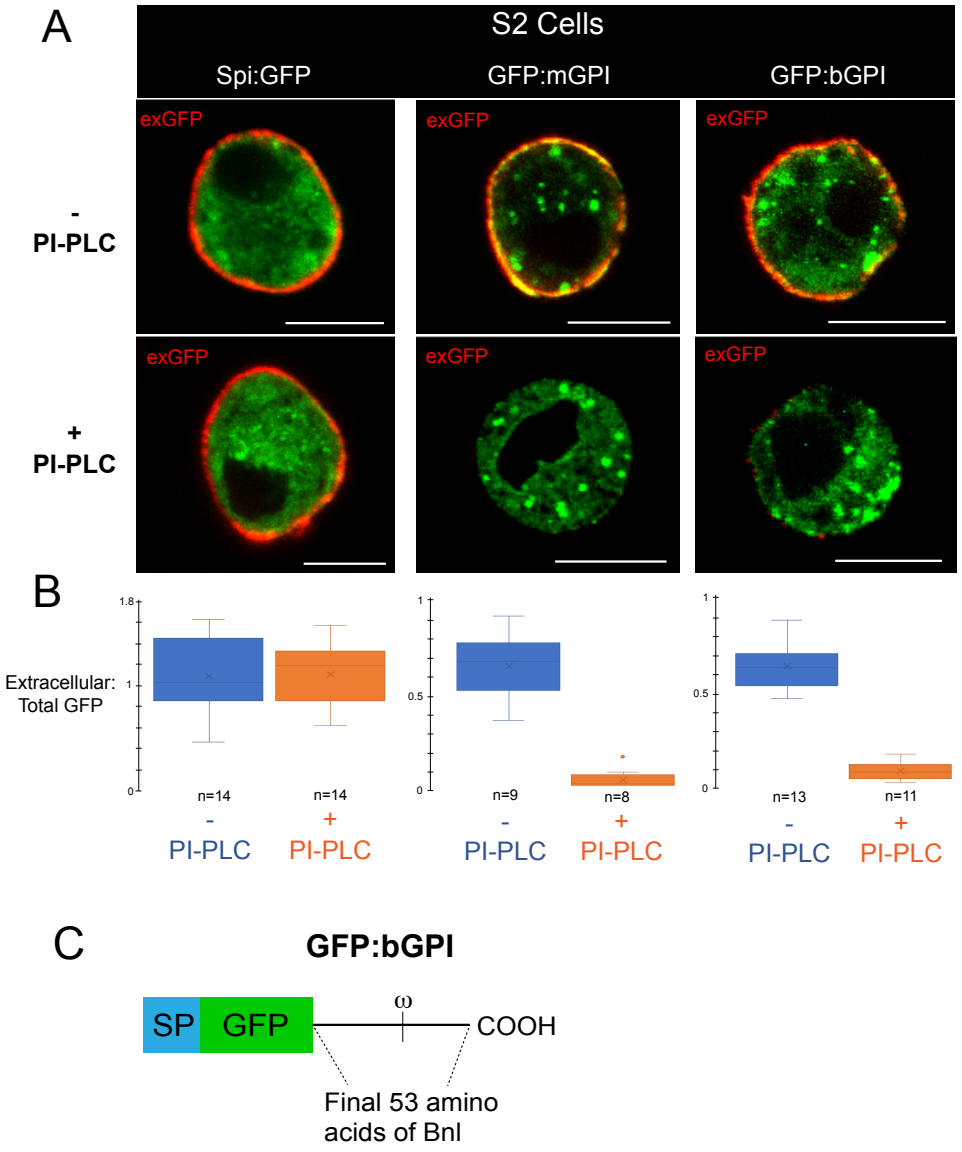

Figure 3-7: PI-PLC treatment on Spi:GFP, GFP:mGPI, and GFP:bGPI

(A) S2 cells transfected with Spi:GFP (left), GFP:mGPI (middle), and GFP:bGPI (right) and treated without PI-PLC (top row) or with PI-PLC (bottom row). All cells were extracellular stained with αGFP. **(B)** Graphs showing the extracellular:total GFP ratios for each group. PI-PLC treatment had no effect on Spi membrane localization, but significantly reduced surface levels of GFP:mGPI and GFP:bGPI (p values <0.001). **(C)** Schematic of the GFP:bGPI construct which contains the Bnl signal peptide (SP), GFP, and the final 53 amino acids from the native Bnl protein that includes the predicted ω site for GPI anchor modification. Scale bars: 10 μm.

similar to the results for Bnl in S2 cells. To further examine whether the C-terminal hydrophobic portion of Bnl is responsible for GPI anchor modification, an additional GFP:bGPI construct was generated. GFP:bGPI contains the N-terminal Bnl signal peptide for secretion, followed by a GFP tag, followed by the final 53 amino acids of native Bnl that contains the predicted Bnl GPI signal sequence and ω site (Figure 3-7, C). When expressed in S2 cells, GFP:bGPI was found to be tethered on the outer cell surface and after treatment with PI-PLC, the extracellular levels of GFP:bGPI on the surface were significantly reduced (Figure 3-7, A and B). Together, these results showed that Bnl is GPI-anchored and PI-PLC effectively and exclusively removes GPI-anchored proteins from the surface of S2 cells.

3.2.5 Generation and analysis of Bnl:GFP_3-dGPI and Bnl:GFP_3-TM

To further test and characterize the GPI-anchoring of Bnl, two different constructs were generated that contained an altered C-terminus in the Bnl:GFP_3 protein. First, a deletion was made after amino Y730 in the native Bnl protein, which is upstream of where the predicted GPI anchor signal sequence and ω site are located (Bnl:GFP_3-dGPI, Figure 3-8, A). Another construct was made in which the transmembrane domain from a CD8 protein was fused to the C-terminus of Bnl:GFP_3-dGPI, which was named Bnl:GFP_3-TM (Figure 3-8, A). In S2 cells expressing Bnl:GFP_3-dGPI, there was no detectable αGFP extracellular stain on the surface either before or after PIPLC treatment, suggesting that this deletion inhibited the ability of Bnl to associate with the membrane (Figure 3-8, B). On the other hand, S2 cells expressing Bnl:GFP_3-TM had a strong extracellular αGFP signal, indicating that the

transmembrane addition to Bnl:GFP$_3$-dGPI allowed it to once again be anchored in the membrane. Furthermore, there was no change in extracellular Bnl:GFP$_3$-TM levels after PI-PLC treatment (Figure 3-8, B), showing that PI-PLC-mediated removal of Bnl requires its intact C-terminus.

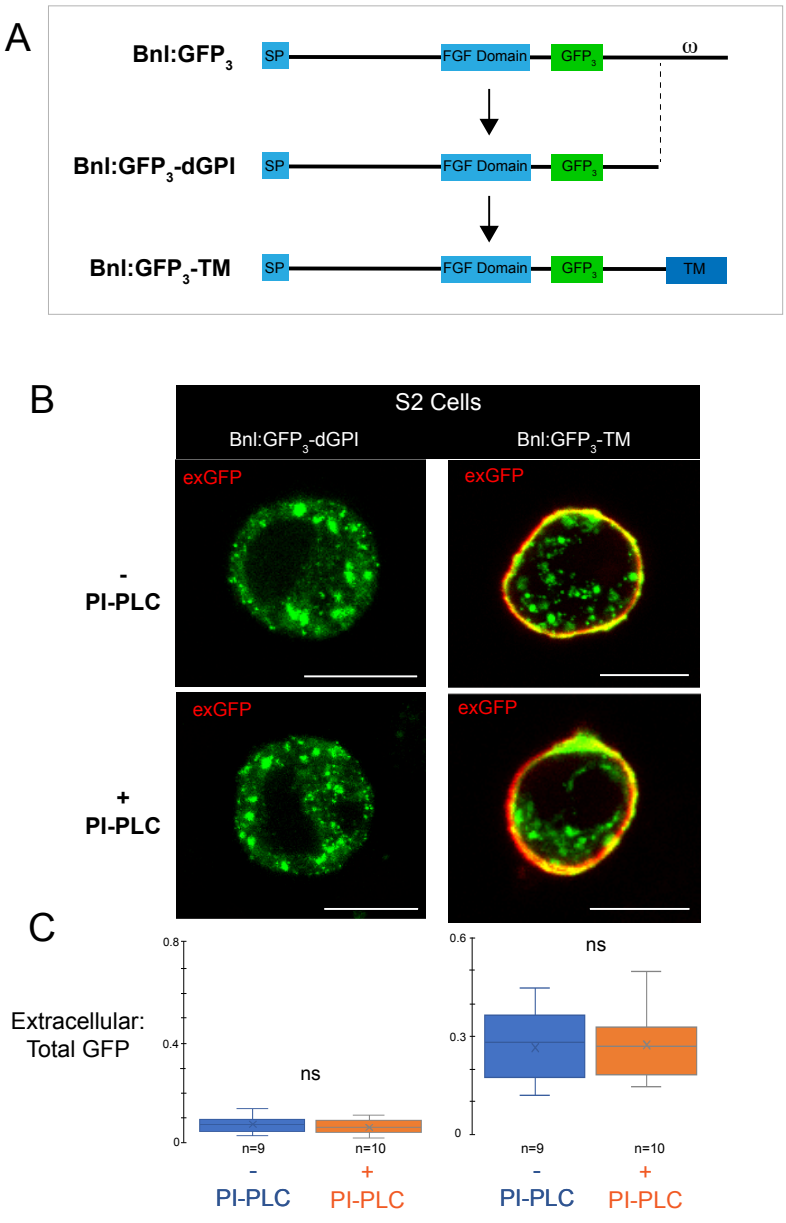

Figure 3-8: Generation of Bnl:GFP$_3$-dGPI and Bnl:GFP$_3$-TM and PI-PLC treatment

(A) Schematics showing how the Bnl:GFP$_3$-dGPI and Bnl:GFP$_3$-TM constructs were created. Bnl:GFP$_3$-dGPI was created by making a deletion at residue Y730 of the native Bnl protein, which is located

upstream of the predicted GPI-anchor ω site. Bnl:GFP_3-TM was created by fusing the transmembrane domain (TM) (cloned from the CD8:GFP construct) onto the end of Bnl:GFP_3-dGPI. **(B)** S2 cells transfected with Bnl:GFP_3-dGPI (left column) or Bnl:GFP_3-TM (right column) and treated with or without PI-PLC. All cells were stained with αGFP^{ex}. **(C)** Graphs showing the extracellular:total GFP ratios for each group. Little to no Bnl:GFP_3-dGPI was detected on the extracellular surface before or after PI-PLC treatment. Bnl:GFP_3-TM was strongly localized on the extracellular surface, but PI-PLC treatment had no effect on extracellular levels. Scale bars: 10 μm.

3.2.6 Analysis of PI-PLC assay using Flow Cytometry

Analysis of PI-PLC treatment on S2 cells by imaging methods naturally represents a relatively small sample out of the total number of successfully transfected cells. Therefore, these results were further investigated by flow cytometry to assess the effect of PI-PLC treatment on S2 cells expressing Bnl:GFP_3, Bnl:GFP_3-dGPI, or Bnl:GFP_3-TM. Flow cytometry provided the ability to analyze each cell within a large population to determine if they exhibited GFP fluorescence (GFP+ or GFP-) and/or extracellular αGFP signal (GFP^{ex}+ or GFP^{ex}-). To ensure that flow cytometry could accurately detect GFP and Alexa-Fluor647 signal, which was the secondary antibody used for extracellular αGFP staining (αGFP^{ex}), a series of controls were performed. First, untransfected and unlabeled S2 cells were analyzed by the flow cytometer and were only seen in quadrant 3 (Q3), the region where there is no GFP or GFP^{ex} signal (GFP-, GFP^{ex}-) (Figure 3-9, A). Unstained S2 cells transfected with Bnl:GFP_3 were only present in Q4 (GFP+, GFP^{ex}-). Finally, S2 cells transfected with Bnl:HA_3 and stained using αHA primary antibody and Alexa-Fluor647 secondary were only localized in Q1 (GFP-, GFP^{ex}+). Therefore, this assay could accurately analyze the fluorophores used in the extracellular staining assay to ultimately measure the effect of PI-PLC treatment.

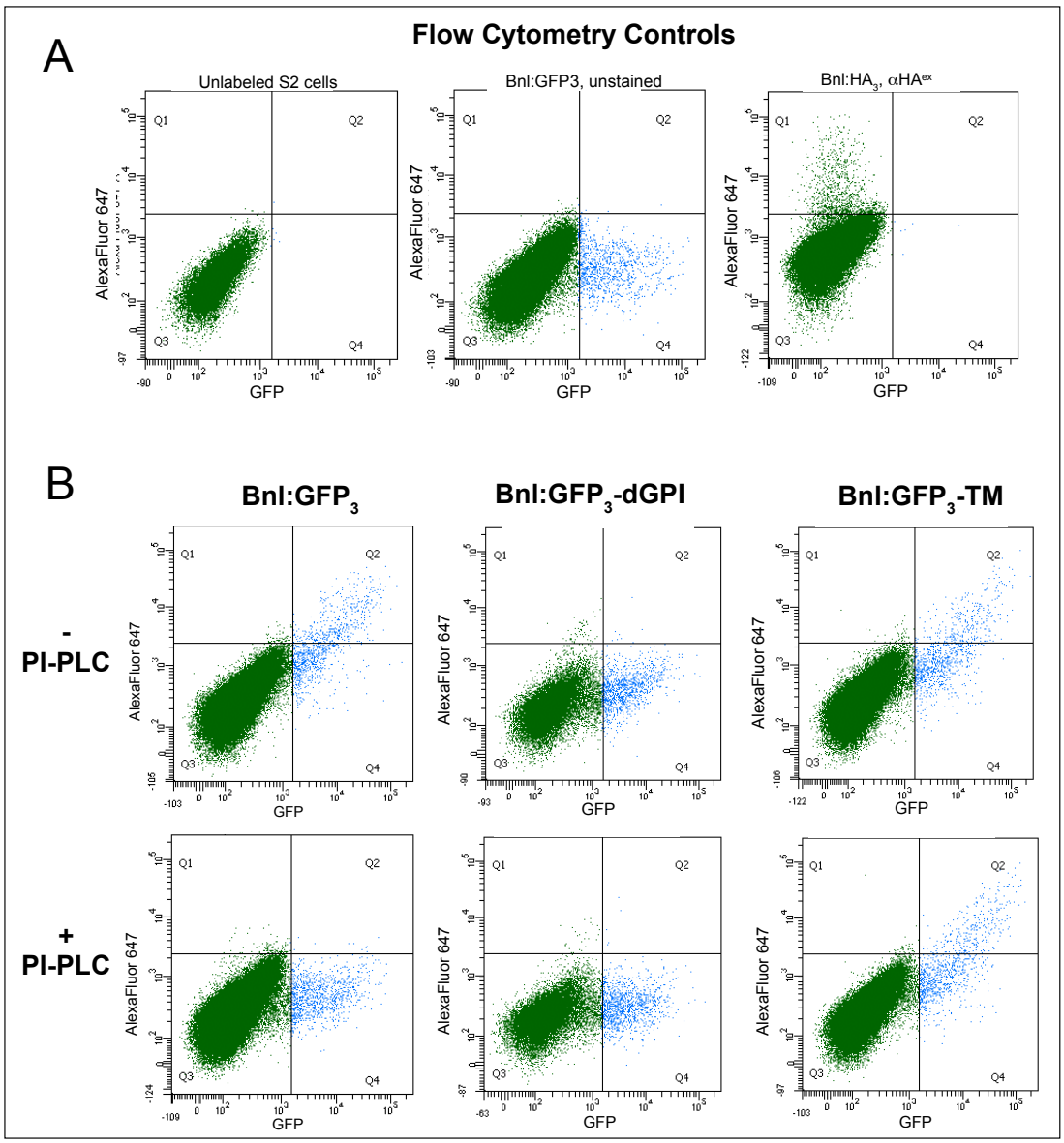

Figure 3-9: Flow Cytometry analysis of PI-PLC treatment on S2 cells expressing Bnl:GFP_3, Bnl:GFP_3-dGPI, or Bnl:GFP_3-TM

(A) Control samples to ensure flow cytometry could accurately analyze the fluorophores used. Left: unlabeled S2 cells were restricted to Q3 where no fluorescence is detected. Middle: Unstained S2 cells transfected with Bnl:GFP_3 were localized in Q4, the region where only GFP+ cells should localize. Right: S2 cells transfected with Bnl:HA_3 and stained with αHA^{ex} using AlexaFluor-647 secondary localized in Q1 only. **(B)** S2 cells transfected with Bnl:GFP_3 (left column), Bnl:GFP_3-dGPI (middle column), or Bnl:GFP_3-TM (right column) and treated with or without PI-PLC and analyzed using flow cytometry after αGFP^{ex} staining. After PI-PLC treatment, Bnl:GFP_3 cells localize in Q4 compared to their Q2 localization in the absence of PI-PLC treatment. Cells expressing Bnl:GFP_3-dGPI were

localized in Q4 regardless of PI-PLC treatment condition. PI-PLC treatment had no effect on cells expressing Bnl:GFP_3-TM that were localized in Q2.

Theoretically, all cells successfully transfected with any of the constructs would be GFP+. If they were also GFP^{ex}+, it indicated that that protein was present on the surface of the cell. S2 cells expressing Bnl:GFP_3 subjected to αGFP^{ex} staining were predominantly localized in Q2 (GFP+, GFP^{ex}+) of the plot before PI-PLC treatment. However, PI-PLC treatment altered this distribution where the majority of cells localized in Q4 (GFP+, GFP^{ex}-), indicating a loss of extracellular Bnl from almost the entire population of transfected cells due to the PI-PLC treatment (Figure 3-9, B). For S2 cells expressing Bnl:GFP_3-dGPI, the entire population was localized in Q2 (GFP+, GFP^{ex}-) regardless of PI-PLC treatment, confirming that the dGPI deletion inhibited the ability of Bnl to localize on the extracellular surface (Figure 3-9, B). The majority of S2 cells transfected with Bnl:GFP_3-TM were localized in Q2 (GFP+, GFP^{ex}+) for both the control and PI-PLC treated groups, showing that PI-PLC treatment had no effect on Bnl:GFP_3-TM extracellular membrane localization. Thus, the flow cytometry data that allowed us to analyze a large population of cells at one time were in alignment with the S2 cell imaging data.

3.2.7 Mutation of the predicted ω site inhibits surface presentation of Bnl

Construction of Bnl:GFP_3-dGPI and Bnl:GFP_3-TM involved complete deletion of the C-terminus of the Bnl protein, including the region that contained the predicted GPI anchor signal sequence and ω site. Therefore, it was important to determine if the predicted ω site at the S741 residue in the native Bnl protein was the actual site of GPI addition. To test this, an additional Bnl construct was generated that contained only a

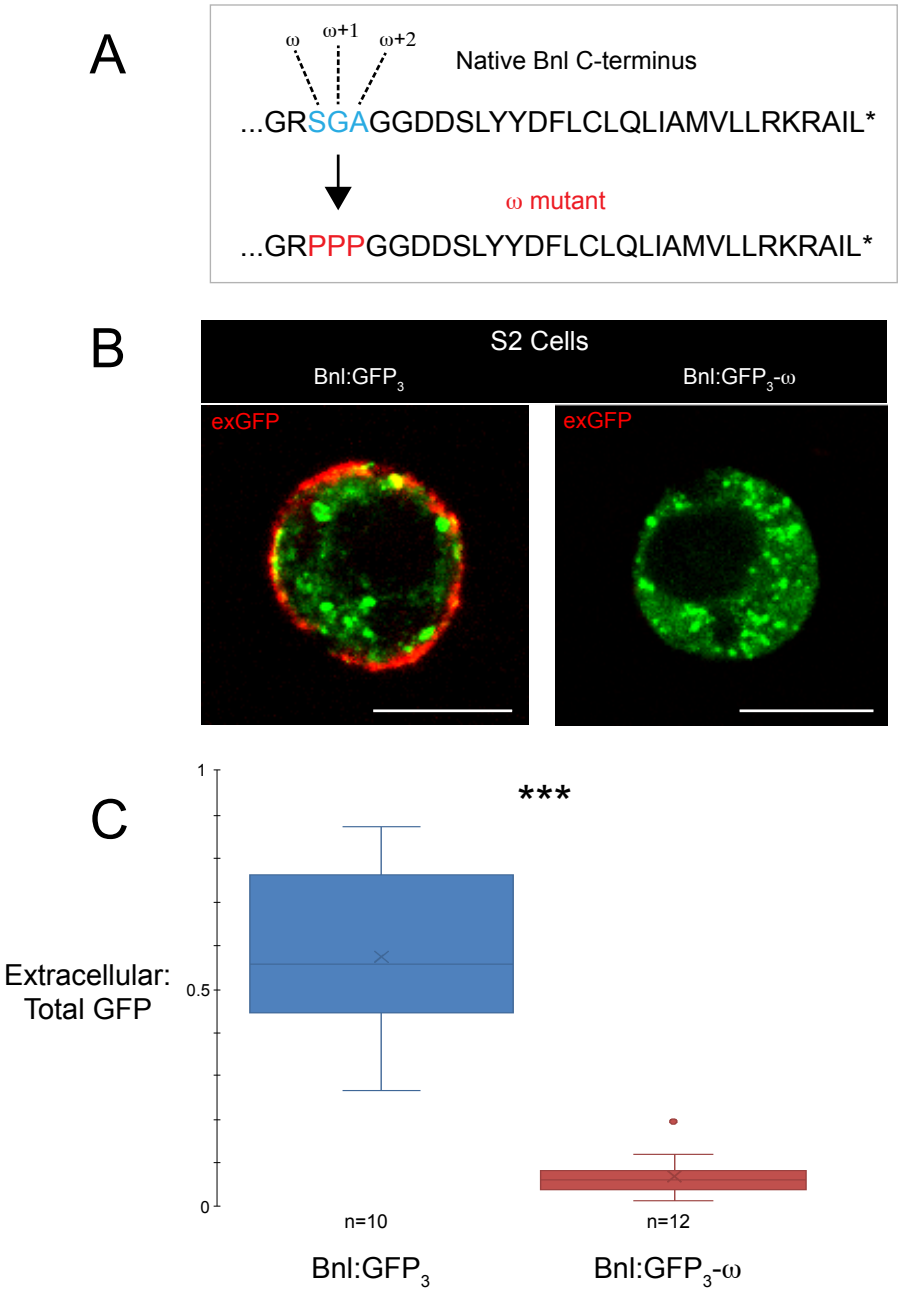

Figure 3-10: Bnl ω site mutation results in impaired surface localization

(A) Schematic of the generation of Bnl:GFP$_3$-ω mutant. The ω, ω+1, and ω+2 amino acids (S^{741}GA) were each substituted with proline in the Bnl:GFP$_3$ protein to create Bnl:GFP$_3$-ω. **(B)** S2 cells transfected with either Bnl:GFP$_3$ (left) or Bnl:GFP$_3$-ω (right) were stained with αGFP^{ex}. Little to no extracellular signal is seen on cells expressing Bnl:GFP$_3$-ω. **(C)** Graph of the extracellular:total GFP ratios shows that the control Bnl:GFP$_3$ surface levels are significantly higher than Bnl:GFP$_3$-ω ($p<0.001$). Scale bars: 10 μm.

disrupted ω site. The ω site as well as the two amino acids immediately downstream of the ω site (ω+1 and ω+2) are critical for GPI anchor addition and proline residues at these sites were shown to inhibit the addition of a GPI anchor (Moran et al., 1991; Eisenhaber et al., 1998). The amino acids at the ω, ω+1, and ω+2 sites were replaced with prolines to make the Bnl:GFP_3-ω construct (Figure 3-10, A). Interestingly, in contrast to the Bnl:GFP_3 control, Bnl:GFP_3-ω could not be detected on the extracellular surface of S2 cells (Figure 3-10, B and C). This result indicates that S741 is the ω site in the Bnl protein and ω site mutation disrupts the ability of the Bnl protein to be tethered to the outer surface of the cell membrane.

3.2.8 Bnl often colocalizes with Cholera-toxin subunit B on the cell surface

Previously, the membrane-binding subunit of cholera toxin, Cholera toxin subunit B (CT-B), was shown to be a *bona fide* marker of lipid rafts. CT-B targets the toxin to host cells by binding with high avidity up to five GM_1 gangliosides that are enriched in membrane rafts (Wolf et al., 1998; 2002). This feature enabled the commercially available non-toxic fluorophore-conjugated CT-B to be used as a common tool for lipid raft research. As GPI-anchored proteins are thought to localize in lipid rafts (Sangiorgio et al., 2004), Bnl might colocalize with CT-B. Indeed, S2 cells expressing Bnl:GFP_3 and stained with CT-B conjugated to Alexa-Fluor647 showed that Bnl does occasionally colocalize with CT-B on the surface of the cells (Figure 3-11). The inconsistency in colocalization of Bnl and CT-B is likely due to the dynamic membrane properties exhibited by GPI-anchored proteins (Saha et al., 2016). This data suggests that Bnl can localize in lipid rafts.

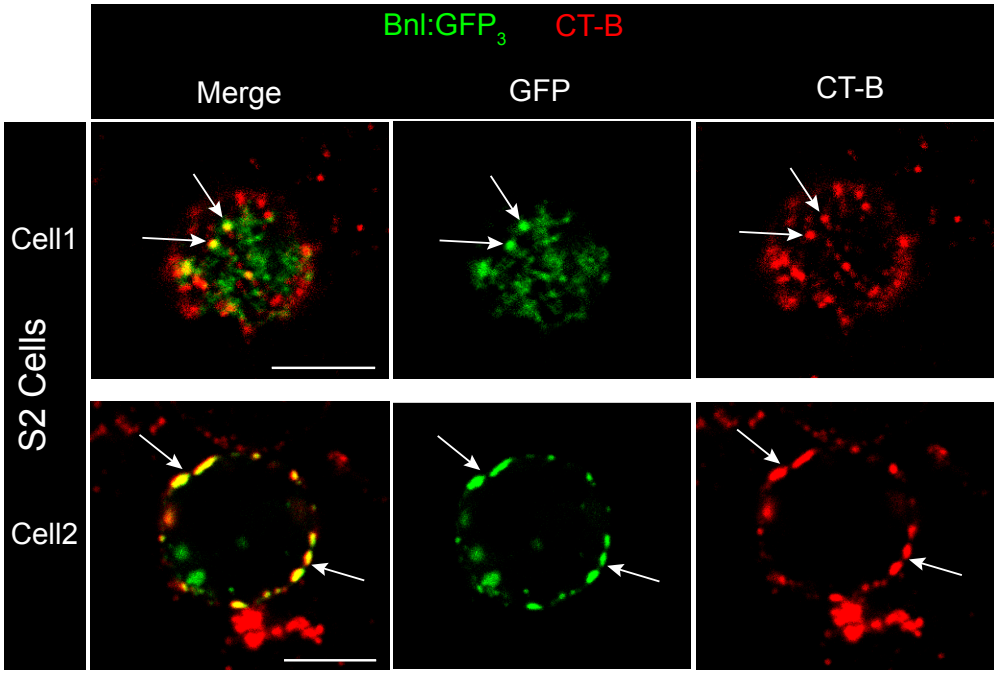

Figure 3-11: Cholera-toxin subunit B and Bnl:GFP$_3$ colocalization

S2 cells transfected with Bnl:GFP$_3$ were stained using Cholera-toxin subunit B (CT-B) conjugated with AlexaFluor-647 (red). Merged and individual channels are shown. Cell 1 is an optical image of a cell close to the coverslip, showing the membrane near the "top" of the cell. Cell 2 is an optical section of the middle of a cell. Bnl:GFP$_3$ colocalization with CT-B likely indicates that Bnl localizes in membrane microdomains, also known as lipid rafts. Scale bars: 10 μm.

3.2.9 Biochemical phase separation analysis of Bnl

Lipid raft association of GPI-anchored proteins is often biochemically determined by lysing cells that are expressing the protein in a detergent solution followed by induction of a phase separation that separates proteins into aqueous or detergent phases depending on their hydrophobicity. A strong detergent such as Triton-X114 is usually used to partition GPI-anchored and other integral membrane proteins into the detergent phase (Bordier, 1981). In this process, soluble proteins should theoretically localize in the aqueous phase while most membrane-bound proteins should partition to the detergent phase. To test how Bnl behaves when phases are

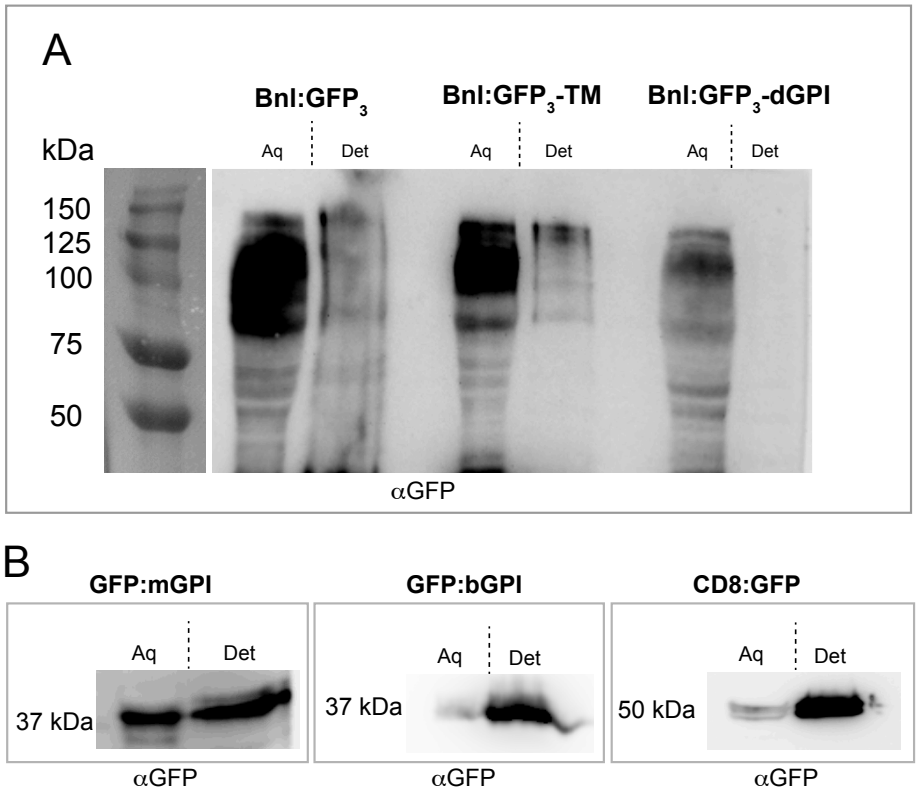

Figure 3-12: Phase Separation of Bnl constructs

(A) Western blot probing with αGFP of proteins isolated from S2 cells expressing Bnl:GFP_3, Bnl:GFP_3-dGPI, or Bnl:GFP_3-TM, as indicated. Following isolation of the proteins, each group was phase separated and the aqueous and detergent phases were isolated. Theoretically, the aqueous phase (Aq) contains hydrophilic proteins, while the detergent phase (Det) contains hydrophobic proteins, including GPI-anchored proteins. All proteins are seen to some degree in the aqueous phase. Low levels of Bnl:GFP_3 and Bnl:GFP_3-TM are observed in the detergent phase, while Bnl:GFP_3-dGPI is not detectable in the detergent phase. **(B)** Western Blots probing with αGFP of phase-separated GFP:mGPI, GFP:bGPI, and CD8:GFP from S2 Cells, as indicated. All of these samples are predominantly localized in the detergent phase after phase separation, with lower levels in the aqueous phase.

separated, S2 cells expressing Bnl:GFP_3, Bnl:GFP_3-dGPI, or Bnl:GFP_3-TM were lysed in a solution containing Triton-X114. Phase separation was induced as described in Chapter 5 (section 5.16) and the separated phases were examined by SDS-PAGE and Western Blotting. Low levels of Bnl:GFP_3 were detected in the detergent phase, but most Bnl:GFP_3 was localized in the aqueous phase. Surprisingly, Bnl:GFP_3-TM had a

very similar pattern to Bnl:GFP_3, where some of the isolated protein partitioned to the detergent phase, yet most was localized in the aqueous phase. Bnl:GFP_3-dGPI, on the other hand, followed the expected pattern and exclusively partitioned to the aqueous phase (Figure 3-12, A). The incomplete partitioning of Bnl:GFP_3 into the detergent phase is not too surprising, as proteins that are known to be GPI-anchored, such as *Drosophila* Mmp1 and Mmp2, were also detected in both the aqueous and detergent phases (LaFever et al., 2017). However, the finding that Bnl:GFP_3 and Bnl:GFP_3-TM were detected in the detergent phase while Bnl:GFP_3-dGPI exclusively partitioned to the aqueous phase may suggest a weak association of Bnl with detergent-resistant lipid rafts.

3.2.10 *In vivo* analysis of Bnl GPI anchoring

To test if the results implicating Bnl as a GPI-anchored protein in S2 cells were consistent *in vivo*, transgenic flies harboring either the *UAS-bnl:GFP_3-dGPI* or *UAS-bnl:GFP_3-TM* construct were generated and a method for treating wing discs with PI-PLC in *ex vivo* conditions was devised (see Chapter 5, section 5.19). Using *bnl-Gal4* to drive expression, Bnl:GFP_3, Bnl:GFP_3-dGPI, or Bnl:GFP_3-TM were expressed in the wing disc Bnl source cells. Next, live discs were dissected, incubated with or without PIPLC, and were then subjected to extracellular αGFP immunostaining. Without PI-PLC treatment, the extracellular profiles of the different Bnl constructs were consistent with their S2 cell profiles. Bnl:GFP_3 and Bnl:GFP_3-TM had strong extracellular signal on the Bnl-producing cells, while Bnl:GFP_3-dGPI exhibited no detectable extracellular surface staining on the source cells (Figure 3-13, A-C). *ex vivo* PI-PLC treatment of wing discs expressing Bnl:GFP_3 significantly reduced the levels

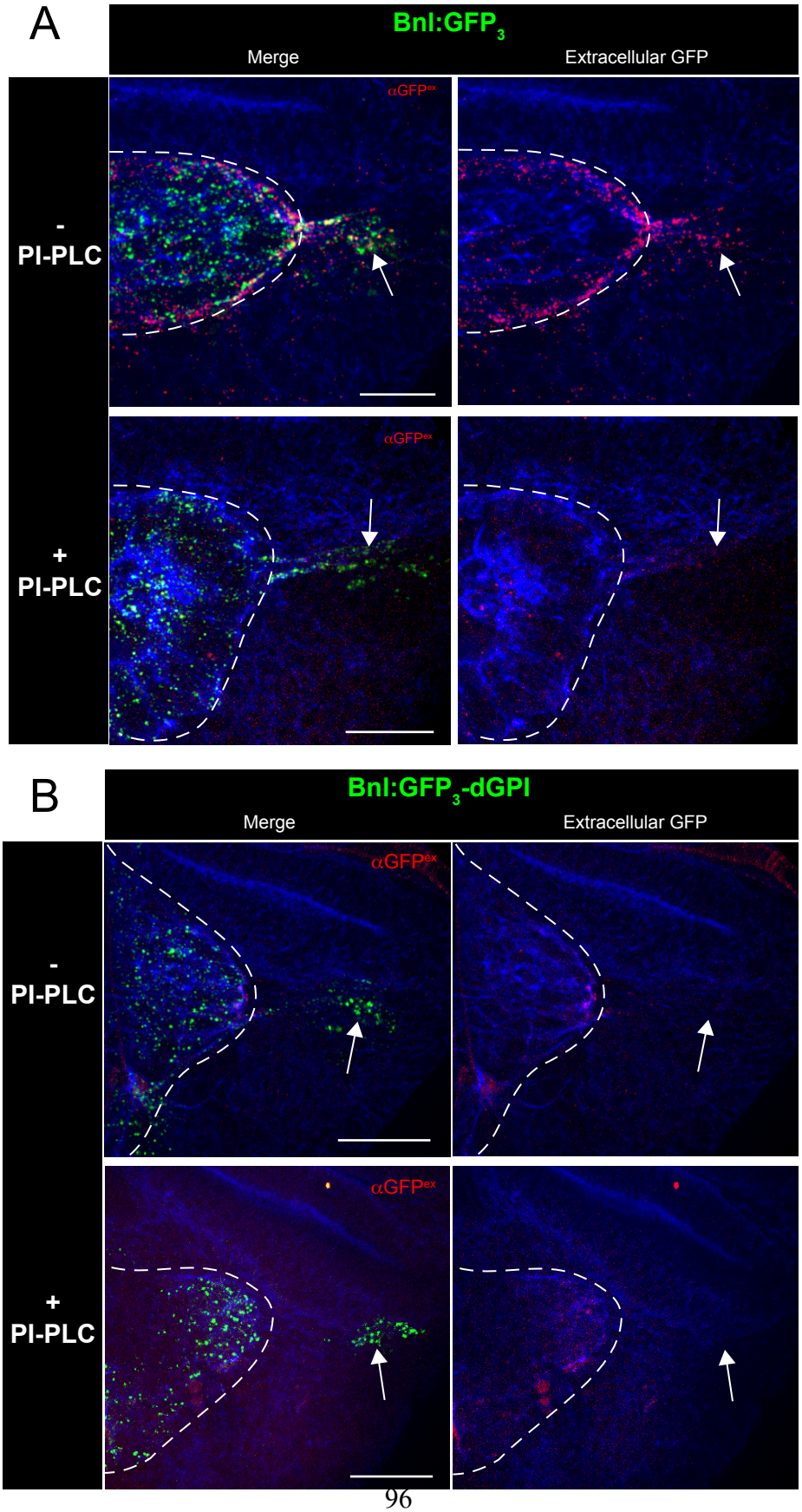
A
Bnl:GFP3
Merge
Extracellular GFP
αGFPex
-
PI-PLC
+
PI-PLC
B
Bnl:GFP3-dGPI
Merge
Extracellular GFP
αGFPex
-
PI-PLC
+
PI-PLC

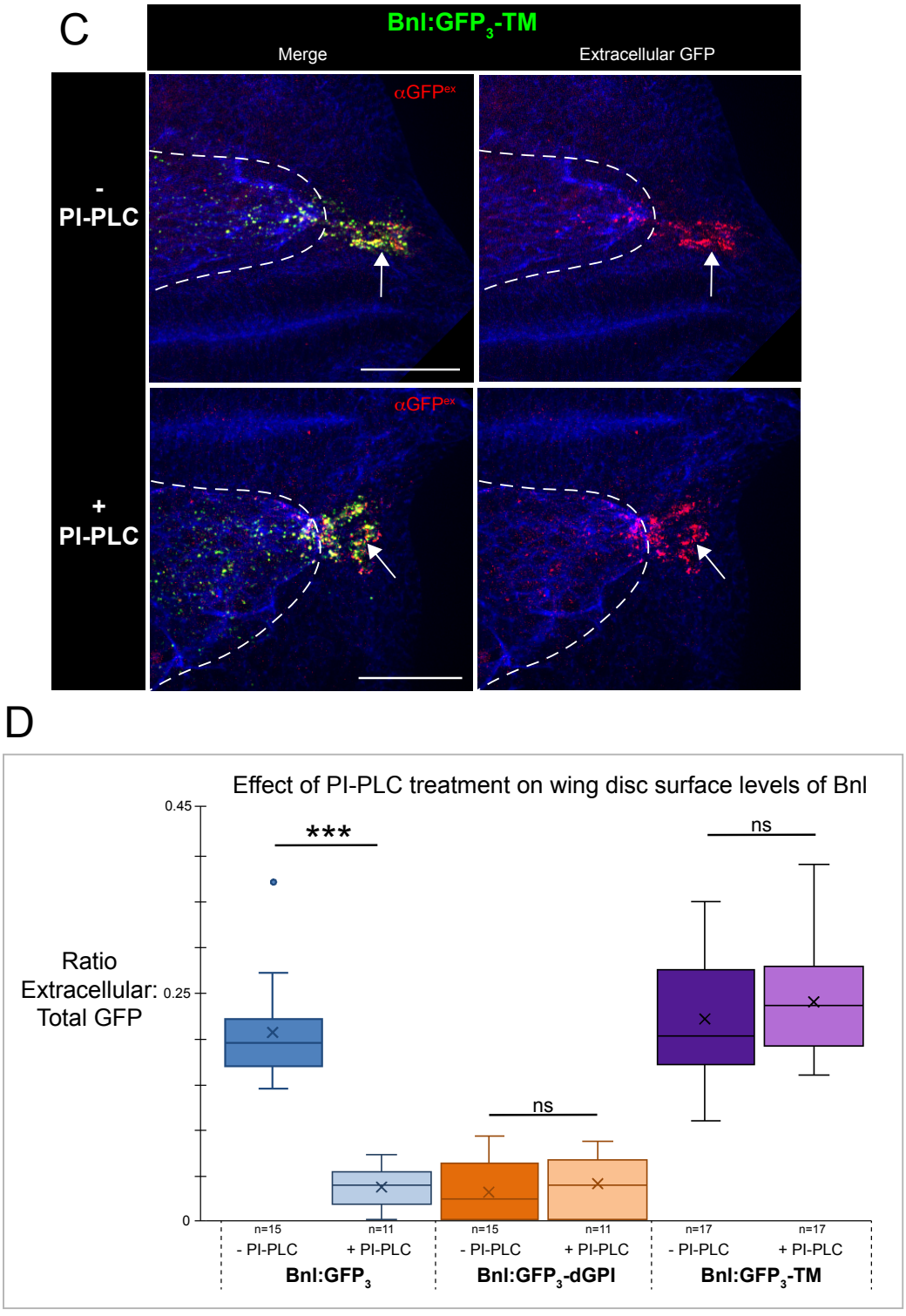

Figure 3-13: Bnl is GPI-anchored *in vivo*

(A-C) PI-PLC treatment on wing discs from flies expressing Bnl:GFP$_3$ (A), Bnl:GFP$_3$-dGPI (B), or Bnl:GFP$_3$-TM (C) under Bnl-Gal4 (*bnl-Gal4 x X*, where *X* = *UAS-bnl:GFP$_3$, UAS-bnl:GFP$_3$-dGPI,* or

UAS-bnl:GFP$_3$-TM). Discs were stained with αGFP^{ex} to visualize surface-localized signal. Merged and extracellular GFP channels are shown. (A-C) Top row: untreated discs. Bottom row: PIPLC-treated discs. **(D)** Graph showing the ratio of extracellular:total GFP fluorescence for the Bnl source cells in the wing disc. PI-PLC treatment significantly reduced the extracellular levels of Bnl:GFP$_3$ on the surface of the source cells ($p<0.001$), but did not significantly alter the levels of Bnl:GFP$_3$-dGPI or Bnl:GFP$_3$-TM on the source surface. Scale bars: 30 μm.

of extracellular Bnl:GFP$_3$ on the surface of the wing disc source cells yet had no effect on the extracellular distribution of Bnl:GFP$_3$-dGPI and Bnl:GFP$_3$-TM (Figure 3-13, A-D). Therefore, these results were in alignment with the data obtained from S2 cell culture and indicate that Bnl is likely GPI-anchored *in vivo.*

3.2.11 *In vivo* analysis of PIG-V knockdown

To determine if Bnl signaling is affected when GPI anchor biosynthesis is disrupted, the effect of PIG-V knockdown in the Bnl source cells was tested. PIG-V is a mannosyltransferase enzyme that is involved in adding the second mannose to the GPI anchor and is essential for normal GPI anchor biosynthesis (Kang et al., 2005). If GPI anchor biosynthesis disrupted Bnl signaling, it may nonautonomously affect growth of the recipient ASP. When RNAi against PIG-V was expressed in the Bnl source using *bnl-Gal4*, corresponding ASPs were abnormally shaped. (Figure 3-13). The ASP:wing disc length ratio was significantly lower in PIG-V RNAi animals compared to the control, showing that PIG-V knockdown ASPs are stunted. Furthermore, they contained significantly fewer cells compared to the control (Figure 3-13, B and C). This phenotype of the PIG-V knockdown ASPs mirrors that of a low level Bnl LOF phenotype (Sohr et al., 2019). These results showed that knockdown of GPI synthesis machinery in the Bnl-producing cells has a non-autonomous effect on

ASP growth and suggested that an intact GPI anchor biosynthesis pathway within the Bnl-producing cells is critical for normal Bnl signaling in the ASP.

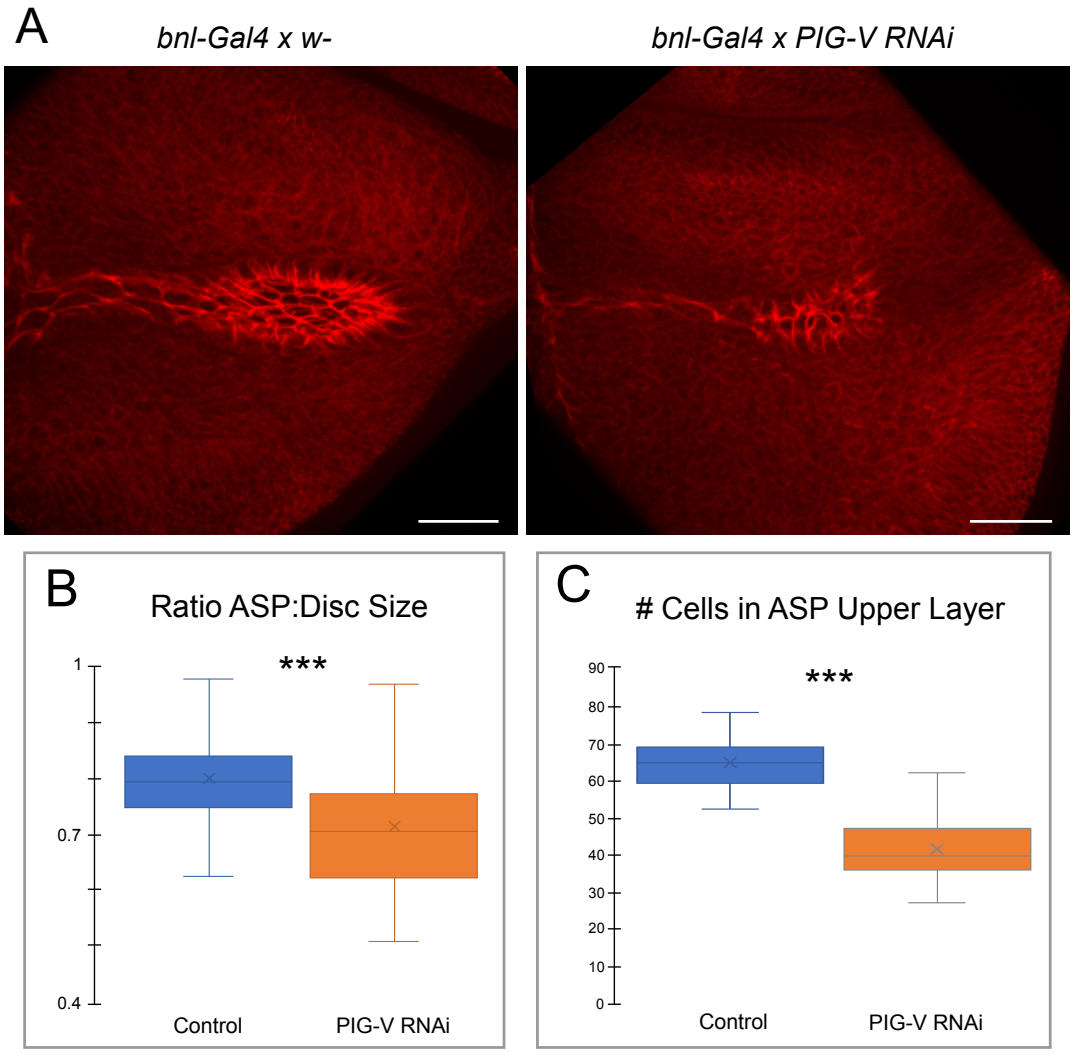

Figure 3-14: Knockdown of PIG-V in the Bnl source affects ASP growth

(A) Images of ASPs from the genotype as indicated, showing that knockdown of *PIG-V* in the Bnl source cells resulted in an abnormal ASP phenotype. **(B)** Graph comparing the ratio of ASP:Disc size for each group, showing that when *PIG-V* was knocked down in the wing disc Bnl source cells, the ASPs were significantly shorter and stunted compared to control ASPs ($p<0.001$, Control: *bnl-G4 x w-*, PIG-V RNAi: *bnl-G4 x PIG-V RNAi*). **(C)** Graph showing a significant reduction in number of cells in the ASP when RNAi against PIG-V was expressed in the Bnl source cells ($p<0.001$, same genotypes as (B)). Scale bars: 30 μm.

3.3 Discussion

In conclusion, these experimental results provide strong evidence that Bnl is modified with the addition of a GPI anchor in the endoplasmic reticulum of the source cells. This is a significant shift in our understanding of what was once thought to be a freely diffusible protein. Furthermore, since we now know that Bnl is transported along recipient cytonemes to the tracheal cells (Du et al., 2018a), the finding that Bnl is GPI-anchored is an important piece to the overall puzzle of the Bnl signaling process. If the Bnl protein were a freely diffusible protein, it would be difficult to regulate its release and transport by cytonemes. Instead, the tethering of Bnl via a GPI anchor allows it to be restricted and presented on the surface of the source cells until cytonemes make contact to receive the signal. This enables the signal to be tightly spatiotemporally regulated and ensures it signals in a target-specific manner.

Although GPI-anchored proteins are known to localize in the detergent-resistant membrane microdomains, Bnl:GFP_3 appeared to be weakly associated with the detergent-rich phase. One reason for such weak association could be that the lipid metabolism in *Drosophila* is different from mammalian cells for which the phase separation experiments at 37^{o}C were standardized. *Drosophila* doesn't thrive beyond 25^{o}C mainly because they lack C20 and C22 polyunsaturated fatty acids (PUFAs). The C20 and C22 PUFAs are critical structural components of the phosopholipids that mammalian cell membranes are comprised of (Shen et al., 2010). Therefore, since *Drosophila* contains fundamentally unique lipid components, the solubility of GPI anchors within the membrane may be altered, which could affect the TritonX-114 extraction and phase partitioning. Furthermore, it has been shown that GPI-anchored

proteins can be diffusely distributed within the plasma membrane, but that with the addition of detergent, GPI-anchored proteins actually redistribute into a more highly clustered conformation, likely into lipid rafts, meaning that GPI-anchored proteins are inherently difficult to dissolve in detergent (Mayor and Maxfield, 1995). In addition to the above possibilities, it is also likely that this method needs to be refined in order to more efficiently separate GPI-anchored proteins and other proteins that contain hydrophobic regions into the detergent phase. For example, the solubility of GPI-anchored proteins is affected by several factors, such as temperature of phase separation and concentration of detergent in solution (Melkonian et al., 1995), so additional conditions may need to be tested in order to optimize the phase separation protocol. However, while examining the phase separation of various proteins, there was a very interesting additional finding that might suggest an uncharacterized regulation of Bnl. GFP:mGPI and GFP:bGPI proteins predominantly partitioned into the detergent phase with relatively low levels in the aqueous phase (Figure 3-12, B). Since GFP:bGPI was created by fusing the GPI signal sequence from Bnl onto the C-terminal end of GFP, it is very intriguing that it strongly partitions to the detergent phase while Bnl:GFP_3 does not. This might suggest that some sequence within the Bnl protein other than the GPI anchor affects its association with the detergent-resistant membrane or perhaps its trafficking within the membrane. This possibility is also supported by the finding that CD8:GFP strongly partitions to the detergent phase as well, but Bnl:GFP_3-TM does not. Bnl:GFP_3-TM was created by replacing the GPI-anchored region in the C-terminus of Bnl with the transmembrane domain from the CD8 portion of CD8:GFP. Thus, it would make sense for Bnl:GFP_3-TM to also partition to the detergent phase similar to

its CD8:GFP counterpart, and yet Bnl:GFP_3-TM localizes mostly in the aqueous phase. This somewhat contradicting result is consistent with the phase separation patterns of GFP:bGPI and Bnl:GFP_3. As GFP:mGPI also localizes predominantly in the detergent phase, it will be essential to create Bnl:mGPI to see if it causes a shift into the aqueous phase as well. If so, this could further confirm that some domain or characteristic of the Bnl protein upstream from the GPI-anchored C-terminus may influence its hydrophobicity and localization within the membrane. Another interesting experiment could be to test phase separation of the uncleaved M1 mutant form of Bnl. It is possible that the cleavage of Bnl, which is a necessary step in its maturation and for its intracellular trafficking, could also somehow affect its membrane localization or trafficking within the membrane. More research needs to be done to examine if and how components within Bnl affect its membrane trafficking and inclusion in membrane microdomains.

Another interesting direction would be to examine if FGFs in other insect species are also lipidated. A phylogenetic analysis was carried out to test if relatives of the Bnl protein in other insect species are also predicted to be GPI-anchored. After compiling and aligning sequences obtained from Bnl protein blast hits, the alignment was organized into a phylogenetic tree. PredGPI (Pierleoni et al., 2008) was used to determine which Branchless homologs are predicted to be GPI-anchored. Interestingly, other than *Drosophila melanogaster* Branchless, only the Branchless homologs in *Drosophila erecta, Stomoxys calcitrans,* a closely related fly, and *Anoplophora glabripennis*, the Asian long-horned beetle, are predicted to be GPI-anchored (Figure 3-15). All other insect Branchless homologs that were analyzed in silico and also mouse

and human Fgf10 were not predicted to be GPI-anchored. However, it is still possible that other Bnl homologs are tethered to the surface of the membrane by an alternative mechanism, such as a cholesterol or palmitic acid lipid modification.

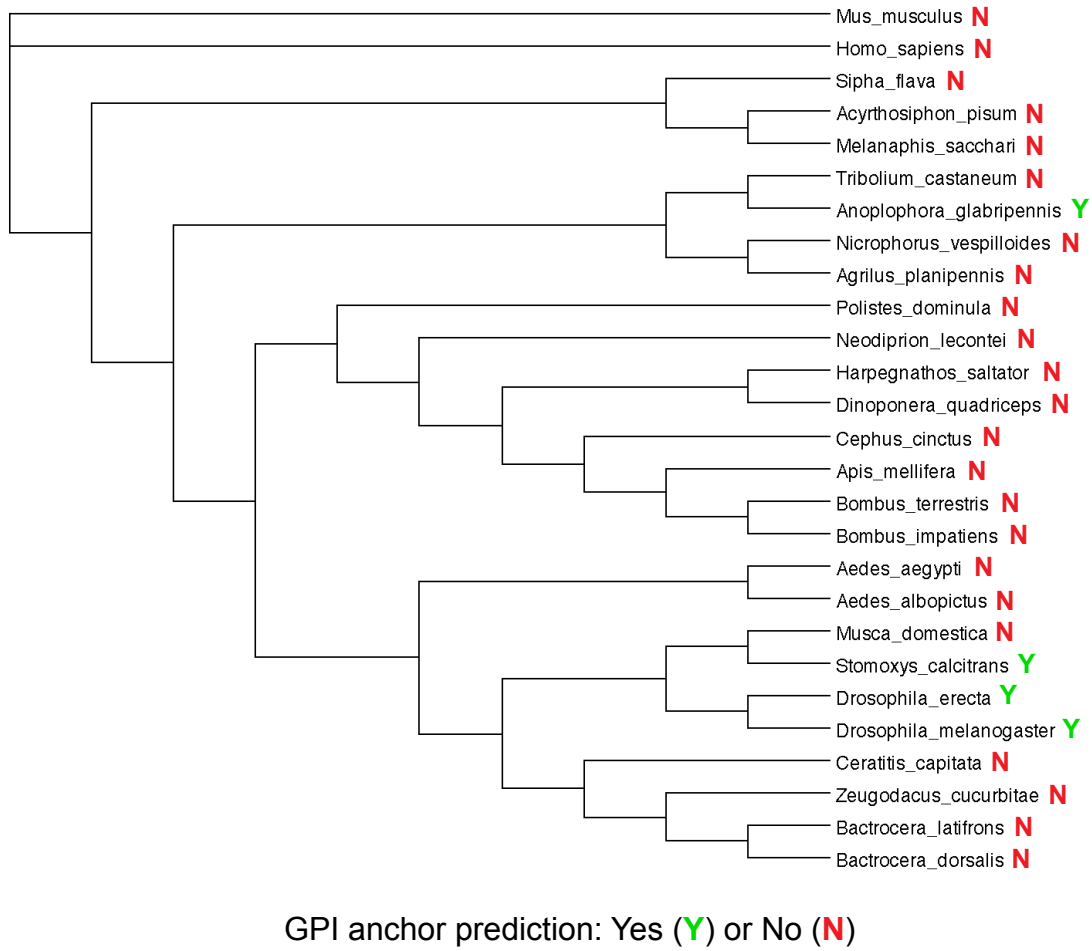

Figure 3-15: Phylogenetic analysis of Branchless and GPI anchor prediction of homologs

Phylogenetic analysis of *Drosophila* Branchless was performed and the closest insect orthologs are shown (indicated as genus and species name), as well as mouse and human Fgf10. Using PredGPI (Pierleoni et al., 2008), each Branchless ortholog was tested to determine if they were predicted to be GPI-anchored (Yes: Green "Y", No: Red "N").

Chapter 4: Summary and Future Directions

4.1 Summary

Prior to this research, intracellular regulation of FGF trafficking and its lipid modification were unknown. Overall, this work discovered two mechanisms that help control cytoneme-mediated Bnl signaling (Figure 4-1). This study revealed how the FGF Branchless is controlled for polarized trafficking within the source cells and that Bnl is tethered to the membrane via a GPI anchor. Both of these post-translational modifications are necessary for Bnl to properly signal and guide the morphogenesis of the *Drosophila* tracheal network.

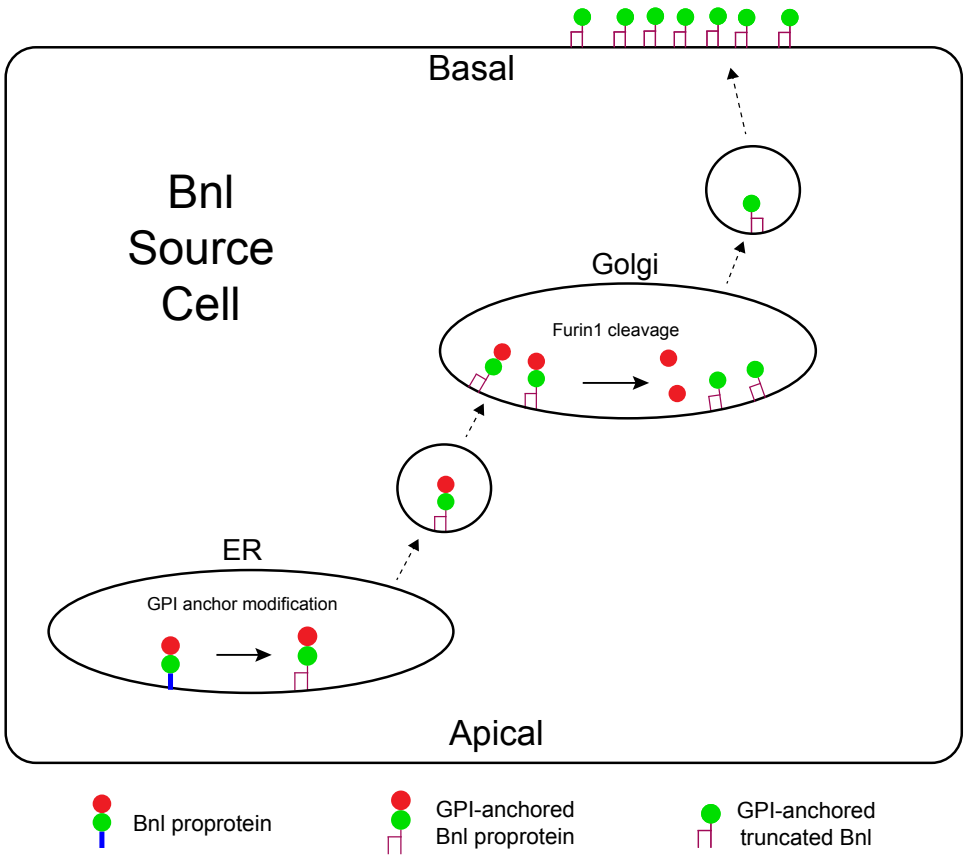

Figure 4-1: Summary of findings

Schematic summarizing the main findings is shown. In the ER, the C-terminus of the Bnl proprotein (blue) is cleaved off and replaced with a GPI anchor. The GPI-anchored Bnl proprotein is then transported to the Golgi, where Furin1-mediated cleavage removes the N-terminal prodomain of Bnl (red). The GPI-anchored, truncated Bnl is asymmetrically transported to the basal surface of Bnl-producing cells where it is tethered on the outer leaflet of the membrane for subsequent retrieval by recipient cell cytonemes.

Based on the localization and activity of separate GFP fusions in the Bnl protein, we suspected that Bnl was proteolytically cleaved prior to its transport to recipient cells. Using a dual-tagged Bnl:HA_1GFP_3 protein, this cleavage was confirmed and the precise site of cleavage in the protein was identified by mutating putative cleavage sites. Next, it was determined that the cleavage is mediated by Furin1 in the Golgi of the source cells. Using CRISPR/Cas-9 genome editing technology, it was shown that when cleavage of the Bnl protein is blocked, signaling is affected, as uncleaved Bnl exhibits a loss of function phenotype. Interestingly, it was confirmed that the uncleaved endogenous form of Bnl could still bind to its receptor, Btl, travel to the ASP, and activate signaling in the recipient cells. However, the levels of uncleaved Bnl traveling to the ASP were significantly reduced, resulting in the loss of function phenotype. An extracellular stain to examine levels of Bnl on the surface of the source cells revealed that the amount of externalized uncleaved Bnl was significantly reduced compared to cleaved Bnl. Within the source cells, it was apparent that cleaved Bnl is preferentially trafficked to the basal surface, which is the only surface that recipient cytonemes can contact to receive the signal. However, uncleaved Bnl was more randomly trafficked within the source cells and instead localized predominantly at the apical domain of the source cells, which is inaccessible to the recipient cytonemes. Thus, the cleavage of Bnl ensures that it is transported to the location in the source cells

where it can be received by recipient cytonemes. When this cleavage is inhibited, the result is a reduced bioavailability of the signal, and although it is still an active signal, the recipient tissue does not receive enough to grow normally.

This study also demonstrated that Bnl localizes on the outer surface of the producing cells, which is consistent with the previous observation of contact-dependent Bnl dispersion through cytonemes (Du et al., 2018a). Examination of a Bnl protein that contained both an intramolecular and also a C-terminal fluorophore (Bnl:$GFP_3Cherry_c$) suggested that the C-terminal hydrophobic stretch of Bnl is cleaved and separated from the rest of the mature protein. This observation, along with the extracellular surface localization of Bnl, led to the hypothesis that Bnl is post-translationally modified with a GPI anchor. Next, various assays were employed to test if Bnl is GPI-anchored. Treatment of cells or tissues with PI-PLC, an enzyme that cleaves within the lipid portion of a GPI anchor, specifically shed Bnl from the membrane of producing cells both *in vitro* and *in vivo.* Furthermore, deletion of the Bnl C-terminus (Bnl:GFP_3-dGPI) eliminated the ability of Bnl to localize on the extracellular surface of producing cells and replacement of the C-terminus with a transmembrane domain (Bnl:GFP_3-TM) resulted in it being tethered to the extracellular surface regardless of PI-PLC treatment conditions. Bnl frequently colocalized with cholera toxin subunit-B (CT-B), which is used to label lipid rafts where GPI-anchored proteins are thought to localize. Phase separation of proteins enabled the independent isolation of hydrophobic membrane-associated proteins and hydrophilic proteins and showed that Bnl:GFP_3 localized in the detergent phase, unlike Bnl:GFP_3-dGPI, which only localized in the aqueous phase. Mutation of the predicted Bnl ω site, the site where GPI anchor modification to the

protein occurs, inhibited the ability of Bnl to localize on the extracellular surface. Thus, the exact site of GPI anchor modification in the Bnl protein was identified. Finally, knockdown of a key member of the GPI anchor biosynthesis pathway in the Bnl-producing wing disc cells resulted in a non-autonomous defect in ASP growth, indicating that GPI anchoring of Bnl is critical for normal signaling *in vivo.* Taken together, all of these results demonstrate that Bnl is a GPI-anchored protein and that this post-translational modification is critical for its signaling function *in vivo*.

4.1 Future Directions

The finding that Bnl cleavage results in altered trafficking of the protein naturally leads to the question of how this cleavage can affect Bnl trafficking within the source cells. One likely scenario is that Bnl cleavage affects its protein-protein interactions within the source cells. It appears that apical sorting is the predominant pathway for full-length Bnl. Therefore, cleavage and removal of the prodomain of Bnl may expose a domain within Bnl that allows it to interact with a protein that chaperones it to the basal domain of the source cells. Alternatively, the prodomain of Bnl could be interacting with a protein that influences it towards the apical sorting pathway, and proteolytic removal of the prodomain redirects truncated Bnl towards the basal sorting pathway. A combination of both of these possibilities could also occur to control Bnl trafficking. More research performed on protein-protein interactions of Bnl, either through biochemical analyses like co-immunoprecipitation or imaging assays such as BiFC (Bimolecular Fluorescence Complementation) could shed more light on how Bnl cleavage affects its intracellular trafficking.

Intriguingly, GPI-anchored proteins have been shown to preferably sort to the apical domain of polarized cells (Helms and Zurzolo, 2004; Schuck and Simons, 2006; Zurzolo and Simons, 2016). However, although Bnl is GPI-anchored, truncated Bnl is predominantly sorted to the basal domain. It will be interesting to examine how the GPI anchoring of Bnl and the proteolytic cleavage in the Golgi cooperate in directing Bnl to the correct location within the source cells. Possibly, full-length Bnl is apically targeted because of its GPI anchor but the cleavage of Bnl somehow enables it to override this signal and sort to the basal domain. It was found that unlipidated Hh was internalized into recipient cells from the basal surface, while lipid-modified Hh was internalized through the apical surface (Callejo et al., 2006). Therefore, in addition to proteolytic cleavage, lipidation could also play a key role in how Bnl is trafficked and released from source cells. Further analysis on the trafficking of Bnl:GFP_3-dGPI and Bnl:GFP_3-TM could help answer how the GPI anchor in Bnl affects the trafficking within source cells.

As Bnl is eventually endocytosed into the Btl-expressing recipient cells, the GPI anchoring of Bnl brings forth a very interesting question: How is Bnl released from the source cell membrane such that it can be received and endocytosed by recipient cells? It seems likely that an additional cleavage upstream of the GPI anchor is required to shed Bnl from the membrane to enable its transport and endocytosis. In Hh signaling, membrane-tethered Hh is released from the membrane via MMP cleavage (Dierker et al., 2009). In a conceptually similar signaling mechanism to Bnl/Btl in which two membrane-anchored proteins interact, Notch/Delta signaling also involves shedding of Notch from the membrane. It is thought that Notch/Delta binding and interaction

induces a conformational change in Notch that exposes a site for an ADAM (a disintegrin and metalloprotease) protease that sheds Notch from the membrane in a type of "lift and cut" mechanism (van Tetering and Vooijs, 2011). It will be interesting to investigate whether a similar mechanism is relevant for Bnl signaling as well.

In the classical RTK signaling pathway, ligand binding induces receptor dimerization which transmits the signaling cascade to within the recipient cell body. However, Bnl/Btl signaling represents an interesting case of RTK signaling since receptor binding actually takes place on cytonemes far from the recipient cell body (Du et al., 2018a). Examination of where downstream signaling events actually occur could open up a new field of how the RTK downstream signaling components are trafficked within the recipient cells. An intriguing example is the protein Dof, which constitutively binds to the cytosolic domain of FGFR/Btl to transduce the signal after receptor dimerization. Since Bnl/Btl interaction occurs at the cytoneme-source contacts, is this also where Dof begins its signal-transducing activity? Thus, cytoneme-mediated signaling may provide a new perspective on how a signal is transduced in the recipient cells.

Chapter 5: Materials and Methods

5.1 *Drosophila* strains and genetic crosses

All crosses were incubated at 25°C. The following strains were used in this study:

Bloomington Stock Center: *UAS-bnlRNAi (#34572), fur1-LacZ (#10341), UAS-fur1RNAi (#25837), UAS-fur1RNAi (#42481), UAS-fur1RNAi (#41914), UAS-fur2RNAi (#51743), UAS-fur2RNAi (#42577), UAS-fur1 (#63077), UAS-fur1-X (#63078), UAS-fur1-CRR (#63079)*.

Other sources: UAS_{attB}*-Bnl:GFP*$_1$, UAS_{attB}*-Bnl:GFP*$_2$, UAS_{attB}*-Bnl:GFP*$_3$, UAS_{attB}*-Bnl:GFP*$_4$, UAS_{attB}*-Bnl:HA*$_1$, UAS_{attB}*-Bnl:HA*$_2$, UAS_{attB}*-Bnl:HA*$_3$, UAS_{attB}*-Bnl:HA*$_4$; *fur2-Gal4 (NP 4074; Kyoto #104593); UAS-CD8:GFP, UAS-CD8:Cherry, btl-Gal4*, *bnl-Gal4* (Roy et al., 2014); *bnl:gfp*^{endo}, *btl:cherry*^{endo} (Du et al., 2018a); *bnl-LexA* (Du et al., 2017).

This study: *UAS-Bnl:GFP*$_1$, *UAS-Bnl:HA*$_1$, *UAS-Bnl:GFP*$_2$, *UAS-Bnl:GFP*$_3$, *UAS-Bnl:HA*$_3$, *UAS-Bnl:GFP*$_4$, *UAS-Bnl:HA*$_1$*GFP*$_3$, *UAS-Bnl:HA*$_1$*GFP*$_3$*-M1*, *UAS-Bnl:HA*$_1$*GFP*$_3$*-M2*, *UAS-Bnl:HA*$_1$*GFP*$_3$*-M1M2*, *bnl:HA*$_1$*GFP*$_3^{endo}$, *bnl:HA*$_1$*GFP*$_3$*-M1*^{endo}, *UAS-Bnl:GFP*$_3$*Cherry*$_c$, *UAS-Bnl:HA*$_1$*GFP*$_3$*-dGPI, UAS-Bnl:HA*$_1$*GFP*$_3$*-TM.*

5.2 Cloning and generation of transgenic *Drosophila* lines

UAS-bnl:GFP and *UAS-bnl:HA* variants

Each of the four Bnl:GFP variants contained an HA-tag upstream to a GFP tag at a single internal site. Bnl:GFP$_1$ contained both HA and GFP tags in tandem inserted between amino acids RSSLVPSAVS^{87} and E^{88}RSVNQPT. Bnl:GFP$_2$ contained the

tags inserted between amino acids SNLDRNERST^{206} and V^{207}PQSHLAWTS. Bnl:GFP$_3$ contained the tags inserted between amino acids KAPPHCSSNT^{432} and S^{433}GSSSSISSS. Bnl:GFP$_4$ contained the tags between amino acids MSSGEEQDQDN^{701} and D^{702}QDQEQSDPGE. Previously, transgenic *Drosophila* lines harboring the Bnl:GFP$_3$ construct at various *attP* loci in the 2nd and 4th chromosomes did not show any detectable Bnl:GFP$_3$ expression when driven by *bnl-Gal4*. Therefore, we subcloned the Bnl:GFP constructs in pUAST vector from the original pUAST-attB constructs and resorted to the random P-element-based transgenesis to avoid any positional effects on Bnl:GFP expression. P-element based transgenesis was carried out as described earlier (Du et al., 2017).

UAS-bnl:HA$_1$GFP$_3$ and LexO-bnl:HA1GFP3

UAS-bnl:HA$_1$GFP$_3$ contained an HA-tag at site 1 (between 87 and 88 amino acid residues of the original protein) and a superfolder (sf) GFP (Pédelacq et al., 2006) at site 3 (between 432 and 433 residues of the original protein). The construct was generated by overlap extension PCR of three fragments using primers (see "Primers"): the N-terminal HA-tagged part, the C-terminal Bnl coding region (amplified from the pUAST-attB-Bnl:HA$_1$, and the middle sfGFP region from a sfGFP-containing construct (Addgene). The final 3060 bp PCR product was cloned into the pCR-Blunt II-TOPO vector. The fully sequence-verified insert was sub-cloned into the pUAST vector at the BglII and XbaI sites. *UAS-bnl:HA$_1$GFP$_3$* was used for analysis in S2 cells and for P-element mediated germline transformation and transgenesis. *LexO-*

bnl:HA$_1$GFP$_3$ was cloned using the BglII and XbaI sites to release *bnl:HA$_1$GFP$_3$* from pUAST and sub-clone this fragment into the pLOT vector.

UAS-bnl:HA$_1$GFP$_3$ mutants

The M1 and M2 variants of Bnl:HA$_1$GFP$_3$ contained the following cleavage site mutations: M1 contained (R/G)TE(R/G)SI(R/G) and M2 contained (R/G)NE(R/G). These mutant constructs were created using overlap extension PCR (see "Primers") with the Bnl:HA$_1$GFP$_3$ construct as a template. The final assembled PCR product was cloned into the pCR-Blunt II-TOPO vector. The sequence-verified constructs were subcloned into the BglII and XbaI sites of the pUAST vector for either analysis in S2 cell culture or for P-element mediated germline transformation and transgenesis.

UAS-bnl:HA$_1$GFP$_4$ and *UAS-bnl:GFP$_1$HA$_4$*

UAS-bnl:HA$_1$GFP$_4$ was cloned using overlap extension PCR to insert a GFP tag at site 4 of *UAS-Bnl:HA$_1$*. Similarly, *UAS-bnl:GFP$_1$HA$_4$* was cloned using overlap extension PCR (see "Primers") to insert a GFP at site 1 of *UAS-bnl:HA$_4$*. These constructs were verified and used in S2 cell culture analyses.

UAS-bnl:GFP$_3$Cherry$_c$

A cherry tag was added to the C-terminus of *bnl:HA$_1$GFP$_3$* by using PCR to amplify *bnl:HA$_1$GFP$_3$* with a C-terminal Cherry overhang (Fragment 1) and Cherry with an N-terminal *bnl:HA$_1$GFP$_3$* overhang (Fragment 2, See "Primers"). These fragments were assembled together into the puc19 vector using Gibson assembly and were

subsequently subcloned into the BglII and Acc65I sites of the pUAST vector for analysis in S2 cell culture or for P-element mediated germline transformation and transgenesis.

UAS-bnl:GFP$_3$-dGPI

To create *bnl:GFP$_3$-dGPI*, a stop codon was inserted into *bnl:HA$_1$GFP$_3$* via PCR after residue Y730 in native Bnl (see "Primers"). This PCR product was cloned into the puc19 vector using Gibson Assembly. Then, the *bnl:HA$_1$GFP$_3$-dGPI* construct was subcloned into the BglII and Acc65I sites of the pUAST vector for analysis in S2 cell culture or for P-element mediated germline transformation and transgenesis.

UAS-bnl:GFP$_3$-TM

The *bnl:GFP$_3$-TM* construct contains a transmembrane domain (TM) at the end of *bnl:GFP$_3$-dGPI.* PCR was used to amplify the transmembrane domain of the mouse CD8 protein with *bnl:GFP$_3$-dGPI* overhang at the N-terminus (Fragment 1). PCR was also used to amplify *bnl:GFP$_3$-dGPI* with the transmembrane domain overhang at the C-terminus (Fragment 2, see "Primers"). These fragments were cloned into the puc19 vector using Gibson assembly to fuse the transmembrane fragment to the *bnl:HA$_1$GFP$_3$-dGPI* fragment after residue Y730 in native Bnl. The *bnl:HA$_1$GFP$_3$-TM* construct was subcloned into the BglII and Acc65I sites of the pUAST vector for analysis in S2 cell culture or for P-element mediated germline transformation and transgenesis.

UAS-bnl:HA$_1$GFP$_3$-ω

The ω mutant was made with PCR using overlapping primers to create two PCR fragments, one that included the N-terminal portion of Bnl with the mutations in the C-terminus of the PCR product (Fragment 1), and the other contained the C-terminal portion of Bnl with the mutations in the N-terminus of the PCR product (Fragment 2, "See Primers). These fragments were assembled into the puc19 vector and fully sequence verified. Then, the *bnl:HA$_1$GFP$_3$-ω* construct was cloned into the BglII and XbaI sites of the pUAST vector for analysis in S2 cell culture.

UAS-bnl:GFP$_1$ cleavage site mutants: The *UAS-bnl:GFP$_1$-M1, UAS-bnl:GFP$_1$-M2,* and *UAS-bnl:GFP$_1$-M1M2* mutants were created using PCR with the *bnl:GFP$_1$* template using the same primers (see "Primers") and strategies that were used to create the mutants in the *bnl:HA$_1$GFP$_3$* protein. These constructs were analyzed biochemically from S2 cell culture.

UAS-hFgf10:HA,GFP

The HA and GFP insertions were cloned into *hFgf10* using PCR and Gibson assembly to stitch together four separate fragments into the puc19 vector: Fragment 1: N-terminus to the HA insertion site; Fragment 2: HA insertion to the GFP insertion site; Fragment 3: GFP fragment containing *hFgf10* overhangs; Fragment 4: GFP insertion site to the C-terminus (see "Primers"). Once fully sequenced, the *hFgf10:HA,GFP* construct was subcloned into the BglII and XbaI sites of the pUAST vector for analysis in S2 cell culture.

5.3 CRISPR/Cas9-based genome editing

The *bnl:HA$_1$GFP$_3$^{endo}* and *bnl:HA$_1$GFP$_3$-M1^{endo}* mutant alleles were generated by in frame insertion of an HA-tag into the first coding exon of a previously characterized *bnl:sfGFP$_3$^{endo}* allele (Du et al., 2018a) using CRISPR/Cas9-based genome editing following previously described protocols (Du et al., 2017; 2018b). The *bnl:HA$_1$GFP$_3$-M1* mutant allele includes the HA$_1$ tag as well as mutations of three Arginines (R) to Glycines (G) at PCS1 that starts 82 amino acids upstream of the conserved FGF domain. For targeting a Cas9-based double-stranded break near tag site 1, a guide RNA (BnlHA1gRNA- CTACGTTCACTCACTGCGCTCGG (underlined bases represent the PAM site)) with zero off targets in the fly genome was cloned by ligating two annealed complimentary oligos into the pCFD3 vector (see "Primers").

The replacement donors, *pDonor-bnl:HA$_1$GFP$_3$* and *pDonor-bnl:HA$_1$GFP$_3$-M1* were designed and generated following Du et al. (2017). These constructs contained either HA$_1$ or the HA$_1$-M1 mutations flanked by ~1 kb long 5'- and 3'- arms that are homologous to the genomic sequence flanking tag site 1. Both 5'- and 3'- homology arms were PCR-amplified from genomic DNA from the *nos-Cas9;;bnl:GFP$_3$^{endo}* parent fly, sequence verified, and assembled together into the pUC19 vector using Gibson Assembly (see "Primers"). To prevent retargeting of the gRNA/Cas9 to the edited genome, a synonymous mutation was introduced into the replacement cassette near the PAM sequence via the primers used for amplification (see "Primers"). The constructs were fully sequenced prior to germline injection.

The gRNA-expressing vector and the respective replacement donor vector were co-injected into the germline cells of *nos-Cas9;;bnl:sfGFP$_3$^{endo}* embryos. For each

genome-editing experiment, a step-wise crossing strategy (Du et al., 2018b) was followed to obtain G0-F2 progenies and establish individual fly lines for screening. The desired "ends-out" homologous directed repair (HDR) was screened for by a three step PCR-based strategy (see "Primers"), followed by sequencing and analyses of tissue-specific expression patterns of the tagged genes under a confocal microscope. The efficiency of genome editing-based generation of the two different genotypes and their phenotypes are summarized in Sohr et al. (2019). During generation of *bnl:HA_1GFP_3-M1 ^{endo}* several lines were obtained that had only the HA_1 insertion without the M1 mutation. We predicted that the HDR had taken place somewhere between the HA_1 tag site and M1 mutation sites (219 bases apart). These lines were fully sequence-verified and found to have normal tissue expression. Therefore, these lines were considered as *bnl:HA_1GFP_3 ^{endo}* lines. For subsequent analyses, we used a *wt^{endo}* and an *$m1^{endo}$* line derived from the same genome-editing experiment. The *wt^{endo}* F4-14 line and *$m1^{endo}$* F4-9 line used in this study were fully sequence verified and established after outcrossing as previously described (Du et al., 2018a).

5.4 Synthesis of double stranded RNA for gene knockdown in S2 cells

Double stranded RNA (dsRNA) was synthesized by PCR from genomic DNA isolated from S2 cells following a previously described protocol (Künnapuu et al., 2009). The following PCR primers were used to synthesize the T7 transcription template carrying the T7 promoter sequence at their 5' ends:

For *fur1*

Fwd: TAATACGACTCACTATAGGGACGCAAAGATCCTCTGTGGCA

Rev: TAATACGACTCACTATAGGGACATTGCTCCCGGAACTGC

For *fur2*

Fwd: TAATACGACTCACTATAGGGACGCTAGAGGCCAATCCGGAA

Rev: TAATACGACTCACTATAGGGACCCTTCTCGCCCCAAAAGTG

Double stranded RNA against *fur1* or *fur2* were synthesized using the MEGAscript RNAi Kit (ThermoFisher).

5.5 Fluorescence in situ hybridization

To probe for *fur1* and *fur2* mRNA, the desired probe regions of 540 bp and 552 bp were PCR-amplified with primers (see "Primers") from respective cDNAs and cloned using Gibson assembly into pSPT18 vector. The vector was linearized and the RNA probe was prepared using the DIG-RNA Labeling Kit (Roche) according to the manufacturer's protocol. RNA *in situ* hybridization on third-instar larval tissues was performed as previously described (Du et al., 2017). Hybridized probes were detected using α-Dig antibody followed by immunofluorescence with Alexa-647-conjugated secondary antibody.

5.6 Cell culture assay

S2 cells were cultured in 25 cm^2 flasks using Shields and Sang M3 insect media (Sigma Aldrich). For transfection, when cells were ~90% confluent, the media was removed and 6 mL of fresh M3 media was added to the flask. Cells were gently resuspended by pipetting and added to a 12-well plate with 1 mL of cells per well. After 2 hours, once the cells had adhered to the bottom of the well, the M3 media was replaced with 1 mL serum-free M3 media and the cells were transfected with 1 μg of

each DNA using Lipofectamine 2000 following the Manufacturer's protocol. After 16 hours the serum-free media was replaced with 1 mL M3 media containing serum. For experiments with *furin RNAi*, 5 μg of dsRNA was used for transfection. Under all conditions, transient expression was examined two-three days post-transfection.

5.7 *Ex vivo* organ culture and Furin inhibitor assay

Ex vivo culturing of wing discs was carried out in WM1 media as described in (Du et al., 2017). The discs were removed from a single pool of culture after 0, 5, and 16 hours of incubation at 25^{o}C, followed by fixation and αHA immunostaining of the tissues. For the Furin inhibition assay, late 3rd instar larval tissues were *ex vivo* cultured in 2 mL of WM1 media in the presence or absence of a cocktail of Furin inhibitor I and II (50 μm final concentration each; Calbiochem 344930 and 344931) following recommended concentrations in (Johnson et al., 2015). The live tissues were incubated for 1, 2.5 or 5 hours. Following incubation, the carcasses were transferred to a centrifuge tube, rinsed three times with 1X PBS, and fixed in 4% PFA before immunostaining.

5.8 Protein analyses

S2 cells were harvested 3 days post-transfection and the cell pellets were washed several times in 1X PBS. The pellet was resuspended in 70 μL RIPA cell lysis buffer (Sigma) in the presence of a cocktail of protease inhibitors (Roche) and kept for 15 minutes at 4^{o}C. An equal volume of lysed cells was combined with 2X Sample Buffer, heated at 95^{o}C for 5 minutes and loaded onto a 10% SDS-PAGE gel. The gel was run at 50V for 10 minutes for stacking and then at 200V until the desired amount

of separation occurred. Proteins were transferred from the gel to a PVDF membrane using Transblot Turbo (BioRad). A standard protocol was followed to perform Western blot analyses using the primary antibodies αGFP (1:1000) or αHA (1:1000) and HRP-conjugated secondary antibody. The HRP activity was detected with ECL substrate (GE) and imaged (Fuji LAS3000).

5.9 Immunostaining

Standard and detergent-free wing disc immunostaining protocols were as previously described (Du et al., 2017). The following antibodies were used in this study: α-Discs large (1:100, DSHB); α-HA (1:1000); α-dpERK (1:100, Cell signaling); α-GFP (1:3000 extracellular, Abcam); α-PH3 (1:2000, Cell Signaling); Alexa Fluor-conjugated secondary antibodies (1:1000 from Molecular Probes) were used for immunofluorescence detection. Phalloidin-conjugated Alexa 647 was often used for marking cell outlines.

Extracellular detergent-free S2 cell staining: Cells were harvested (700g, 5 minutes) and washed with 500 μL stain buffer (PBS, 5% NGS, 0.1% azide). Cells were resuspended in stain buffer containing the primary antibody and rotated for 1 minute to mix. Cells were incubated on ice for 30 minutes with occasional inversion to mix. Cells were washed with stain buffer, and then fixed in 2% PFA in PBS for 20 minutes at room temperature. Cells were washed with PBS and then resuspended in PBS containing the secondary antibody. After mixing for 1 minute by rotation, cells were incubated on ice for 30 minutes with occasional inversion to mix. Cells were washed

in PBS, and then resuspended in mounting media (Vectashield) and mounted on a slide for imaging or resuspended in 300 μL PBS for analysis via flow cytometry.

5.10 Microscopic imaging

For live imaging, wing imaginal discs and their associated trachea were prepared following (Roy et al., 2014). Images were obtained as previously described (Du et al., 2018a) using a Leica SP5X with HyD detector or an CSUX1 Yokogawa spinning disc confocal equipped with an Andor iXon897 EMCCD camera. The images were processed and analyzed with FIJI. Maximum intensity projections of sections were shown for most images. All images were obtained using a 40X objective in the microscopes, except for the images in Figure 2-12, J-N which were obtained with a 20X objective. All XZY images were obtained using the Leica SP5X with a 40X objective for S2 cells and 20X objective for wing discs.

5.11 Analysis of ASP size

ASP length was measured from the transverse connective (TC) along the longest (major) Distal-Proximal axis to the ASP tip. The disc size was determined by measuring from the TC, along the ASP major axis to the edge of the disc. A ratio of the ASP:disc size was used to compare different genotypes and conditions.

5.12 Sholl analysis for terminal branching

Salivary Glands were gently dissected out from fixed larval tissues overexpressing the different variants of Bnl and imaged under transmitted light to visualize tracheal invasion. In WT overexpressing tissue, the terminal tracheal branches

ramified radially from a preexisting central branch point. Due to its morphological resemblance with neuronal dendritic arbors, we employed Sholl analysis (Binley et al., 2014) using FIJI to measure the frequency of terminal branching. The analysis created 20 concentric circles in increments of 5 μm radius from the point of origin up to 100 μm and counted the number of times any tracheal branch crossed these circles. These values were averaged across several samples and compared between the different Bnl variants expressed in the salivary gland.

5.13 Flow cytometry

After extracellular staining, individual cell fluorescence was quantitated using a flow cytometer (BD CantoII, BD Biosciences) and the data were analyzed using FACSDiva (BD Biosciences).

5.14 Survival assay

For each genotype (*w*-, *bnl:HA$_1$GFP$_3$^{endo}*, and *bnl:HA$_1$GFP$_3$-M1^{endo}*) 90 males and females were collected within 2 days of their eclosure. The males and females were kept together for 2 days to allow them to mate, and then each sex was separated into three separate fly food tubes, with 30 flies in each. Thus, for each genotype and sex, there were three tubes of 30 mated flies used for the survival assay. Every other day, each group was changed to a new tube of fly food and dead flies were scored until there were no flies remaining.

5.15 Cholera toxin subunit B (CT-B) staining

S2 cells transfected with *bnl:HA$_1$GFP$_3$* were plated on a cover slip resting inside a 6-well plate. The cells were allowed to settle and adhere to the coverslip for 30 minutes, and then were subsequently chilled on ice for 15 minutes. Cells were briefly rinsed 3 times with ice-cold PBS. Then, cells were incubated with 3 μg/mL CT-B-AlexaFluor647 conjugate (Invitrogen) for 30 minutes at 4°C, protected from light. Cells were washed with ice-cold PBS 3 times and then were fixed with 4% PFA for 10 minutes. Finally, cells were washed 3 times with PBS and the cell-coated coverslip was placed onto a slide containing Vectashield mounting media for imaging.

5.16 Phase separation

Phase separation was performed as in (LaFever et al., 2017). In brief, one well of transfected S2 cells from a 12-well plate was harvested (700g, 5 minutes) and the media was removed. Cells were then resuspended in 180 μL ice cold TBS with protease inhibitors and 30 μL of precondensed Triton X-114 (~12% detergent) was added. After thorough mixing, cells were lysed for 15 minutes on ice with occasional mixing. Lysed material was spun at high speeds (>13,000 rpm) at 4°C to remove insoluble material. The cleared lysate was warmed to 37°C for 5 minutes and spun at 1000g for 10 minutes at room temperature. The aqueous (upper) and detergent (lower) phases were isolated separately. The detergent phase was diluted five-fold with TBS prior to performing SDS-PAGE and western blotting.

5.17 Quantitative analyses of fluorescence intensities

For Bnl levels, all fluorescent intensity measurements were background corrected. 3D image stacks representing only either the wing disc sections or the ASP were transformed into 2D by maximum intensity projections. The density of fluorescence intensity was measured from a selected ROI of the 2D images, either outlining the Bnl source cells or the recipient ASP. For the recipient ASP, the ROI encompassed the distal tip of the ASP (a region with ~3-4 cell diameter that receives the highest levels Bnl from the source). Likewise, the density of the surface-localized Bnl:GFP variants, probed by αGFP immunostaining was measured from selected ROIs on the maximum intensity projections of the relevant optical sections encompassing either the ASP or wing disc source. For salivary gland fluorescence quantitation, the ROIs represented each salivary gland cell including the cell junctions and the density of the red and green channel intensities were measured from the maximum intensity projections of optical sections within the 5 μm Z-stack from the basal surface. The ratio of surface GFP (red) to total GFP (green) was expected to be <1. However, some average ratios were slightly greater than 1, probably due to the immunofluorescent signal amplification of the surface-exposed proteins obtained through αGFP-immunostaining. Secondly, as reported earlier (Du et al., 2018a) the surface exposed GFP was rapidly quenched, reducing its levels of detection on the cell surface. ROIs representing the basal or apical part of the wing disc source cells were selected from maximum intensity projections of the XZY sections. GFP intensities measured from the ROIs were normalized to the total intensity from the total source cell area.

For colocalization analyses in S2 cells, maximum intensity projections of ~4-5 stacks around the center of the cell were produced. An I_{corr} value was obtained using the Colocalization Colormap plugin on FIJI to determine the degree of colocalization of two selected channels (HA immunostain and GFP).

For measuring fluorescence intensities in S2 cells, 3-4 z-slices around the middle of the cell were flattened (~1.5-2 μm in total z-depth). A region of interest (ROI) was drawn around the cell, and each fluorescent channel was measured and background corrected. If applicable, a ratio of background-corrected measurements was taken (i.e. for "Extracelllular:Total GFP", the background-corrected αGFP^{ex} measurement was divided by the background-corrected GFP measurement for each cell).

Gradients of intensities of Bnl:GFP variants in the ASP were obtained along the ASP D-P axes as reported earlier (Du et al., 2018a). For the normalized gradients, individual gradients from homozygous wt^{endo} (n=9) or $m1^{endo}$ (n=12) ASPs were measured. Each position (x) within an ASP was normalized by length of the ASP (L) to obtain x/L, the x-axis of the plot. Similarly, GFP intensity was normalized by dividing each intensity value in a single sample by the highest intensity value from that sample for the y-axis. Normalized intensity values from each sample were taken at 0.05 x/L increments from 0-1 (i.e., 21 data points from each sample). The normalized intensity values from each group (WT or M1) were averaged together and plotted along the x/L axis.

5.18 Cytoneme analysis

ASP cytoneme number was quantitated microscopically as previously described (Roy et al., 2014; Du et al., 2018a; Roy et al., 2011). In brief, cytonemes >15 μm in length that extended from a 60 μm total perimeter region (30 μm from the tip of the ASP in both directions) were counted.

5.19 PI-PLC treatment

S2 cells: Transfected S2 cells (1 mL) were harvested (700g, 5 minutes) in a 1.7 mL eppendorf tube. The media was saved for further analysis or discarded if not needed. The cells were then resuspended in 500 μL PBS, harvested, and washed once more in PBS in the same way. After the last wash, cells were resuspended in a PI-PLC/PBS mixture (1 U/mL PI-PLC). Cells were incubated at 25^{o}C for 30 minutes with light agitation. Then, cells were then harvested subjected to the extracellular staining protocol.

Wing discs: 3rd instar larvae were dissected in WM1 media (Zartman et al., 2013) and carcasses were placed into an Eppendorf tube on ice containing WM1 media. After all larvae were dissected, the carcasses were briefly rinsed with WM1 media 3 times. Carcasses were then incubated with PI-PLC (1 U/mL) in WM1 media for 30 minutes at room temperature with light agitation. Carcasses were briefly rinsed 3 times in WM1 media, and then were subjected to the extracellular staining protocol.

5.20 Phylogenetic analysis of Bnl

The *Drosophila* Branchless conserved FGF domain protein sequence was blasted (blastp) against the insect database and mammalian database in NCBI. The top hits from the insect database were collected, and mouse (*Mus musculus)* and human (*Homo sapiens*) were chosen and collected from the mammalian database. All protein sequences were aligned in Clustal Omega (Li et al., 2015). The resulting alignment was imported into TOPALi v2 (Milne et al., 2009) where the phylogenetic analysis and tree was created using the RaxML, JTT+G model. Additional formatting of the tree was done using Dendoscope3 (Huson and Scornavacca, 2012).

5.21 Statistical analyses

Statistical significance was determined with two-tailed t-tests or a one-way ANOVA followed by Tukey honestly significant different (HSD) tests. All p values in the legends were obtained using a t-test, unless otherwise stated.

5.22 Primers

Primers used for cloning	**Sequence (5'-3')**
UAS-bnl:HA$_1$GFP$_3$	
5' Bnl BglII	GCTGCTAGATCTATGCGAAGAAACCTGCGCTTAGAC
BnlR GFP N overhang	CTCCTCGCCCTTGGACATAGTGTTGCTGCTGCAATGTGG
GFP F Bnl overhang	CCACATTGCAGCAGCAACACTATGTCCAAGGGCGAGGAG
GFP R Bnl overhang	CTGCTGCTGCTGCCACTCTTGTACAGCTCATCCATGCCC
BnlF GFP C overhang	GGGCATGGATGAGCTGTACAAGAGTGGCAGCAGCAGCAG
3' Bnl-XbaI	TCTAGATTACAGGATGGCTCTTTTTCGGAGCAAAAC

UAS-bnl:HA$_1$GFP$_3$-M1	
5’ Bnl BglII	GCTGCTAGATCTATGCGAAGAAACCTGCGCTTAGAC
R bnl M1 mutant R G	CTGCTGCTGATTCTGGTGACcAATGCTGCcTTCGGTACcCGACAGGACCGCC
F bnl M1 mutant R G	GGCGGTCCTGTCGgGTACCGAAgGCAGCATTgGTCACCAGAATCAGCAGCAG
3’ Bnl-XbaI	TCTAGATTACAGGATGGCTCTTTTTCGGAGCAAAAC
UAS-bnl:HA$_1$GFP$_3$-M2	
5’ Bnl BglII	GCTGCTAGATCTATGCGAAGAAACCTGCGCTTAGAC
R bnl M2 mutant R G	CTGTGGCACCGTGGATCcTTCGTTACcGTCCAGATTGCTGATGGGC
F bnl M2 mutant R G	GCCCATCAGCAATCTGGACgGTAACGAAgGATCCACGGTGCCACAG
3’ Bnl-XbaI	TCTAGATTACAGGATGGCTCTTTTTCGGAGCAAAAC
UAS-bnl:HA$_1$GFP$_4$	
5’ Bnl BglII	GCTGCTAGATCTATGCGAAGAAACCTGCGCTTAGAC
Bnl R GFP4 overhang	GCGGCGAGGAGCAGGATCAGGATAACATGAGTAAAGGAGAAGAACTTTTCACTGGAG
GFP4 F Bnl overhang	CTCCAGTGAAAAGTTCTTCTCCTTTACTCATGTTATCC TGATCCTGCTCCTCGCCGC
3’ Bnl-XbaI	TCTAGATTACAGGATGGCTCTTTTTCGGAGCAAAAC
UAS-bnl:GFP$_1$HA$_4$	
5’ Bnl BglII	GCTGCTAGATCTATGCGAAGAAACCTGCGCTTAGAC
Bnl R GFP1 overhang	GTAGTAGTTTAGTGCCGAGCGCAGTGAGTATGAGTAAAGGAGAAGAACTTTTCA
GFP1 F Bnl overhang	CTCCAGTGAAAAGTTCTTCTCCTTTACTCATACTCACTGCGCTCGGCACTAAAC
3’ Bnl-XbaI	TCTAGATTACAGGATGGCTCTTTTTCGGAGCAAAAC
UAS-bnl:GFP$_3$Cherry$_c$	
Cherryc 1 F	GCTGCTAGATCTATGCGAAGAAACCTGCGCTTAGAC
Cherryc 1 R	GCCCTTGCTCACCATCAGGATGGCTCTTTTTCGGAGC
Cherryc 2 F	GTTTTGCTCCGAAAAAGAGCCATCCTGATGGTGAGCAAGGGCGAGGAG
Cherryc 2 R	GCTGCTGGTACCTTACTTGTACAGCTCGTCCATGCCG
UAS-bnl:GFP$_3$-dGPI	
dGPI F	AATTCGAGCTCGGTACAGATCTATGCGAAGAAACCTGCGC
dGPI R	GCCAAGCTTGCATGCCGGTACCTTAGTAGCTCGCATCTTCTAGGGATCC
UAS-bnl:GFP$_3$-TM	
TM 1 F	CCCTAGAAGATGCGAGCTACGACTTCGCCTGTGATATTTACATCTGG
TM 1 R	GCCAAGCTTGCATGCCGGTACCTTAGTGGTAGCAGATGAGAGTGATGATC
TM 2 F	AATTCGAGCTCGGTACAGATCTATGCGAAGAAACCTGCGC
TM 2 R	GATGTAAATATCACAGGCGAAGTCGTAGCTCGCATCTTCTAGGGATCC

UAS-bnl:HA$_1$GFP$_3$-ω	
omega 1 F	AATTCGAGCTCGGTACAGATCTATGCGAAGAAACCTGCGC
omega 1 R	CGAATCGTCGCCGCCTGGTGGGGGGCGTCCTTGGGCCTCG
omega 2 F	CGAGGCCCAAGGACGCCCCCCACCAGGCGGCGACGATTCG
omega 2 R	GCCAAGCTTGCATGCCATATATTCTAGATTACAGGATGGCTCTTTTTCGG
UAS-hFgf10:HA,GFP	
hFgf10 1 F	AATTCGAGCTCGGTACAGATCTATGTGGAAATGGATACTGACACATTGTG
hFgf10 1 R	GGCGTAGTCTGGGACATCATATGGATATGGTGACACCATGTCCTGACC
hFgf10 2 F	TATCCATATGATGTCCCAGACTACGCCGAGGCCACCAACTCTTCTTCC
hFgf10 2 R	CCTTGGACATAAGGTGATTGTAGCTCCGCAC
hFgf10 3 F	CTACAATCACCTTATGTCCAAGGGCGAGGAGC
hFgf10 3 R	CATCTCCTTGCTTGTACAGCTCATCCATGCCC
hFgf10 4 F	GAGCTGTACAAGCAAGGAGATGTCCGCTGGAG
hFgf10 4 R	GCCAAGCTTGCATGCCATATATTCTAGATTATGAGTGTACCACCATTGGAAGG
In situ probe synthesis	
Fur1 probe-F	GACTCTAGAGGATCCCCGCCGATGCGGTTGCCAA
Fur1 probe-R	TCGAGCTCGGTACCCGTTGGCGGTGGCTGCC
Fur2 probe-F	GACTCTAGAGGATCCCCTGTCCATTCTGGACGATGGCATTC
Fur2 probe-R	TCGAGCTCGGTACCCAGGAGCACTCCTCCAGGTAC
CRISPR/Cas9-based genome editing	
gRNA cloning	
bnl HA1 gRNA fwd	AAACAGCGCAGTGAGTGAACGTAG
bnl HA1 gRNA rev	GTCGCTACGTTCACTCACTGCGCT
HDR donor construction	
bnlHA1 N-fwd	AATTCGAGCTCGGTACGCTGAAGAATTTATGTACAATTTGGCTTAATCC
bnlHA1 N-rev	GGCGTAGTCTGGGACATCATATGGATAACTCACTGCACTCGGCACTAAACTACTACG
bnlHA1 C-fwd	TATCCATATGATGTCCCAGACTACGCCGAACGTAGTGTAAATCAACCCACAAATC
bnlHA1 C-rev	GCCAAGCTTGCATGCCGAATGGGTGGTTCGAAGTTCG
bnlHA1M1 N-fwd	AATTCGAGCTCGGTACGCTGAAGAATTTATGTACAATTTGGCTTAATCC
bnlHA1M1 N-rev	GGCGTAGTCTGGGACATCATATGGATAACTCACTGCACTCGGCACTAAACTACTACG
bnlHA1M1 mid-fwd	TATCCATATGATGTCCCAGACTACGCCGAACGTAGTGTAAATCAACCCACAAATC
bnlHA1M1 mid-rev	CTGCTGCTGATTCTGGTGACcAATGCTGCcTTCGGTACcCGACAGGACCGCC
bnlHA1M1 C-fwd	GGCGGTCCTGTCGgGTACCGAAgGCAGCATTgGTCACCAGAATCAGCAGCAG
bnlHA1M1 C-rev	GCCAAGCTTGCATGCCGAATGGGTGGTTCGAAGTTCG
HDR screening and sequencing	
bnlHA1 scr F	CGCATAAACAAGCTGAAATTGCTTCATTC
bnlHA1 scr R	GGCGTAGTCTGGGACATCATATGGATA

bnlHA1 seq fwd1	GGGGCTTTCCCTCTCACTCTC
bnlHA1 seq rev1	GGGTTGCTCAGTCTTTTCGATTTCG
bnlHA1 seq fwd2	ATCCAATCCCAATACCCATCGC
bnlHA1 seq rev2	CTTGTGGGCGCTCGACATATG

Primers Table: F, forward; R, reverse; lowercase nucleotides in the primers for the M1 and M2 overexpression constructs introduced R-to-G mutations at the M1 and M2 sites; lowercase nucleotides in the primers for the Bnl:HA1-M1 donor construct indicate nucleotides that will create the M1 mutations; underlined sequences were for Gibson assembly cloning of the *fur* in situ probe constructs into the pSPT18 vector. The M1M2 double mutant was cloned using M2 mutant primers with the M1 mutant template. Primers were used to introduce synonymous mutations at the gRNA recognition sites in the HDR donor construct. Nucleotides in bold caused the synonymous mutations to the protospacer sequence.

References

Abrami, L., M. Fivaz, E. Decroly, N.G. Seidah, F. Jean, G. Thomas, S.H. Leppla, J.T. Buckley, and F.G. van der Goot. 1998. The pore-forming toxin proaerolysin is activated by furin. *J. Biol. Chem.* 273:32656–32661. doi:10.1074/jbc.273.49.32656.

Ahmad, S.M., and B.S. Baker. 2002. Sex-specific deployment of FGF signaling in Drosophila recruits mesodermal cells into the male genital imaginal disc. *Cell*. 109:651–661. doi:10.1016/s0092-8674(02)00744-4.

Anderson, E.D., S.S. Molloy, F. Jean, H. Fei, S. Shimamura, and G. Thomas. 2002. The ordered and compartment-specific autoproteolytic removal of the furin intramolecular chaperone is required for enzyme activation. *J. Biol. Chem.* 277:12879–12890. doi:10.1074/jbc.M108740200.

Anderson, E.N., and K.A. Wharton. 2017. Alternative cleavage of the bone morphogenetic protein (BMP), Gbb, produces ligands with distinct developmental functions and receptor preferences. *J. Biol. Chem.* 292:19160–19178. doi:10.1074/jbc.M117.793513.

Aznavoorian, S., B.A. Moore, L.D. Alexander-Lister, S.L. Hallit, L.J. Windsor, and J.A. Engler. 2001. Membrane type I-matrix metalloproteinase-mediated degradation of type I collagen by oral squamous cell carcinoma cells. *Cancer Res.* 61:6264–6275.

Bassi, D.E., H. Mahloogi, L. Al-Saleem, R. Lopez De Cicco, J.A. Ridge, and A.J. Klein-Szanto. 2001a. Elevated furin expression in aggressive human head and neck tumors and tumor cell lines. *Mol. Carcinog.* 31:224–232.

Bassi, D.E., R. Lopez De Cicco, H. Mahloogi, S. Zucker, G. Thomas, and A.J. Klein-Szanto. 2001b. Furin inhibition results in absent or decreased invasiveness and tumorigenicity of human cancer cells. *Proc. Natl. Acad. Sci. U.S.A.* 98:10326–10331. doi:10.1073/pnas.191199198.

Battersby, A., A. Csiszár, M. Leptin, and R. Wilson. 2003. Isolation of proteins that interact with the signal transduction molecule Dof and identification of a functional domain conserved between Dof and vertebrate BCAP. *J. Mol. Biol.* 329:479–493.

Beauchamp, A., M.O. Lively, A. Mintz, D. Gibo, J. Wykosky, and W. Debinski. 2012. EphrinA1 is released in three forms from cancer cells by matrix metalloproteases. *Molecular and Cellular Biology*. 32:3253–3264. doi:10.1128/MCB.06791-11.

Beenken, A., and M. Mohammadi. 2009. The FGF family: biology, pathophysiology and therapy. *Nat Rev Drug Discov*. 8:235–253. doi:10.1038/nrd2792.

Beiman, M., B.Z. Shilo, and T. Volk. 1996. Heartless, a Drosophila FGF receptor homolog, is essential for cell migration and establishment of several mesodermal lineages. *Genes & Development*. 10:2993–3002.

Bellusci, S., J. Grindley, H. Emoto, N. Itoh, and B.L. Hogan. 1997. Fibroblast growth factor 10 (FGF10) and branching morphogenesis in the embryonic mouse lung. *Development*. 124:4867–4878.

Bellusci, S., R. Henderson, G. Winnier, T. Oikawa, and B.L. Hogan. 1996. Evidence from normal expression and targeted misexpression that bone morphogenetic protein (Bmp-4) plays a role in mouse embryonic lung morphogenesis. *Development*. 122:1693–1702.

Bergwitz, C., and H. Jüppner. 2012. FGF23 and syndromes of abnormal renal phosphate handling. *Adv. Exp. Med. Biol.* 728:41–64. doi:10.1007/978-1-4614-0887-1_3.

Binley, K.E., W.S. Ng, J.R. Tribble, B. Song, and J.E. Morgan. 2014. Sholl analysis: a quantitative comparison of semi-automated methods. *J. Neurosci. Methods*. 225:65–70. doi:10.1016/j.jneumeth.2014.01.017.

Blanchette, F., N. Rivard, P. Rudd, F. Grondin, L. Attisano, and C.M. Dubois. 2001. Cross-talk between the p42/p44 MAP kinase and Smad pathways in transforming growth factor beta 1-induced furin gene transactivation. *J. Biol. Chem.* 276:33986–33994. doi:10.1074/jbc.M100093200.

Blanchette, F., R. Day, W. Dong, M.H. Laprise, and C.M. Dubois. 1997. TGFbeta1 regulates gene expression of its own converting enzyme furin. *J. Clin. Invest.* 99:1974–1983. doi:10.1172/JCI119365.

Bordier, C. 1981. Phase separation of integral membrane proteins in Triton X-114 solution. *J. Biol. Chem.* 256:1604–1607.

Brisken, C., S. Park, T. Vass, J.P. Lydon, B.W. O'Malley, and R.A. Weinberg. 1998. A paracrine role for the epithelial progesterone receptor in mammary gland development. *Proc. Natl. Acad. Sci. U.S.A.* 95:5076–5081. doi:10.1073/pnas.95.9.5076.

Buglino, J.A., and M.D. Resh. 2008. Hhat is a palmitoylacyltransferase with specificity for N-palmitoylation of Sonic Hedgehog. *J. Biol. Chem.* 283:22076–22088. doi:10.1074/jbc.M803901200.

Callejo, A., C. Torroja, L. Quijada, and I. Guerrero. 2006. Hedgehog lipid modifications are required for Hedgehog stabilization in the extracellular matrix. *Development*. 133:471–483. doi:10.1242/dev.02217.

Caras, I.W. 1991. An internally positioned signal can direct attachment of a glycophospholipid membrane anchor. *J Cell Biol*. 113:77–85. doi:10.1083/jcb.113.1.77.

Caussinus, E., J. Colombelli, and M. Affolter. 2008. Tip-cell migration controls stalk-cell intercalation during Drosophila tracheal tube elongation. *Curr. Biol.* 18:1727–1734. doi:10.1016/j.cub.2008.10.062.

Chamoun, Z., R.K. Mann, D. Nellen, D.P. von Kessler, M. Bellotto, P.A. Beachy, and K. Basler. 2001. Skinny hedgehog, an acyltransferase required for palmitoylation and activity of the hedgehog signal. *Science*. 293:2080–2084. doi:10.1126/science.1064437.

Charng, W.-L., S. Yamamoto, M. Jaiswal, V. Bayat, B. Xiong, K. Zhang, H. Sandoval, G. David, S. Gibbs, H.-C. Lu, K. Chen, N. Giagtzoglou, and H.J. Bellen. 2014. Drosophila Tempura, a novel protein prenyltransferase α subunit, regulates notch signaling via Rab1 and Rab11. *PLoS Biol*. 12:e1001777. doi:10.1371/journal.pbio.1001777.

Chen, M.-H., Y.-J. Li, T. Kawakami, S.-M. Xu, and P.-T. Chuang. 2004. Palmitoylation is required for the production of a soluble multimeric Hedgehog protein complex and long-range signaling in vertebrates. *Genes & Development*. 18:641–659. doi:10.1101/gad.1185804.

Chen, W., H. Huang, R. Hatori, and T.B. Kornberg. 2017. Essential basal cytonemes take up Hedgehog in the Drosophila wing imaginal disc. *Development*. 144:3134–3144. doi:10.1242/dev.149856.

Chrétien, M., and C.H. Li. 1967. Isolation, purification, and characterization of gamma-lipotropic hormone from sheep pituitary glands. *Can. J. Biochem.* 45:1163–1174.

Chu, T., M. Chiu, E. Zhang, and S. Kunes. 2006. A C-terminal motif targets Hedgehog to axons, coordinating assembly of the Drosophila eye and brain. *Developmental Cell*. 10:635–646. doi:10.1016/j.devcel.2006.03.003.

Ciruna, B., and J. Rossant. 2001. FGF signaling regulates mesoderm cell fate specification and morphogenetic movement at the primitive streak. *Developmental Cell*. 1:37–49.

Clark, I.B.N., V. Muha, A. Klingseisen, M. Leptin, and H.-A.J. Müller. 2011. Fibroblast growth factor signaling controls successive cell behaviours during mesoderm layer formation in Drosophila. *Development*. 138:2705–2715. doi:10.1242/dev.060277.

Constam, D.B. 2014. Regulation of TGFβ and related signals by precursor processing. *Semin. Cell Dev. Biol.* 32:85–97. doi:10.1016/j.semcdb.2014.01.008.

Costantini, F. 2006. Renal branching morphogenesis: concepts, questions, and recent advances. *Differentiation*. 74:402–421. doi:10.1111/j.1432-0436.2006.00106.x.

Csiszár, A., E. Vogelsang, H. Beug, and M. Leptin. 2010. A novel conserved phosphotyrosine motif in the Drosophila fibroblast growth factor signaling adaptor Dof with a redundant role in signal transmission. *Molecular and Cellular Biology*. 30:2017–2027. doi:10.1128/MCB.01436-09.

Daniele, J.R., T. Chu, and S. Kunes. 2017. A novel proteolytic event controls Hedgehog intracellular sorting and distribution to receptive fields. *Biol Open*. 6:540–550. doi:10.1242/bio.024083.

De Moerlooze, L., B. Spencer-Dene, J.M. Revest, M. Hajihosseini, I. Rosewell, and C. Dickson. 2000. An important role for the IIIb isoform of fibroblast growth factor receptor 2 (FGFR2) in mesenchymal-epithelial signaling during mouse organogenesis. *Development*. 127:483–492.

Degnin, C., F. Jean, G. Thomas, and J.L. Christian. 2004. Cleavages within the prodomain direct intracellular trafficking and degradation of mature bone morphogenetic protein-4. *Mol. Biol. Cell*. 15:5012–5020. doi:10.1091/mbc.e04-08-0673.

Dierker, T., R. Dreier, A. Petersen, C. Bordych, and K. Grobe. 2009. Heparan sulfate-modulated, metalloprotease-mediated sonic hedgehog release from producing cells. *J. Biol. Chem.* 284:8013–8022. doi:10.1074/jbc.M806838200.

Du, L., A. Sohr, G. Yan, and S. Roy. 2018a. Feedback regulation of cytoneme-mediated transport shapes a tissue-specific FGF morphogen gradient. *Elife*. 7:831. doi:10.7554/eLife.38137.

Du, L., A. Zhou, A. Patel, M. Rao, K. Anderson, and S. Roy. 2017. Unique patterns of organization and migration of FGF-expressing cells during Drosophila morphogenesis. *Developmental Biology*. 427:35–48. doi:10.1016/j.ydbio.2017.05.009.

Du, L., A. Zhou, A. Sohr, and S. Roy. 2018b. An Efficient Strategy for Generating Tissue-specific Binary Transcription Systems in Drosophila by Genome Editing. *J Vis Exp*. doi:10.3791/58268.

Duckert, P., S. Brunak, and N. Blom. 2004. Prediction of proprotein convertase cleavage sites. *Protein Eng. Des. Sel.* 17:107–112. doi:10.1093/protein/gzh013.

Duckworth, W.C., F.B. Stentz, M. Heinemann, and A.E. Kitabchi. 1979. Initial site of insulin cleavage by insulin protease. *Proc. Natl. Acad. Sci. U.S.A.* 76:635–639. doi:10.1073/pnas.76.2.635.

Eaton, S. 2006. Release and trafficking of lipid-linked morphogens. *Current Opinion in Genetics & Development*. 16:17–22. doi:10.1016/j.gde.2005.12.006.

Eblaghie, M.C., M. Reedy, T. Oliver, Y. Mishina, and B.L.M. Hogan. 2006. Evidence that autocrine signaling through Bmpr1a regulates the proliferation, survival and morphogenetic behavior of distal lung epithelial cells. *Developmental Biology*. 291:67–82. doi:10.1016/j.ydbio.2005.12.006.

Eisenhaber, B., P. Bork, and F. Eisenhaber. 1998. Sequence properties of GPI-anchored proteins near the omega-site: constraints for the polypeptide binding site of the putative transamidase. *Protein Eng.* 11:1155–1161.

Eswarakumar, V.P., I. Lax, and J. Schlessinger. 2005. Cellular signaling by fibroblast growth factor receptors. *Cytokine & Growth Factor Reviews*. 16:139–149. doi:10.1016/j.cytogfr.2005.01.001.

Fisher, C.E., and S.E.M. Howie. 2006. The role of megalin (LRP-2/Gp330) during development. *Developmental Biology*. 296:279–297. doi:10.1016/j.ydbio.2006.06.007.

Franch-Marro, X., F. Wendler, J. Griffith, M.M. Maurice, and J.-P. Vincent. 2008. In vivo role of lipid adducts on Wingless. *J. Cell. Sci.* 121:1587–1592. doi:10.1242/jcs.015958.

Fritsch, C., A. Sawala, R. Harris, A. Maartens, C. Sutcliffe, H.L. Ashe, and R.P. Ray. 2012. Different requirements for proteolytic processing of bone morphogenetic protein 5/6/7/8 ligands in Drosophila melanogaster. *J. Biol. Chem.* 287:5942–5953. doi:10.1074/jbc.M111.316745.

Fuller, R.S., A.J. Brake, and J. Thorner. 1989. Intracellular targeting and structural conservation of a prohormone-processing endoprotease. *Science*. 246:482–486. doi:10.1126/science.2683070.

Gale, N.W., and G.D. Yancopoulos. 1997. Ephrins and their receptors: a repulsive topic? *Cell Tissue Res*. 290:227–241.

Galian, C., P. Björkholm, N. Bulleid, and G. von Heijne. 2012. Efficient glycosylphosphatidylinositol (GPI) modification of membrane proteins requires a C-terminal anchoring signal of marginal hydrophobicity. *J. Biol. Chem.* 287:16399–16409. doi:10.1074/jbc.M112.350009.

Galli, L.M., T.L. Barnes, S.S. Secrest, T. Kadowaki, and L.W. Burrus. 2007. Porcupine-mediated lipid-modification regulates the activity and distribution of Wnt proteins in the chick neural tube. *Development*. 134:3339–3348. doi:10.1242/dev.02881.

Gerhardt, H., M. Golding, M. Fruttiger, C. Ruhrberg, A. Lundkvist, A. Abramsson, M. Jeltsch, C. Mitchell, K. Alitalo, D. Shima, and C. Betsholtz. 2003. VEGF guides

angiogenic sprouting utilizing endothelial tip cell filopodia. *J Cell Biol*. 161:1163–1177. doi:10.1083/jcb.200302047.

Gisselbrecht, S., J.B. Skeath, C.Q. Doe, and A.M. Michelson. 1996. heartless encodes a fibroblast growth factor receptor (DFR1/DFGF-R2) involved in the directional migration of early mesodermal cells in the Drosophila embryo. *Genes & Development*. 10:3003–3017.

Gjorevski, N., and C.M. Nelson. 2011. Integrated morphodynamic signalling of the mammary gland. *Nat Rev Mol Cell Biol*. 12:581–593. doi:10.1038/nrm3168.

Goldfarb, M. 2005. Fibroblast growth factor homologous factors: evolution, structure, and function. *Cytokine & Growth Factor Reviews*. 16:215–220. doi:10.1016/j.cytogfr.2005.02.002.

Goldfarb, M., J. Schoorlemmer, A. Williams, S. Diwakar, Q. Wang, X. Huang, J. Giza, D. Tchetchik, K. Kelley, A. Vega, G. Matthews, P. Rossi, D.M. Ornitz, and E. D'Angelo. 2007. Fibroblast growth factor homologous factors control neuronal excitability through modulation of voltage-gated sodium channels. *Neuron*. 55:449–463. doi:10.1016/j.neuron.2007.07.006.

González-Gaitán, M. 2003. Signal dispersal and transduction through the endocytic pathway. *Nat Rev Mol Cell Biol*. 4:213–224. doi:10.1038/nrm1053.

González-Méndez, L., I. Seijo-Barandiarán, and I. Guerrero. 2017. Cytoneme-mediated cell-cell contacts for Hedgehog reception. *Elife*. 6:605. doi:10.7554/eLife.24045.

Gordon, V.M., R. Benz, K. Fujii, S.H. Leppla, and R.K. Tweten. 1997. Clostridium septicum alpha-toxin is proteolytically activated by furin. *Infect. Immun.* 65:4130–4134.

Gospodarowicz, D. 1974. Purification of a Fibroblast Growth Factor from Bovine Pituitary. *J. Biol. Chem.* 250:2515–2520.

Gospodarowicz, D., H. Bialecki, and G. Greenburg. 1978. Purification of the fibroblast growth factor activity from bovine brain. *J. Biol. Chem.* 253:3736–3743.

Greco, V., M. Hannus, and S. Eaton. 2001. Argosomes: a potential vehicle for the spread of morphogens through epithelia. *Cell*. 106:633–645. doi:10.1016/s0092-8674(01)00484-6.

Green, J.B.A., and J. Sharpe. 2015. Positional information and reaction-diffusion: two big ideas in developmental biology combine. *Development*. 142:1203–1211. doi:10.1242/dev.114991.

Gryzik, T., and H.-A.J. Müller. 2004. FGF8-like1 and FGF8-like2 encode putative ligands of the FGF receptor Htl and are required for mesoderm migration in the Drosophila gastrula. *Curr. Biol.* 14:659–667. doi:10.1016/j.cub.2004.03.058.

Guerrero, I., and T.B. Kornberg. 2014. Hedgehog and its circuitous journey from producing to target cells. *Semin. Cell Dev. Biol.* 33:52–62. doi:10.1016/j.semcdb.2014.06.016.

Hacohen, N., S. Kramer, D. Sutherland, Y. Hiromi, and M.A. Krasnow. 1998. sprouty encodes a novel antagonist of FGF signaling that patterns apical branching of the Drosophila airways. *Cell*. 92:253–263.

Hanafusa, H., S. Torii, T. Yasunaga, and E. Nishida. 2002. Sprouty1 and Sprouty2 provide a control mechanism for the Ras/MAPK signalling pathway. *Nat Cell Biol*. 4:850–858. doi:10.1038/ncb867.

He, X., M. Semenov, K. Tamai, and X. Zeng. 2004. LDL receptor-related proteins 5 and 6 in Wnt/beta-catenin signaling: arrows point the way. *Development*. 131:1663–1677. doi:10.1242/dev.01117.

Helms, J.B., and C. Zurzolo. 2004. Lipids as targeting signals: lipid rafts and intracellular trafficking. *Traffic*. 5:247–254. doi:10.1111/j.1600-0854.2004.0181.x.

Hens, J.R., and J.J. Wysolmerski. 2005. Key stages of mammary gland development: molecular mechanisms involved in the formation of the embryonic mammary gland. *Breast Cancer Res.* 7:220–224. doi:10.1186/bcr1306.

Hens, J.R., P. Dann, J.-P. Zhang, S. Harris, G.W. Robinson, and J. Wysolmerski. 2007. BMP4 and PTHrP interact to stimulate ductal outgrowth during embryonic mammary development and to inhibit hair follicle induction. *Development*. 134:1221–1230. doi:10.1242/dev.000182.

Hoff, P.M., and K.K. Machado. 2012. Role of angiogenesis in the pathogenesis of cancer. *Cancer Treat. Rev.* 38:825–833. doi:10.1016/j.ctrv.2012.04.006.

Hook, V., L. Funkelstein, D. Lu, S. Bark, J. Wegrzyn, and S.-R. Hwang. 2008. Proteases for processing proneuropeptides into peptide neurotransmitters and hormones. *Annu. Rev. Pharmacol. Toxicol.* 48:393–423. doi:10.1146/annurev.pharmtox.48.113006.094812.

Hsiung, F., F.-A. Ramirez-Weber, D.D. Iwaki, and T.B. Kornberg. 2005. Dependence of Drosophila wing imaginal disc cytonemes on Decapentaplegic. *Nature*. 437:560–563. doi:10.1038/nature03951.

Huang, H., and T.B. Kornberg. 2015. Myoblast cytonemes mediate Wg signaling from the wing imaginal disc and Delta-Notch signaling to the air sac primordium. *Elife*. 4:e06114. doi:10.7554/eLife.06114.

Huang, P., and M.J. Stern. 2005. FGF signaling in flies and worms: more and more relevant to vertebrate biology. *Cytokine & Growth Factor Reviews*. 16:151–158. doi:10.1016/j.cytogfr.2005.03.002.

Huang, Z., and S. Kunes. 1996. Hedgehog, transmitted along retinal axons, triggers neurogenesis in the developing visual centers of the Drosophila brain. *Cell*. 86:411–422. doi:10.1016/s0092-8674(00)80114-2.

Hufnagel, L., J. Kreuger, S.M. Cohen, and B.I. Shraiman. 2006. On the role of glypicans in the process of morphogen gradient formation. *Developmental Biology*. 300:512–522. doi:10.1016/j.ydbio.2006.08.076.

Huson, D.H., and C. Scornavacca. 2012. Dendroscope 3: an interactive tool for rooted phylogenetic trees and networks. *Syst. Biol.* 61:1061–1067. doi:10.1093/sysbio/sys062.

Itoh, N., and D.M. Ornitz. 2004. Evolution of the Fgf and Fgfr gene families. *Trends in Genetics*. 20:563–569. doi:10.1016/j.tig.2004.08.007.

Itoh, N., and D.M. Ornitz. 2007. Functional evolutionary history of the mouse Fgf gene family. *Dev. Dyn.* 237:18–27. doi:10.1002/dvdy.21388.

Itoh, N., and D.M. Ornitz. 2011. Fibroblast growth factors: from molecular evolution to roles in development, metabolism and disease. *Journal of Biochemistry*. 149:121–130. doi:10.1093/jb/mvq121.

Janes, P.W., N. Saha, W.A. Barton, M.V. Kolev, S.H. Wimmer-Kleikamp, E. Nievergall, C.P. Blobel, J.-P. Himanen, M. Lackmann, and D.B. Nikolov. 2005. Adam meets Eph: an ADAM substrate recognition module acts as a molecular switch for ephrin cleavage in trans. *Cell*. 123:291–304. doi:10.1016/j.cell.2005.08.014.

Jarecki, J., E. Johnson, and M.A. Krasnow. 1999. Oxygen regulation of airway branching in Drosophila is mediated by branchless FGF. *Cell*. 99:211–220. doi:10.1016/s0092-8674(00)81652-9.

Jaskolski, F., C. Mulle, and O.J. Manzoni. 2005. An automated method to quantify and visualize colocalized fluorescent signals. *J. Neurosci. Methods*. 146:42–49. doi:10.1016/j.jneumeth.2005.01.012.

Jean, F., K. Stella, L. Thomas, G. Liu, Y. Xiang, A.J. Reason, and G. Thomas. 1998. alpha1-Antitrypsin Portland, a bioengineered serpin highly selective for furin: application as an antipathogenic agent. *Proc. Natl. Acad. Sci. U.S.A.* 95:7293–7298. doi:10.1073/pnas.95.13.7293.

Johnson, T.K., M.A. Henstridge, A. Herr, K.A. Moore, J.C. Whisstock, and C.G. Warr. 2015. Torso-like mediates extracellular accumulation of Furin-cleaved Trunk to pattern the Drosophila embryo termini. *Nat Commun*. 6:8759–6. doi:10.1038/ncomms9759.

Julius, D., A. Brake, L. Blair, R. Kunisawa, and J. Thorner. 1984. Isolation of the putative structural gene for the lysine-arginine-cleaving endopeptidase required for processing of yeast prepro-alpha-factor. *Cell*. 37:1075–1089. doi:10.1016/0092-8674(84)90442-2.

Kadam, S., A. McMahon, P. Tzou, and A. Stathopoulos. 2009. FGF ligands in Drosophila have distinct activities required to support cell migration and differentiation. *Development*. 136:739–747. doi:10.1242/dev.027904.

Kadowaki, T., E. Wilder, J. Klingensmith, K. Zachary, and N. Perrimon. 1996. The segment polarity gene porcupine encodes a putative multitransmembrane protein involved in Wingless processing. *Genes & Development*. 10:3116–3128.

Kang, J.Y., Y. Hong, H. Ashida, N. Shishioh, Y. Murakami, Y.S. Morita, Y. Maeda, and T. Kinoshita. 2005. PIG-V involved in transferring the second mannose in glycosylphosphatidylinositol. *J. Biol. Chem.* 280:9489–9497. doi:10.1074/jbc.M413867200.

Kerbel, R.S. 2008. Tumor angiogenesis. *N. Engl. J. Med.* 358:2039–2049. doi:10.1056/NEJMra0706596.

Khatib, A.M., G. Siegfried, A. Prat, J. Luis, M. Chrétien, P. Metrakos, and N.G. Seidah. 2001. Inhibition of proprotein convertases is associated with loss of growth and tumorigenicity of HT-29 human colon carcinoma cells: importance of insulin-like growth factor-1 (IGF-1) receptor processing in IGF-1-mediated functions. *J. Biol. Chem.* 276:30686–30693. doi:10.1074/jbc.M101725200.

Kicheva, A., P. Pantazis, T. Bollenbach, Y. Kalaidzidis, T. Bittig, F. Jülicher, and M. González-Gaitán. 2007. Kinetics of morphogen gradient formation. *Science*. 315:521–525. doi:10.1126/science.1135774.

Kim, W., R. Essalmani, D. Szumska, J.W.M. Creemers, A.J.M. Roebroek, P. D'Orleans-Juste, S. Bhattacharya, N.G. Seidah, and A. Prat. 2012. Loss of endothelial furin leads to cardiac malformation and early postnatal death. *Molecular and Cellular Biology*. 32:3382–3391. doi:10.1128/MCB.06331-11.

Kinoshita, T. 2016. Glycosylphosphatidylinositol (GPI) Anchors: Biochemistry and Cell Biology: Introduction to a Thematic Review Series. *J. Lipid Res.* 57:4–5. doi:10.1194/jlr.E065417.

Klämbt, C., L. Glazer, and B.Z. Shilo. 1992. breathless, a Drosophila FGF receptor homolog, is essential for migration of tracheal and specific midline glial cells. *Genes & Development*. 6:1668–1678. doi:10.1101/gad.6.9.1668.

Klingseisen, A., I.B.N. Clark, T. Gryzik, and H.-A.J. Müller. 2009. Differential and overlapping functions of two closely related Drosophila FGF8-like growth factors in mesoderm development. *Development*. 136:2393–2402. doi:10.1242/dev.035451.

Koizumi, K., K. Takano, A. Kaneyasu, H. Watanabe-Takano, E. Tokuda, T. Abe, N. Watanabe, T. Takenawa, and T. Endo. 2012. RhoD activated by fibroblast growth factor induces cytoneme-like cellular protrusions through mDia3C. *Mol. Biol. Cell*. 23:4647–4661. doi:10.1091/mbc.E12-04-0315.

Kornberg, T.B. 2011. Barcoding Hedgehog for intracellular transport. *Sci Signal*. 4:pe44–pe44. doi:10.1126/scisignal.2002447.

Kornberg, T.B. 2014. Cytonemes and the dispersion of morphogens. *WIREs Dev Biol*. 3:445–463. doi:10.1002/wdev.151.

Kornberg, T.B., and A. Guha. 2007. Understanding morphogen gradients: a problem of dispersion and containment. *Current Opinion in Genetics & Development*. 17:264–271. doi:10.1016/j.gde.2007.05.010.

Kornberg, T.B., and S. Roy. 2014. Cytonemes as specialized signaling filopodia. *Development*. 141:729–736. doi:10.1242/dev.086223.

Künnapuu, J., I. Björkgren, and O. Shimmi. 2009. The Drosophila DPP signal is produced by cleavage of its proprotein at evolutionary diversified furin-recognition sites. *Proc. Natl. Acad. Sci. U.S.A.* 106:8501–8506. doi:10.1073/pnas.0809885106.

Künnapuu, J., P.M. Tauscher, N. Tiusanen, M. Nguyen, A. Löytynoja, K. Arora, and O. Shimmi. 2014. Cleavage of the Drosophila screw prodomain is critical for a dynamic BMP morphogen gradient in embryogenesis. *Developmental Biology*. 389:149–159. doi:10.1016/j.ydbio.2014.02.007.

LaFever, K.S., X. Wang, P. Page-McCaw, G. Bhave, and A. Page-McCaw. 2017. Both Drosophila matrix metalloproteinases have released and membrane-tethered forms but have different substrates. *Sci Rep*. 7:44560. doi:10.1038/srep44560.

Lebeche, D., S. Malpel, and W.V. Cardoso. 1999. Fibroblast growth factor interactions in the developing lung. *Mech. Dev.* 86:125–136.

Lee, J.D., and J.E. Treisman. 2001. Sightless has homology to transmembrane acyltransferases and is required to generate active Hedgehog protein. *Curr. Biol.* 11:1147–1152.

Lee, J.J., S.C. Ekker, D.P. von Kessler, J.A. Porter, B.I. Sun, and P.A. Beachy. 1994. Autoproteolysis in hedgehog protein biogenesis. *Science*. 266:1528–1537. doi:10.1126/science.7985023.

Lee, J.R., S. Urban, C.F. Garvey, and M. Freeman. 2001a. Regulated intracellular ligand transport and proteolysis control EGF signal activation in Drosophila. *Cell*. 107:161–171. doi:10.1016/s0092-8674(01)00526-8.

Lee, R., P. Kermani, K.K. Teng, and B.L. Hempstead. 2001b. Regulation of cell survival by secreted proneurotrophins. *Science*. 294:1945–1948. doi:10.1126/science.1065057.

LeMosy, E.K. 2006. Proteolytic regulatory mechanisms in the formation of extracellular morphogen gradients. *Birth Defects Res. C Embryo Today*. 78:243–255. doi:10.1002/bdrc.20074.

Li, W., A. Cowley, M. Uludag, T. Gur, H. McWilliam, S. Squizzato, Y.M. Park, N. Buso, and R. Lopez. 2015. The EMBL-EBI bioinformatics web and programmatic tools framework. *Nucleic Acids Res.* 43:W580–4. doi:10.1093/nar/gkv279.

Liu, Z.-J., T. Shirakawa, Y. Li, A. Soma, M. Oka, G.P. Dotto, R.M. Fairman, O.C. Velazquez, and M. Herlyn. 2003. Regulation of Notch1 and Dll4 by vascular endothelial growth factor in arterial endothelial cells: implications for modulating arteriogenesis and angiogenesis. *Molecular and Cellular Biology*. 23:14–25. doi:10.1128/mcb.23.1.14-25.2003.

Lohela, M., M. Bry, T. Tammela, and K. Alitalo. 2009. VEGFs and receptors involved in angiogenesis versus lymphangiogenesis. *Curr. Opin. Cell Biol.* 21:154–165. doi:10.1016/j.ceb.2008.12.012.

Mallepell, S., A. Krust, P. Chambon, and C. Brisken. 2006. Paracrine signaling through the epithelial estrogen receptor alpha is required for proliferation and morphogenesis in the mammary gland. *Proc. Natl. Acad. Sci. U.S.A.* 103:2196–2201. doi:10.1073/pnas.0510974103.

Manning, G., and M.A. Krasnow. 1993. Development of the Drosophila tracheal system. *In* The Development of Drosophila melanogaster. M. Bate and A. Martinez-Arias, editors. Cold Spring Harbor, NY.

Mashayekhi, F., M. Hadavi, H.R. Vaziri, and M. Naji. 2010. Increased acidic fibroblast growth factor concentrations in the serum and cerebrospinal fluid of patients with Alzheimer's disease. *J Clin Neurosci*. 17:357–359. doi:10.1016/j.jocn.2009.05.037.

Mayor, S., and F.R. Maxfield. 1995. Insolubility and redistribution of GPI-anchored proteins at the cell surface after detergent treatment. *Mol. Biol. Cell*. 6:929–944. doi:10.1091/mbc.6.7.929.

Mbikay, M., F. Sirois, J. Yao, N.G. Seidah, and M. Chrétien. 1997. Comparative analysis of expression of the proprotein convertases furin, PACE4, PC1 and PC2 in human lung tumours. *Br. J. Cancer*. 75:1509–1514. doi:10.1038/bjc.1997.258.

Melkonian, K.A., T. Chu, L.B. Tortorella, and D.A. Brown. 1995. Characterization of proteins in detergent-resistant membrane complexes from Madin-Darby canine kidney epithelial cells. *Biochemistry*. 34:16161–16170. doi:10.1021/bi00049a031.

Metzger, R.J., and M.A. Krasnow. 1999. Genetic control of branching morphogenesis. *Science*. 284:1635–1639.

Micchelli, C.A., I. The, E. Selva, V. Mogila, and N. Perrimon. 2002. Rasp, a putative transmembrane acyltransferase, is required for Hedgehog signaling. *Development*. 129:843–851.

Milne, I., D. Lindner, M. Bayer, D. Husmeier, G. McGuire, D.F. Marshall, and F. Wright. 2009. TOPALi v2: a rich graphical interface for evolutionary analyses of multiple alignments on HPC clusters and multi-core desktops. *Bioinformatics*. 25:126–127. doi:10.1093/bioinformatics/btn575.

Miura, G.I., J. Buglino, D. Alvarado, M.A. Lemmon, M.D. Resh, and J.E. Treisman. 2006. Palmitoylation of the EGFR ligand Spitz by Rasp increases Spitz activity by restricting its diffusion. *Developmental Cell*. 10:167–176. doi:10.1016/j.devcel.2005.11.017.

Molloy, S.S., E.D. Anderson, F. Jean, and G. Thomas. 1999. Bi-cycling the furin pathway: from TGN localization to pathogen activation and embryogenesis. *Trends in Cell Biology*. 9:28–35.

Molloy, S.S., P.A. Bresnahan, S.H. Leppla, K.R. Klimpel, and G. Thomas. 1992. Human furin is a calcium-dependent serine endoprotease that recognizes the sequence Arg-X-X-Arg and efficiently cleaves anthrax toxin protective antigen. *J. Biol. Chem.* 267:16396–16402.

Moran, P., H. Raab, W.J. Kohr, and I.W. Caras. 1991. Glycophospholipid membrane anchor attachment. Molecular analysis of the cleavage/attachment site. *J. Biol. Chem.* 266:1250–1257.

Moriconi, C., A. Ordoñez, G. Lupo, B. Gooptu, J.A. Irving, R. Noto, V. Martorana, M. Manno, V. Timpano, N.A. Guadagno, L. Dalton, S.J. Marciniak, D.A. Lomas, and

E. Miranda. 2015. Interactions between N-linked glycosylation and polymerisation of neuroserpin within the endoplasmic reticulum. *FEBS J.* 282:4565–4579. doi:10.1111/febs.13517.

Muha, V., and H.-A.J. Müller. 2013. Functions and Mechanisms of Fibroblast Growth Factor (FGF) Signalling in Drosophila melanogaster. *IJMS.* 14:5920–5937. doi:10.3390/ijms14035920.

Mukherjee, T., I. Choi, and U. Banerjee. 2012. Genetic analysis of fibroblast growth factor signaling in the Drosophila eye. *G3 (Bethesda)*. 2:23–28. doi:10.1534/g3.111.001495.

Müller, P., K.W. Rogers, S.R. Yu, M. Brand, and A.F. Schier. 2013. Morphogen transport. *Development*. 140:1621–1638. doi:10.1242/dev.083519.

Neumann, S., M. Harterink, and H. Sprong. 2007. Hitch-hiking between cells on lipoprotein particles. *Traffic*. 8:331–338. doi:10.1111/j.1600-0854.2006.00532.x.

Nies, V.J.M., G. Sancar, W. Liu, T. van Zutphen, D. Struik, R.T. Yu, A.R. Atkins, R.M. Evans, J.W. Jonker, and M.R. Downes. 2015. Fibroblast Growth Factor Signaling in Metabolic Regulation. *Front Endocrinol (Lausanne)*. 6:193. doi:10.3389/fendo.2015.00193.

Ochoa-Espinosa, A., and M. Affolter. 2012. Branching morphogenesis: from cells to organs and back. *Cold Spring Harbor Perspectives in Biology*. 4:a008243–a008243. doi:10.1101/cshperspect.a008243.

Ohshiro, T., Y. Emori, and K. Saigo. 2002. Ligand-dependent activation of breathless FGF receptor gene in Drosophila developing trachea. *Mech. Dev.* 114:3–11. doi:10.1016/s0925-4773(02)00042-4.

Ornitz, D.M., and N. Itoh. 2001. Fibroblast growth factors. *Genome Biol.* 2:1–12.

Ornitz, D.M., and N. Itoh. 2015. The Fibroblast Growth Factor signaling pathway. *WIREs Dev Biol*. 4:215–266. doi:10.1002/wdev.176.

Panáková, D., H. Sprong, E. Marois, C. Thiele, and S. Eaton. 2005. Lipoprotein particles are required for Hedgehog and Wingless signalling. *Nature*. 435:58–65. doi:10.1038/nature03504.

Pasquale, E.B. 2008. Eph-ephrin bidirectional signaling in physiology and disease. *Cell*. 133:38–52. doi:10.1016/j.cell.2008.03.011.

Paulick, M.G., and C.R. Bertozzi. 2008. The glycosylphosphatidylinositol anchor: a complex membrane-anchoring structure for proteins. *Biochemistry*. 47:6991–7000. doi:10.1021/bi8006324.

Pepinsky, R.B., C. Zeng, D. Wen, P. Rayhorn, D.P. Baker, K.P. Williams, S.A. Bixler, C.M. Ambrose, E.A. Garber, K. Miatkowski, F.R. Taylor, E.A. Wang, and A. Galdes. 1998. Identification of a palmitic acid-modified form of human Sonic hedgehog. *J. Biol. Chem.* 273:14037–14045. doi:10.1074/jbc.273.22.14037.

Perrimon, N., C. Pitsouli, and B.-Z. Shilo. 2012. Signaling mechanisms controlling cell fate and embryonic patterning. *Cold Spring Harbor Perspectives in Biology*. 4:a005975–a005975. doi:10.1101/cshperspect.a005975.

Peterson, S.J., and M.A. Krasnow. 2015. Subcellular trafficking of FGF controls tracheal invasion of Drosophila flight muscle. *Cell*. 160:313–323. doi:10.1016/j.cell.2014.11.043.

Petit, V., U. Nussbaumer, C. Dossenbach, and M. Affolter. 2004. Downstream-of-FGFR is a fibroblast growth factor-specific scaffolding protein and recruits

Corkscrew upon receptor activation. *Molecular and Cellular Biology*. 24:3769–3781. doi:10.1128/MCB.24.9.3769-3781.2004.

Pierleoni, A., P.L. Martelli, and R. Casadio. 2008. PredGPI: a GPI-anchor predictor. *BMC Bioinformatics*. 9:392–11. doi:10.1186/1471-2105-9-392.

Porter, J.A., K.E. Young, and P.A. Beachy. 1996. Cholesterol modification of hedgehog signaling proteins in animal development. *Science*. 274:255–259.

Ramírez-Weber, F.A., and T.B. Kornberg. 1999. Cytonemes: cellular processes that project to the principal signaling center in Drosophila imaginal discs. *Cell*. 97:599–607. doi:10.1016/s0092-8674(00)80771-0.

Resh, M.D. 2006. Trafficking and signaling by fatty-acylated and prenylated proteins. *Nat. Chem. Biol.* 2:584–590. doi:10.1038/nchembio834.

Ridley, A.J. 2006. Rho GTPases and actin dynamics in membrane protrusions and vesicle trafficking. *Trends in Cell Biology*. 16:522–529. doi:10.1016/j.tcb.2006.08.006.

Rietveld, A., S. Neutz, K. Simons, and S. Eaton. 1999. Association of sterol- and glycosylphosphatidylinositol-linked proteins with Drosophila raft lipid microdomains. *J. Biol. Chem.* 274:12049–12054. doi:10.1074/jbc.274.17.12049.

Roebroek, A.J., I.G. Pauli, Y. Zhang, and W.J. van de Ven. 1991. cDNA sequence of a Drosophila melanogaster gene, Dfur1, encoding a protein structurally related to the subtilisin-like proprotein processing enzyme furin. *FEBS Lett.* 289:133–137. doi:10.1016/0014-5793(91)81052-a.

Roebroek, A.J., J.W. Creemers, I.G. Pauli, T. Bogaert, and W.J. van de Ven. 1993. Generation of structural and functional diversity in furin-like proteins in

Drosophila melanogaster by alternative splicing of the Dfur1 gene. *EMBO J*. 12:1853–1870.

Roebroek, A.J., J.W. Creemers, I.G. Pauli, U. Kurzik-Dumke, M. Rentrop, E.A. Gateff, J.A. Leunissen, and W.J. van de Ven. 1992. Cloning and functional expression of Dfurin2, a subtilisin-like proprotein processing enzyme of Drosophila melanogaster with multiple repeats of a cysteine motif. *J. Biol. Chem.* 267:17208–17215.

Roebroek, A.J., L. Umans, I.G. Pauli, E.J. Robertson, F. van Leuven, W.J. van de Ven, and D.B. Constam. 1998. Failure of ventral closure and axial rotation in embryos lacking the proprotein convertase Furin. *Development*. 125:4863–4876.

Rojas-Ríos, P., I. Guerrero, and A. González-Reyes. 2012. Cytoneme-mediated delivery of hedgehog regulates the expression of bone morphogenetic proteins to maintain germline stem cells in Drosophila. *PLoS Biol*. 10:e1001298. doi:10.1371/journal.pbio.1001298.

Roy, S., and T.B. Kornberg. 2015. Paracrine signaling mediated at cell-cell contacts. *BioEssays*. 37:25–33. doi:10.1002/bies.201400122.

Roy, S., F. Hsiung, and T.B. Kornberg. 2011. Specificity of Drosophila cytonemes for distinct signaling pathways. *Science*. 332:354–358. doi:10.1126/science.1198949.

Roy, S., H. Huang, S. Liu, and T.B. Kornberg. 2014. Cytoneme-mediated contact-dependent transport of the Drosophila decapentaplegic signaling protein. *Science*. 343:1244624–1244624. doi:10.1126/science.1244624.

Sagar, F. Pröls, C. Wiegreffe, and M. Scaal. 2015. Communication between distant epithelial cells by filopodia-like protrusions during embryonic development. *Development*. 142:665–671. doi:10.1242/dev.115964.

Saha, S., A.A. Anilkumar, and S. Mayor. 2016. GPI-anchored protein organization and dynamics at the cell surface. *J. Lipid Res.* 57:159–175. doi:10.1194/jlr.R062885.

Sai, X., and R.K. Ladher. 2008. FGF signaling regulates cytoskeletal remodeling during epithelial morphogenesis. *Curr. Biol.* 18:976–981. doi:10.1016/j.cub.2008.05.049.

Sanders, T.A., E. Llagostera, and M. Barna. 2013. Specialized filopodia direct long-range transport of SHH during vertebrate tissue patterning. *Nature*. 497:628–632. doi:10.1038/nature12157.

Sangiorgio, V., M. Pitto, P. Palestini, and M. Masserini. 2004. GPI-anchored proteins and lipid rafts. *Ital. J. Biochem.* 53:98–111.

Sato, M., and T.B. Kornberg. 2002. FGF is an essential mitogen and chemoattractant for the air sacs of the drosophila tracheal system. *Developmental Cell*. 3:195–207.

Schuck, S., and K. Simons. 2006. Controversy fuels trafficking of GPI-anchored proteins. *J Cell Biol*. 172:963–965. doi:10.1083/jcb.200603015.

Schweitzer, R., M. Shaharabany, R. Seger, and B.Z. Shilo. 1995. Secreted Spitz triggers the DER signaling pathway and is a limiting component in embryonic ventral ectoderm determination. *Genes & Development*. 9:1518–1529. doi:10.1101/gad.9.12.1518.

Seidah, N.G., and M. Chrétien. 1999. Proprotein and prohormone convertases: a family of subtilases generating diverse bioactive polypeptides. *Brain Res.* 848:45–62. doi:10.1016/s0006-8993(99)01909-5.

Seidah, N.G., R. Day, M. Marcinkiewicz, and M. Chrétien. 1998. Precursor convertases: an evolutionary ancient, cell-specific, combinatorial mechanism yielding diverse bioactive peptides and proteins. *Ann. N. Y. Acad. Sci.* 839:9–24. doi:10.1111/j.1749-6632.1998.tb10727.x.

Sekine, K., H. Ohuchi, M. Fujiwara, M. Yamasaki, T. Yoshizawa, T. Sato, N. Yagishita, D. Matsui, Y. Koga, N. Itoh, and S. Kato. 1999. Fgf10 is essential for limb and lung formation. *Nat. Genet.* 21:138–141. doi:10.1038/5096.

Shen, L.R., C.Q. Lai, X. Feng, L.D. Parnell, J.B. Wan, J.D. Wang, D. Li, J.M. Ordovas, and J.X. Kang. 2010. Drosophila lacks C20 and C22 PUFAs. *J. Lipid Res.* 51:2985–2992. doi:10.1194/jlr.M008524.

Shimada, T., T. Muto, I. Urakawa, T. Yoneya, Y. Yamazaki, K. Okawa, Y. Takeuchi, T. Fujita, S. Fukumoto, and T. Yamashita. 2002. Mutant FGF-23 responsible for autosomal dominant hypophosphatemic rickets is resistant to proteolytic cleavage and causes hypophosphatemia in vivo. *Endocrinology*. 143:3179–3182. doi:10.1210/endo.143.8.8795.

Shishido, E., N. Ono, T. Kojima, and K. Saigo. 1997. Requirements of DFR1/Heartless, a mesoderm-specific Drosophila FGF-receptor, for the formation of heart, visceral and somatic muscles, and ensheathing of longitudinal axon tracts in CNS. *Development*. 124:2119–2128.

Shishido, E., S. Higashijima, Y. Emori, and K. Saigo. 1993. Two FGF-receptor homologues of Drosophila: one is expressed in mesodermal primordium in early embryos. *Development*. 117:751–761.

Simmen, T., M. Nobile, J.S. Bonifacino, and W. Hunziker. 1999. Basolateral sorting of furin in MDCK cells requires a phenylalanine-isoleucine motif together with an acidic amino acid cluster. *Molecular and Cellular Biology*. 19:3136–3144. doi:10.1128/mcb.19.4.3136.

Simmen, T., S. Höning, A. Icking, R. Tikkanen, and W. Hunziker. 2002. AP-4 binds basolateral signals and participates in basolateral sorting in epithelial MDCK cells. *Nat Cell Biol*. 4:154–159. doi:10.1038/ncb745.

Sohr, A., L. Du, R. Wang, L. Lin, and S. Roy. 2019. Drosophila FGF cleavage is required for efficient intracellular sorting and intercellular dispersal. *J Cell Biol*. 218:1653–1669. doi:10.1083/jcb.201810138.

Sopory, S., S. Kwon, M. Wehrli, and J.L. Christian. 2010. Regulation of Dpp activity by tissue-specific cleavage of an upstream site within the prodomain. *Developmental Biology*. 346:102–112. doi:10.1016/j.ydbio.2010.07.019.

Sounni, N.E., E.N. Baramova, C. Munaut, E. Maquoi, F. Frankenne, J.-M. Foidart, and A. Noël. 2002. Expression of membrane type 1 matrix metalloproteinase (MT1-MMP) in A2058 melanoma cells is associated with MMP-2 activation and increased tumor growth and vascularization. *Int. J. Cancer*. 98:23–28. doi:10.1002/ijc.10134.

Spemann, H., and H. Mangold. 1924. Uber Weckung

organisatorischer Fahigkeiten durch Verplanzung

in organisatorische Umgebung. *Rouxs Arch*. 109:557–577.

Stanganello, E., A.I.H. Hagemann, B. Mattes, C. Sinner, D. Meyen, S. Weber, A. Schug, E. Raz, and S. Scholpp. 2015. Filopodia-based Wnt transport during vertebrate tissue patterning. *Nat Commun*. 6:5846. doi:10.1038/ncomms6846.

Stathopoulos, A., B. Tam, M. Ronshaugen, M. Frasch, and M. Levine. 2004. pyramus and thisbe: FGF genes that pattern the mesoderm of Drosophila embryos. *Genes & Development*. 18:687–699. doi:10.1101/gad.1166404.

Steiner, D.F., J.L. Clark, C. Nolan, A.H. Rubenstein, E. Margoliash, B. Aten, and P.E. Oyer. 1969. Proinsulin and the biosynthesis of insulin. *Recent Prog. Horm. Res.* 25:207–282.

Sternlicht, M.D. 2006. Key stages in mammary gland development: the cues that regulate ductal branching morphogenesis. *Breast Cancer Res.* 8:201. doi:10.1186/bcr1368.

Stewart, D.P., S. Marada, W.J. Bodeen, A. Truong, S.M. Sakurada, T. Pandit, S.M. Pruett-Miller, and S.K. Ogden. 2018. Cleavage activates dispatched for Sonic Hedgehog ligand release. *Elife*. 7:5119. doi:10.7554/eLife.31678.

Sutherland, D., C. Samakovlis, and M.A. Krasnow. 1996. branchless encodes a Drosophila FGF homolog that controls tracheal cell migration and the pattern of branching. *Cell*. 87:1091–1101. doi:10.1016/s0092-8674(00)81803-6.

Swift, M.R., and B.M. Weinstein. 2009. Arterial-venous specification during development. *Circ. Res.* 104:576–588. doi:10.1161/CIRCRESAHA.108.188805.

Takada, R., Y. Satomi, T. Kurata, N. Ueno, S. Norioka, H. Kondoh, T. Takao, and S. Takada. 2006. Monounsaturated fatty acid modification of Wnt protein: its role in

Wnt secretion. *Developmental Cell*. 11:791–801. doi:10.1016/j.devcel.2006.10.003.

Tang, B.L. 2001. ADAMTS: a novel family of extracellular matrix proteases. *Int. J. Biochem. Cell Biol.* 33:33–44.

Teleman, A.A., and S.M. Cohen. 2000. Dpp gradient formation in the Drosophila wing imaginal disc. *Cell*. 103:971–980. doi:10.1016/s0092-8674(00)00199-9.

Tefft, J.D., M. Lee, S. Smith, M. Leinwand, J. Zhao, P. Bringas, D.L. Crowe, and D. Warburton. 1999. Conserved function of mSpry-2, a murine homolog of Drosophila sprouty, which negatively modulates respiratory organogenesis. *Curr. Biol.* 9:219–222.

Teven, C.M., E.M. Farina, J. Rivas, and R.R. Reid. 2014. Fibroblast growth factor (FGF) signaling in development and skeletal diseases. *Genes Diseases*. 1:199–213. doi:10.1016/j.gendis.2014.09.005.

Thacker, C., and A.M. Rose. 2000. A look at the Caenorhabditis elegans Kex2/Subtilisin-like proprotein convertase family. *BioEssays*. 22:545–553. doi:10.1002/(SICI)1521-1878(200006)22:6<545::AID-BIES7>3.0.CO;2-F.

Thomas, G. 2002. Furin at the cutting edge: from protein traffic to embryogenesis and disease. *Nat Rev Mol Cell Biol*. 3:753–766. doi:10.1038/nrm934.

Thomas, G., B.A. Thorne, L. Thomas, R.G. Allen, D.E. Hruby, R. Fuller, and J. Thorner. 1988. Yeast KEX2 endopeptidase correctly cleaves a neuroendocrine prohormone in mammalian cells. *Science*. 241:226–230. doi:10.1126/science.3291117.

Tímár, J., B. Döme, K. Fazekas, A. Janovics, and S. Paku. 2001. Angiogenesis-dependent diseases and angiogenesis therapy. *Pathol. Oncol. Res.* 7:85–94.

Tokhunts, R., S. Singh, T. Chu, G. D'Angelo, V. Baubet, J.A. Goetz, Z. Huang, Z. Yuan, M. Ascano, Y. Zavros, P.P. Thérond, S. Kunes, N. Dahmane, and D.J. Robbins. 2010. The full-length unprocessed hedgehog protein is an active signaling molecule. *J. Biol. Chem.* 285:2562–2568. doi:10.1074/jbc.M109.078626.

Tulin, S., and A. Stathopoulos. 2010. Analysis of Thisbe and Pyramus functional domains reveals evidence for cleavage of Drosophila FGFs. *BMC Dev. Biol.* 10:83–18. doi:10.1186/1471-213X-10-83.

Turing, A.M. 1952. The Chemical Basis of Morphogenesis. *Philos Trans R Soc Lond*. 237:37–72.

Turner, N., and R. Grose. 2010. Fibroblast growth factor signalling: from development to cancer. *Nature Reviews Cancer*. 10:116–129. doi:10.1038/nrc2780.

Urban, S., J.R. Lee, and M. Freeman. 2001. Drosophila rhomboid-1 defines a family of putative intramembrane serine proteases. *Cell*. 107:173–182. doi:10.1016/s0092-8674(01)00525-6.

van den Heuvel, M., C. Harryman-Samos, J. Klingensmith, N. Perrimon, and R. Nusse. 1993. Mutations in the segment polarity genes wingless and porcupine impair secretion of the wingless protein. *EMBO J.* 12:5293–5302.

van Tetering, G., and M. Vooijs. 2011. Proteolytic cleavage of Notch: "HIT and RUN". *Curr. Mol. Med.* 11:255–269.

Vempati, P., A.S. Popel, and F. Mac Gabhann. 2014. Extracellular regulation of VEGF: isoforms, proteolysis, and vascular patterning. *Cytokine & Growth Factor Reviews*. 25:1–19. doi:10.1016/j.cytogfr.2013.11.002.

Volchkov, V.E., H. Feldmann, V.A. Volchkova, and H.D. Klenk. 1998. Processing of the Ebola virus glycoprotein by the proprotein convertase furin. *Proc. Natl. Acad. Sci. U.S.A.* 95:5762–5767. doi:10.1073/pnas.95.10.5762.

Volckaert, T., and S. De Langhe. 2014. Lung epithelial stem cells and their niches: Fgf10 takes center stage. *Fibrogenesis Tissue Repair*. 7:8. doi:10.1186/1755-1536-7-8.

Vyas, N., D. Goswami, A. Manonmani, P. Sharma, H.A. Ranganath, K. VijayRaghavan, L.S. Shashidhara, R. Sowdhamini, and S. Mayor. 2008. Nanoscale organization of hedgehog is essential for long-range signaling. *Cell*. 133:1214–1227. doi:10.1016/j.cell.2008.05.026.

Walker, J.A., S.S. Molloy, G. Thomas, T. Sakaguchi, T. Yoshida, T.M. Chambers, and Y. Kawaoka. 1994. Sequence specificity of furin, a proprotein-processing endoprotease, for the hemagglutinin of a virulent avian influenza virus. *J. Virol.* 68:1213–1218.

Wassarman, D.A., M. Therrien, and G.M. Rubin. 1995. The Ras signaling pathway in Drosophila. *Current Opinion in Genetics & Development*. 5:44–50.

Wharton, K.A., and M. Serpe. 2013. Fine-tuned shuttles for bone morphogenetic proteins. *Current Opinion in Genetics & Development*. 23:374–384. doi:10.1016/j.gde.2013.04.012.

Willert, K., J.D. Brown, E. Danenberg, A.W. Duncan, I.L. Weissman, T. Reya, J.R. Yates, and R. Nusse. 2003. Wnt proteins are lipid-modified and can act as stem cell growth factors. *Nature*. 423:448–452. doi:10.1038/nature01611.

Wolf, A.A., M.G. Jobling, S. Wimer-Mackin, M. Ferguson-Maltzman, J.L. Madara, R.K. Holmes, and W.I. Lencer. 1998. Ganglioside structure dictates signal transduction by cholera toxin and association with caveolae-like membrane domains in polarized epithelia. *J Cell Biol*. 141:917–927. doi:10.1083/jcb.141.4.917.

Wolf, A.A., Y. Fujinaga, and W.I. Lencer. 2002. Uncoupling of the cholera toxin-G(M1) ganglioside receptor complex from endocytosis, retrograde Golgi trafficking, and downstream signal transduction by depletion of membrane cholesterol. *J. Biol. Chem.* 277:16249–16256. doi:10.1074/jbc.M109834200.

Wolpert, L. 1969. Positional information and the spatial pattern of cellular differentiation. *J. Theor. Biol.* 25:1–47. doi:10.1016/s0022-5193(69)80016-0.

Wolpert, L. 1971. Positional information and pattern formation. *Curr. Top. Dev. Biol.* 6:183–224.

Wu, Y., S. Yakar, L. Zhao, L. Hennighausen, and D. LeRoith. 2002. Circulating insulin-like growth factor-I levels regulate colon cancer growth and metastasis. *Cancer Res.* 62:1030–1035.

Wykosky, J., and W. Debinski. 2008. The EphA2 receptor and ephrinA1 ligand in solid tumors: function and therapeutic targeting. *Mol. Cancer Res.* 6:1795–1806. doi:10.1158/1541-7786.MCR-08-0244.

Xia, F., J. Li, G.W. Hickey, A. Tsurumi, K. Larson, D. Guo, S.-J. Yan, L. Silver-Morse, and W.X. Li. 2008. Raf activation is regulated by tyrosine 510 phosphorylation in Drosophila. *PLoS Biol*. 6:e128. doi:10.1371/journal.pbio.0060128.

Yamanishi, Y., D.L. Boyle, M. Clark, R.A. Maki, M.D. Tortorella, E.C. Arner, and G.S. Firestein. 2002. Expression and regulation of aggrecanase in arthritis: the role of TGF-beta. *J. Immunol.* 168:1405–1412. doi:10.4049/jimmunol.168.3.1405.

Yamashita, Y.M., M. Inaba, and M. Buszczak. 2018. Specialized Intercellular Communications via Cytonemes and Nanotubes. *Annu. Rev. Cell Dev. Biol.* 34:59–84. doi:10.1146/annurev-cellbio-100617-062932.

Yu, S.R., M. Burkhardt, M. Nowak, J. Ries, Z. Petrásek, S. Scholpp, P. Schwille, and M. Brand. 2009. Fgf8 morphogen gradient forms by a source-sink mechanism with freely diffusing molecules. *Nature*. 461:533–536. doi:10.1038/nature08391.

Zartman, J., S. Restrepo, and K. Basler. 2013. A high-throughput template for optimizing Drosophila organ culture with response-surface methods. *Development*. 140:667–674. doi:10.1242/dev.088872.

Zhai, L., D. Chaturvedi, and S. Cumberledge. 2004. Drosophila wnt-1 undergoes a hydrophobic modification and is targeted to lipid rafts, a process that requires porcupine. *J. Biol. Chem.* 279:33220–33227. doi:10.1074/jbc.M403407200.

Zhang, X., J.G. Abreu, C. Yokota, B.T. MacDonald, S. Singh, K.L.A. Coburn, S.-M. Cheong, M.M. Zhang, Q.-Z. Ye, H.C. Hang, H. Steen, and X. He. 2012. Tiki1 is required for head formation via Wnt cleavage-oxidation and inactivation. *Cell*. 149:1565–1577. doi:10.1016/j.cell.2012.04.039.

Zhang, X., O.A. Ibrahimi, S.K. Olsen, H. Umemori, M. Mohammadi, and D.M. Ornitz. 2006. Receptor specificity of the fibroblast growth factor family. The complete mammalian FGF family. *J. Biol. Chem.* 281:15694–15700. doi:10.1074/jbc.M601252200.

Zhou, A., S. Martin, G. Lipkind, J. LaMendola, and D.F. Steiner. 1998. Regulatory roles of the P domain of the subtilisin-like prohormone convertases. *J. Biol. Chem.* 273:11107–11114. doi:10.1074/jbc.273.18.11107.

Zurzolo, C., and K. Simons. 2016. Glycosylphosphatidylinositol-anchored proteins: Membrane organization and transport. *Biochim. Biophys. Acta*. 1858:632–639. doi:10.1016/j.bbamem.2015.12.018.